DESIGN AND ANALYSIS OF A MAGNETORHEOLOGICAL DAMPER FOR VIBRATION CONTROL OF WASHING MACHINE

By

Syed Muhammad Anas Gilani

A Thesis Submitted to the

Graduate School of Engineering

in Partial Fulfillment of the Requirements for

the Degree of

Master of Science

in

Mechanical Engineering

Koc University

January 2016

Koc University

Graduate School of Sciences and Engineering

This is to certify that I have examined this copy of a master's thesis by

Syed Muhammad Anas Gilani

and have found that it is complete and satisfactory in all respects,

and that any and all revisions required by the final

examining committee have been made.

Committee Members:

Prof. İsmail Lazoğlu, Ph. D. (Advisor)

Prof. Özgen Akalın, Ph. D.

Prof. Funda Yağcı Acar, Ph. D.

Date:

ABSTRACT

Magnetorheological (MR) dampers are state of the art adaptive devices that can change damping capability within milliseconds to control undesired vibrations in the dynamic systems. A novel magnetorheological friction damper has been developed to control the vibration of washing machine drum. A 2-D axis symmetric model of MR damper has been developed in finite element analysis software for magnetic analysis and parameter optimization. This analysis will help designers to design an efficient electromagnet capable of delivering maximum magnetic flux and force with less electrical energy and compact geometry.

The hardware design of MR damper has been developed based on magnetic analysis, force and stroke requirements in the washing machine. Experimental modal analysis was performed to determine the dynamic characteristics of MR damper. An experimental test setup was developed to test and validate the performance such as force-velocity and force-displacement relationships. Off-state friction characteristics were studied to determine the behavior of damper without applied current. On-state damping characteristics have been studied using hysteretic model. Damper mathematical model parameters such as damping coefficient, stiffness and hysteresis are identified using mathematical and experimental data. Parameter optimization techniques like least square fit, fmincon, and fminuncon and multistart methods were applied to obtain the trends of damping coefficient and stiffness against various excitation amplitudes of displacement, velocities and frequencies.

The displacement and speed of washing machine drum has been analyzed using sensors at full range of drum speeds. The data was recorded first with conventional passive dampers installed in washing machine. Then passive dampers were replaced by MR dampers and the data is recorded again to compare the performance of both types of dampers. The damping force is adjusted by changing the current through look-up controller. The current is adjusted on the basis of displacement and speed of the drum. Finally a performance comparison was presented that justifies that MR damper can control the vibration of washing machine far better than conventional passive dampers.

ÖZET

Magnetorheological (MR) damperler istenmeyen titreşimleri kontrol etmek için kullanılan ve sönümleme özelliğini milisaniye içerisinde değiştirebilen araçlardır. Özgün magnetorheological sürtünme damperi çamaşır makinesinin titreşimlerini control etmek için geliştirildi. Sonlu parça analizi yazılımında manyetik analizler ve parametre optimizasyonu yapılmak üzere 2-D eksen simetrik MR damper modeli geliştirildi. Bu analizler maksimum manyetik flux ve kuvveti daha az elektrik enerjisi ve geometri kompaktlığı ile sağlayan verimli elektromıknatıs üretimi için dizaynırlara yardımcı olacaktır.

MR damperlerin hardware dizaynı manyetik analizler, kuvvet ve çalışma mesafesi gereklilikleri baz alınarak yapılmıştır. MR damperin dinamik özelliklerini tanımlamak için deneysel modal analizler gerçekleştirildi. Kuvvet-hız ve kuvvet-yer değiştirme(deplasman) ilişkilerini test etmek ve doğrulamak için deneysel test düzeneği kuruldu. Sistemin kapalı durumdaki sürtünme özelliği akım uygulanmadığındaki davranışı belirmek için incelendi. Sistemin çalışır vaziyetteki sönümleme özelliği hysteretic model kullanılarak incelendi. Damperin sönümleme(damping) katsayısı, sertlik(stiffness) ve hysteresis gibi matematiksel parametreleri matematiksel ve deneysel veriler kullanılarak belirlendi. Değişik yer değiştirme, hız ve frekans uyarmalarında sönümleme katsayısı ve sertliğin değişim trendini elde etmk için least square fit, fmincon, fminuncon and multistart gibi parametre optimizasyon teknikleri kullanıldı.

ACKNOWLEDGMENTS

First of all I want to thank to my advisor Prof.Dr. Ismail Lazoglu for giving me the chance to be a part of his team and the resources he provided during the research. I am very grateful for his faith and patience on me.

I would like to thank my project fellow Abasin Ulasyar for working equally hard, days and nights in this project. Without his help and support it will be very difficult to achieve the goal on time.

I specially thank my friend Adnan Hassan for providing valuable advice and technical support whenever it is required.

Several other colleagues and friends deserve special thanks. I thank my friends and MARC members Mohammad Akmal, Sarmad Shams, Haris Shehzad, Talha Irfan Khan, Abbas Hussein, Shahid Mustafa, Caglar Ozturk, Ali Memedov, Basar Aka, Armin Bijanzad, Erdem Kundakcioglu, Ugur Mumtaz, Mohammad Isa, Ismail Enes Yigit and Ehsan Layegh Khavidaki for sharing their knowledge and supporting me in every possible way.

I extremely appreciate the technical support from Muzaffer Butun. Without his help this project would be unaccomplished.

I would like to thank my parents for their prayers and support throughout my stay in Turkey. I would especially like to thank my wife for all the support encouragement and attention and to my daughter Mia for all the welcome hugs and byes that encourage me to work even harder through the day. Last but not the least, I would like to thank to my parents in law, brother and sisters in law for supporting me spiritually throughout my study and my life in general.

TABLE OF CONTENTS

LIST OF TABLES

LIST OF FIGURES

Chapter 1

1 INTRODUCTION

1.1 Overview

Dynamic systems deal with kinematics and kinetics i.e. motions and forces. For a stable dynamic system, all the forces acting on a machine system need to be balanced, but sometimes these forces cause imbalance in the system. The imbalance or the state when the system is displaced from its equilibrium position is called vibration. Dynamic system can be displaced from equilibrium due to many factors, for example force imbalance, loose connections, degradation of structure or mass changes, etc. Several ways are adopted to reduce and suppress vibrations, i.e. changing the dynamics of the system, balancing the unbalanced forces and masses and absorbing the vibration energy or simply damping the vibrations of the system. Dampers are used to dissipate energy which is generated due to disturbances and retain the system back to equilibrium state. Vibration dampers can be classified as passive, active and semi active. Passive dampers are simpler in design and have fixed damping characteristics. Passive dampers have fixed vibration suppression frequency and cannot suppress a broad range of vibration excitations. Active dampers can suppress vibrations in a broader range by adjusting the damping parameters through control signals. However active dampers usually require large power sources to provide desired active forces which make them bulky and costly and make the control system more complex. Semi active vibration dampers can provide both the simplicity of a passive system while maintaining the adaptability of active vibration dampers without requiring a complex control technique and large power sources. One of the main advantages of the semi active damper over active damper is fail safe design. In case of power failure active dampers fail to work almost completely while semi active damper can still work due to passive mode.

1.2 Problem Statement

One of the examples of vibrations due to force imbalance and mass changes are washing machines. Modern day washing machines are front loaded; it means the dirty clothes are loaded inside from the front of washing machine rather than from the top. The spinning process in washing machines is a source of undesired vibrations and noise. It is the main cause of discomfort for the user and the environment as well as for the machine as it affects performance and lifetime reliability of the machine. It also limits the capacity of washing machines. The tub of front loaded washing machine, which contains water to flow in and out of the clothes, is suspended from housing by a number of coil springs. In addition to providing mechanical support, the high stiffness springs allow the tube to move at low frequency while providing vibration isolation at high frequency. Due to gravity the load or mass is not concentric with the spin axis of the drum located inside the tub. During spin cycle the mass imbalance produces the disturbing centrifugal force that excites the vibratory motion of the tub. The motion of the tub can become excessive when drum speed approaches the tub resonance frequency as illustrated in Figure 1-1.

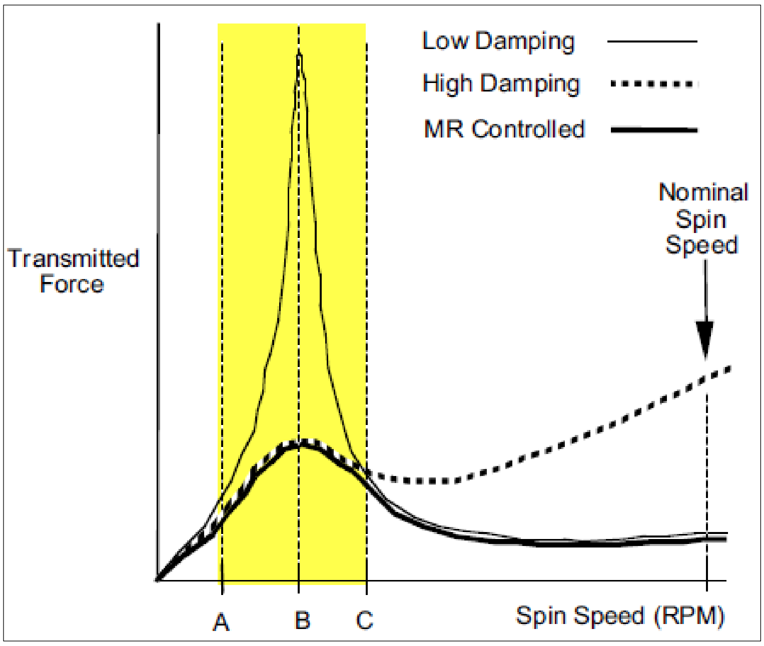

Figure 1-1: Typical force transmissibility curve of front-loaded washing machines [1]

1.3 Methodology

In this study the problem statement is deeply addressed step by step from designing of magnetorheological damper to its final installment into washing machine. In the end preliminary testing with on-off control and performance comparison has been made with currently available passive dampers.

Chapter 2 provides necessary background and literature review on MR dampers. A wide literature search on the use of MR fluid in different application was discussed. Later a complete review of MR dampers in different application available in literature has been presented. Designs of MR dampers are discussed in detail based on types, structure, magnetic circuits and valve configurations. Finally an optimal design solution has been selected for washing machine application and advantages of solution have been presented.

Chapter 3 describes the complete finite element analysis and design of magnetic circuit for MR damper. Chapter starts with the discussion about magnetic circuit theory together with magnetic materials. Reluctance method is discussed and proposed for designing of magnetic circuit. Finite element analysis is conducted in two phases; first phase design parameters are chosen arbitrarily to verify the magnetic flux and magnetic force calculations. In second phase optimization of design parameters is conducted to select the optimal parameters based on magnetic flux and force requirements.

Chapter 4 describes the magnetorheological fluid theory, mathematical model and operating point calculations. Specification of MR fluid is presented including BH curve and yield stress vs applied magnetic field intensity. Operating point is selected based on magnetic circuit parameters discussed in chapter 3 and shear stress is calculated.

Chapter 5 details the complete mechanical design of MR damper. Active part (bobbin) of damper has been modelled based on magnetic circuit design parameters concluded in previous chapter. The stroke, length and end fittings of damper have been finalized based on the space and fitting requirements of available washing machine. In addition to that dynamic frequency response analysis of MR damper is conducted using experimental modal analysis techniques to find out the natural frequencies, modal stiffness and damping ratio of the damper. In the end details of experimental test setup are presented along with test setup components specifications are listed.

Chapter 6 discusses the complete mathematical modelling of MR damper. It starts with discussion of passive state (no current) modelling known as friction characteristics. Later experimental tests are conducted to validate total force calculation and energy dissipation characteristics. Equivalent damping coefficient and energy dissipation graphs are presented using experimental tests at different currents. In the end damper parameters such as stiffness, damping constant and hysteresis has been identified using different experimental tests at several frequencies and currents. Trends of parameters with amplitude, current and frequency parameters are discussed.

Chapter 7 describes the performance comparison of MR damper with available passive dampers onto the washing machine. First the displacement data of washing machine drum has been recorded with passive dampers. The drum speed (RPM) is also measured simultaneously with displacement. In next step passive dampers are replaced by MR dampers and displacement data is again recorded for similar drum speeds. During operation MR damper current is controlled by on-off controller. The controller switches current based on drum speed. In the end comparison of both passive and MR damper performance is compared.

Chapter 2

2 LITERATURE REVIEW

2.1 Overview

This chapter provides necessary background and literature review on MR dampers. A wide literature search on the use of MR fluid in different application were discussed initially. Later on a complete review of MR dampers in different application available in literature has been presented. Designs of MR dampers are discussed in detail based on types, structure, magnetic circuits and valve configurations. Finally an optimal design solution has been selected for washing machine application and advantages of solution have been presented.

2.2 Magnetorheological (MR) Fluid

Magnetorheological fluids are smart fluids that change apparent viscosity when subjected to magnetic field. Jacob Rabinow has been considered as the inventor of MR fluid as he received the first patent for MR fluid in 1940s when working for US National Bureau of Standards [2]. MR fluids consist of synthetic hydrocarbon or silicon base coupled with a suspension of magnetically soft particles. In the off-state magnetic particles are suspended freely in the carrier fluid and exhibit Newtonian behavior. However in the on-state when magnetic field applied the magnetic particles get aligned in the direction of magnetic field to form chains in the fluid. The yield strength of fluid can be controlled accurately by varying the magnetic field intensity. At higher magnetic field the fluid becomes viscoelastic solid. The ability of fluid to be controlled by electromagnet give rise to many possible control based applications. MR fluid can be used in three different ways which are called modes of operation of MR damper as shown in Fig 2-1.

Figure 2-1: MR fluid in liquid form in the absence of magnetic field turns solid when magnetic field is applied .

2.3 Magnetorheological Fluid Applications

MR fluid has many applications nowadays. Kordonski et al. used MR fluid to polish optical glasses using jet finishing process. MR fluid helped to resolve a challenging problem of finishing steep concave surfaces and cavities [4]. Cheng et al. used MR fluid for assistive polishing of optical aspheric components. Cheng et al. used 2-axis wheel shaped tool supporting dual magnetic fields [5]. Sidpara et al. used MR fluid for finishing of flat, curved and free form metal surfaces [6]. Magnetorheological based finishing is a Nano finishing process, when magnetic field is applied stiffness of MR fluid increases. Material can be removed by using the stiffness and abrasive properties of MR fluid to finish and polish the work-piece.

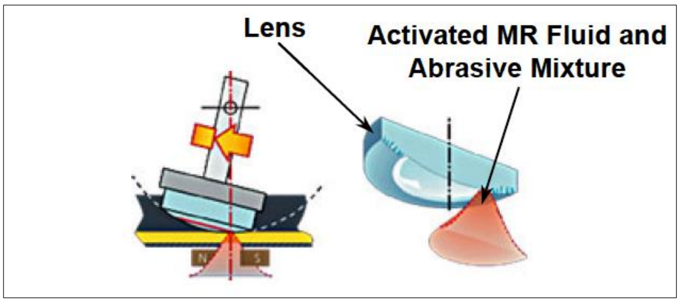

Figure 2-2: Basic principle of MR fluid – assistive optical polishing [7]

Singh et al. used ball end milling process for finishing flat and 3D work pieces. MR fluid used to flow through the center of the rotating tool core and gets stiffened in the form of magnetically controlled ball end shape at the tip surface of the tool [8]. Jung et al. used MR finishing process for hard materials using sintered using iron-CNT compound abrasives on Al_2O_3-TIC hard disk slider [9].

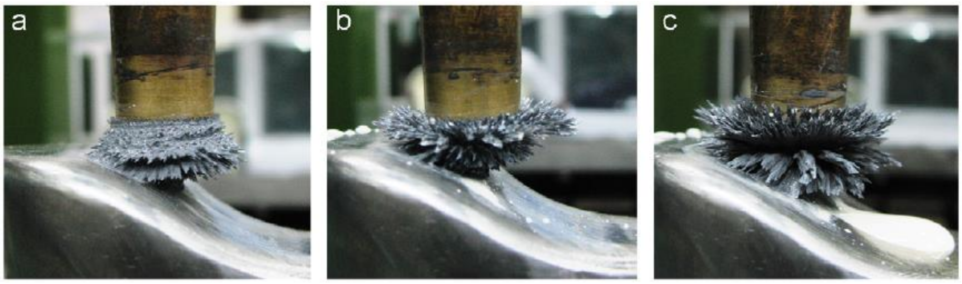

Figure 2-3: MR fluid used for finishing and polishing of free form surfaces [6]

Pettersson et al. used MR fluid in robot gripper for handling of delicate food products with varying shapes [10]. Robot grippers are filled with MR fluid and molded around the product's contours. Through the activation of an electromagnet in the gripper arm, a large increase in the MR fluids yield stress grips the product in the mold produced with gripper surfaces, allowing it to be lifted.

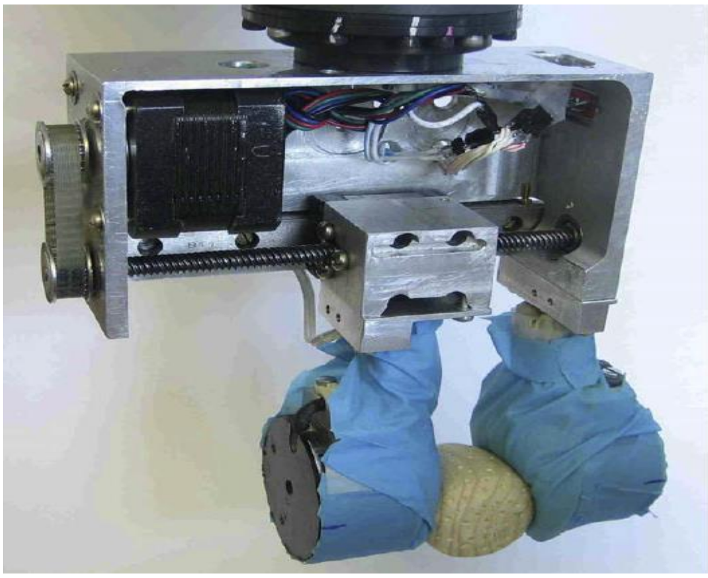

Figure 2-4: MR fluid filled pouches on grippers holding a model strawberry [10]

Zhong et al. used MR fluid on sheet metal flexible-die forming. Zhong showed that viscosity has the great effect on the formability of sheet metal in viscous pressure forming. MR fluid is used as flexible die medium and viscosity adjusted by changing the magnetic field during the forming process [11].

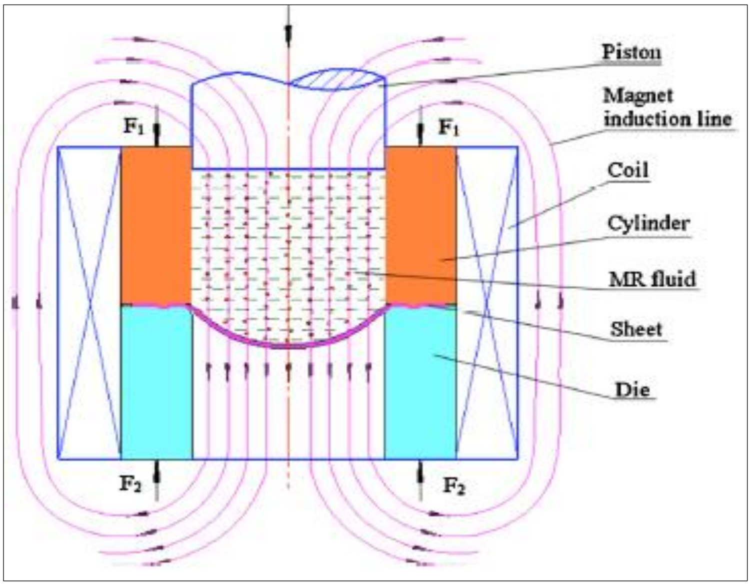

Figure 2-5: Schematic drawing of magnetorheological pressure forming process [11]

Yang et al. developed miniature tunable stiffness display for haptic applications using MR fluid. Commercial tactile information devices use AC or DC motors as actuators due to which these devices have instability problems and are bulky to be incorporated in hand held devices. MR fluids are used because controllable fluids not only allow the stiffness display to have a simple mechanical structure but also allow the stiffness display to avoid any stability problems [12].

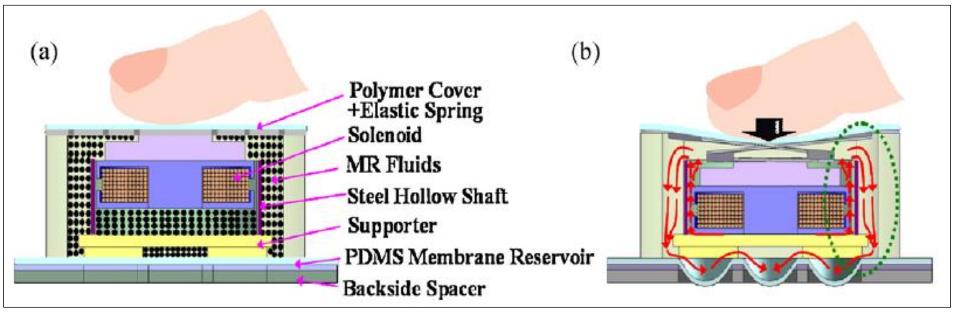

Figure 2-6: Schematic illustration of working principle and mechanism of stiffness display: (a) before pressing and (b) after pressing [12]

Farzad Ahmadkhanlou et al. developed 5-DOF MR sponge based haptic system (master) for controlling a tele robotic arm used in tele robotic surgery. The master 5-DOF joystick controls the movement of a 5-DOF slave (Lynx 5 by Lynxmotion). A novel multi-axis force sensor is designed with authors and used at the end effector (EE) of the slave for force feedback control. Force and displacement sensors in the slave sense the environment conditions along which the end effector moves. When the EE contacts a solid object or barrier, the exerted force is sensed with force sensor and the signals are sent to the 5-DOF MR based master to activate the MR dampers accordingly to replicate the force. The user feels the force from master joystick proportional to the force encountered at the slave. For example if the slave encounters soft tissue (low force, small to no deceleration) a relatively small current signal is sent to the MR damper which will give the user the slight resistance associated with soft tissue. Likewise if the slave encounters bone (high force, large deceleration) a large signal is sent to the MR damper, which will give the user a larger resistance [13].

2.4 MR Damper Applications

The most promising applications of MR fluid are semi active dampers. There have been developed many applications where MR fluid dampers are used and are discussed here.

There are three operational modes in which MR fluid can be used in dampers [15]. Carlson et al. used MR damper in smart human prosthetics. In such system MR damper is used to control in real time the motion of an artificial limb based on inputs from a group of sensors [14].

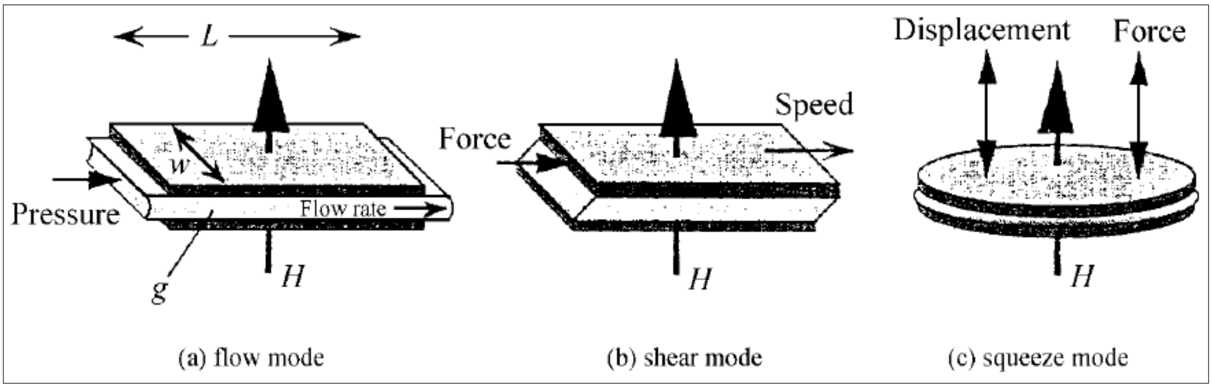

Figure 2-7: Operational modes of MR fluid devices [15]

Tomori et al. used MR fluid brake for the vibration control of an artificial muscle manipulator. A straight-fiber-type artificial muscle actuator has been developed which operates by air. The actuator is flexible light and so it vibrated when there is a high load.

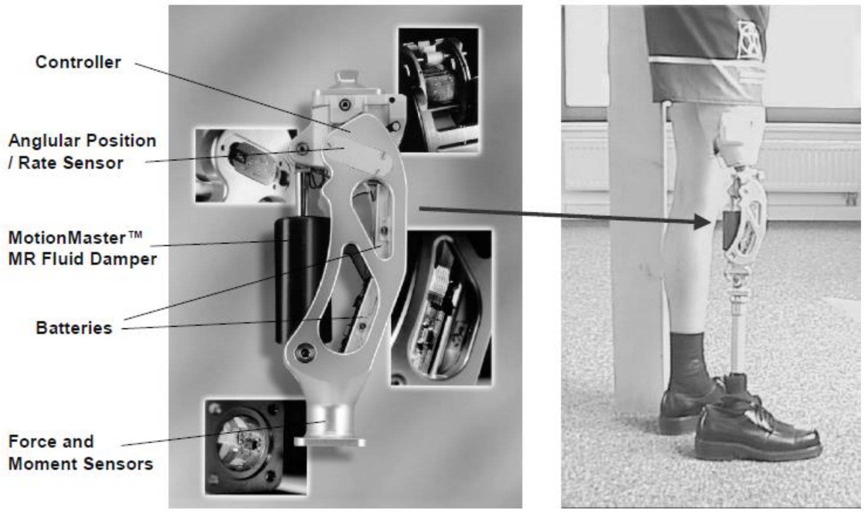

Figure 2-8: Commercial smart Magnetix™ above knee prosthesis with real time control provided by MotionMaster™ MR fluid damper [16]

Therefore magnetorheological fluid brake is used to suppress vibration by applying magnetic field and changing the apparent viscosity [17]. Dong et al. used MR fluid damper for adaptive force regulation of muscle strengthening rehabilitation device. Rehabilitation device is adaptive and used to strengthen different muscle groups based on the torque generating capability of the muscle that changes with joint angle. A digital adaptive control attached to MR rehabilitation device is capable of regulating exercise force precisely following the muscle strengthening profile prescribed by a physical therapist [16]

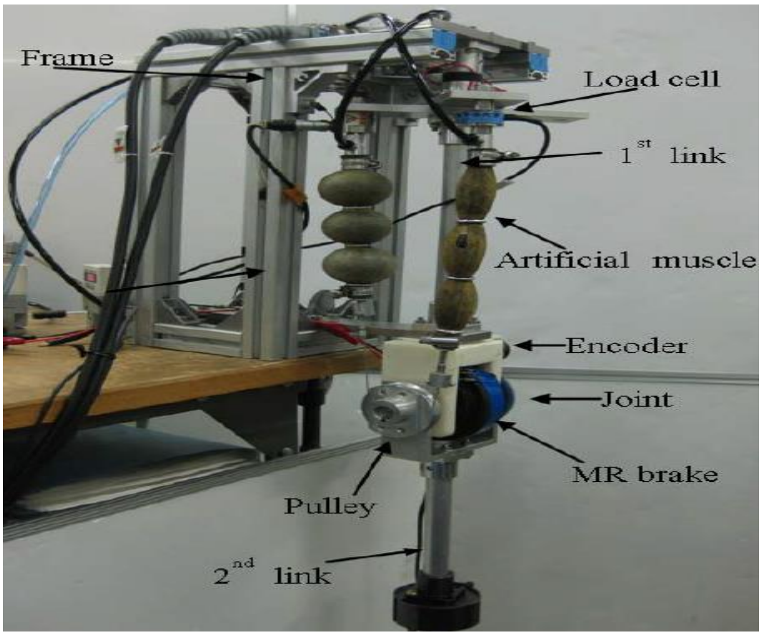

Figure 2-9: Artificial muscle manipulator with MR brake [17].

Kong et al. used MR damper for targeted suppression of vibration in deep hole drilling. Deep hole drilling process is susceptible to dynamic disturbances, chatter and spiraling. MR damper has been designed to suppress the dominant vibration upon its emergence by variable damping or to force the harmful vibration morph into less harmful by different damper position [18]. David case et al. employed the MR damper in the development of upper limb orthosis for tremor attenuation in patients suffering from pathological disease [19].

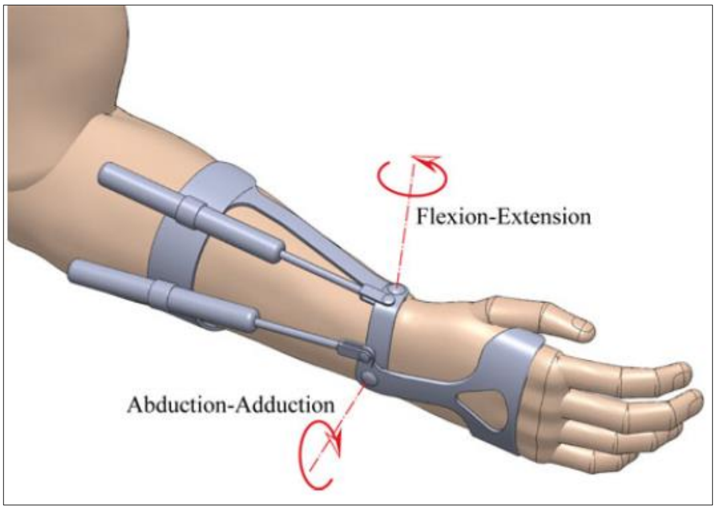

Figure 2-10: CAD representation of orthosis design as worn on the arm of the patient [19]

Mei et al. developed an innovative method based on MR fluid controlled boring bar for chatter suppression. Stiffness and natural frequency of boring bar is changed during boring operation to suppress chatter by changing the stiffness of MR fluid [20].

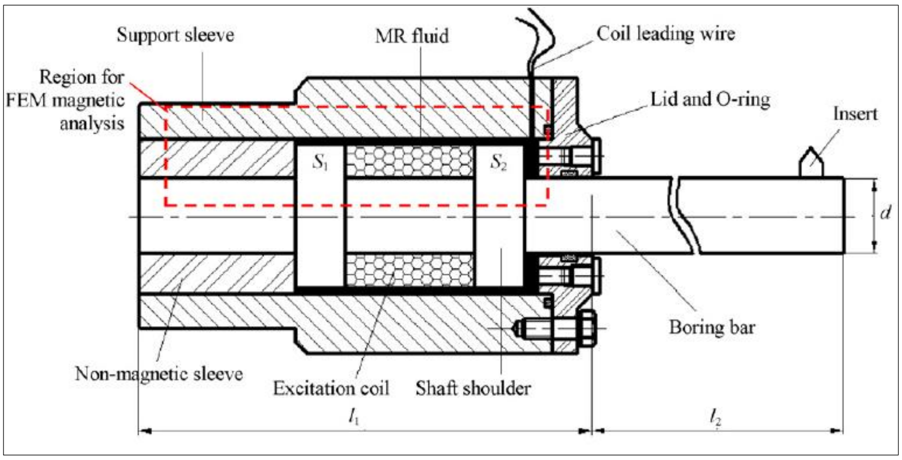

Figure 2-11: Structure of MR fluid-controlled boring bar with chatter suppression [20]

Choi et al. used a mixed mode MR fluid mount for optimal control of structural beam subjected to external disturbances. Rubber material used in mount is flexible and good for dampening high frequency vibrations but poor performance at low frequencies so MR fluid mount has been developed to counter vibrations at low and high frequencies [21].

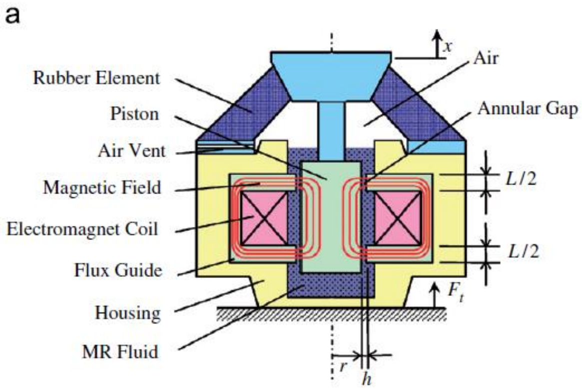

Figure 2-12: MR mount (a) configuration (b) picture of MR mount [21]

MR dampers available today mostly used in heavy industrial applications. A major application is earth quake proof structures and seismic applications by absorbing detrimental shock waves and oscillations. Spenser et al. studied MR fluid dampers for seismic protection of structures. Spenser said "*Because of their mechanical simplicity, high dynamic range, low power requirements, large force capacity and robustness, magneto-rheological (MR) fluid dampers have been shown to be semi-active control devices that mesh well with application demands and constraints to offer an attractive means of protecting civil infrastructure systems against severe earthquake and wind loading*" [22].

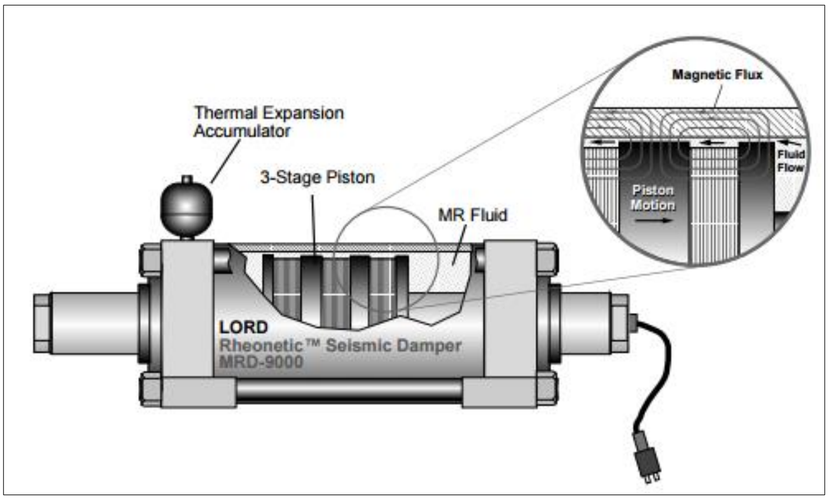

Figure 2-13: Schematic of 20 ton MR fluid damper for seismic applications [22].

Lots of study has been done regarding use of MR damper in vehicle technology. Delphi corporation developed MagneRide™ an adaptive suspension with magnetorheological damper and debuted on the Cadillac Seville STS [23].

Figure 2-14: MagneRide™ can be found on these and other quality vehicles [23]

Figure 2-15:First MagneRide™ introduced in 2002 (Left), the third-gen Audi TT launched with MagneRide™ Dampers(Right) [23].

2.5 MR Damper Designs - A study

This chapter also discusses about the study being done and currently going on the different designs of MR Dampers. The purpose of study is to analyze and select the best suitable design of MR damper for washing machine applications. Zhu et al. did the comprehensive literature review on the structural design and analysis of MR dampers [24]. Authors discussed and divided the different structural functions and configurations in the following fundamental aspects (a) Operational modes of MR dampers (b) Structural design of MR dampers and (c) MR control valves.

2.5.1 Monotube Structure

The Monotube MR damper is basically based on single rod cylinder structure which has only one reservoir of MR fluid which is divided into extension chamber and compression chamber by moving piston [7]. During piston movement, MR fluid in the cylinder passes through the MR control valve that is assembled in the piston, a pressure differential created in the valve for the flow of fluids and consequently generating damping force proportional to the pressure difference is produced.

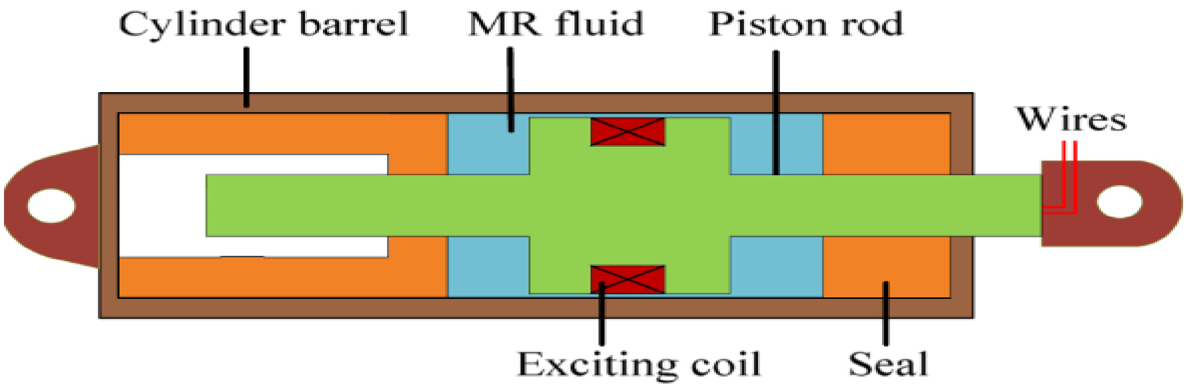

Figure 2-16: Monotube MR Damper [25]

An accumulator with the compressed gas is fitted to one side of piston separated by diaphragm and has been used for the following three advantages. First, the accumulator is used to accommodate the volume change of the incompressible MR fluid due to piston movement. Second, the accumulator provide the pressure offset so that the low pressure side of MR control valve should not reduce to cause cavitation of MR fluid. Third, the gas chamber adds a spring effect to the force generated by damper simultaneously and maintains the damper at its extended length when no force is applied [26]. In addition the bearing at the end of the extension chamber is utilized to guide the piston rod movement and the adjacent seals for preventing leakage of MR fluid. Generally Monotube dampers have advantage of simpler mechanical structure in terms of manufacturing and are being lighter due to fewer parts and have the disadvantages of having higher gas pressure normally more than 10 bar and having a cylinder that is more susceptible to damage compared to that of twin tube damper [26].

2.5.2 Twin Tube Structure

Basic structure of passive twin tube damper is shown in Fig 2-17. The twin tube MR damper has inner and outer housing. The inner housing is filled with MR fluid and guides the piston rod assembly same as the housing of Monotube damper. The outer housing that is partially filled with MR fluid accommodates volume changes due to piston movement fulfilling the same purpose as the pneumatic accumulator mechanism in Monotube damper.

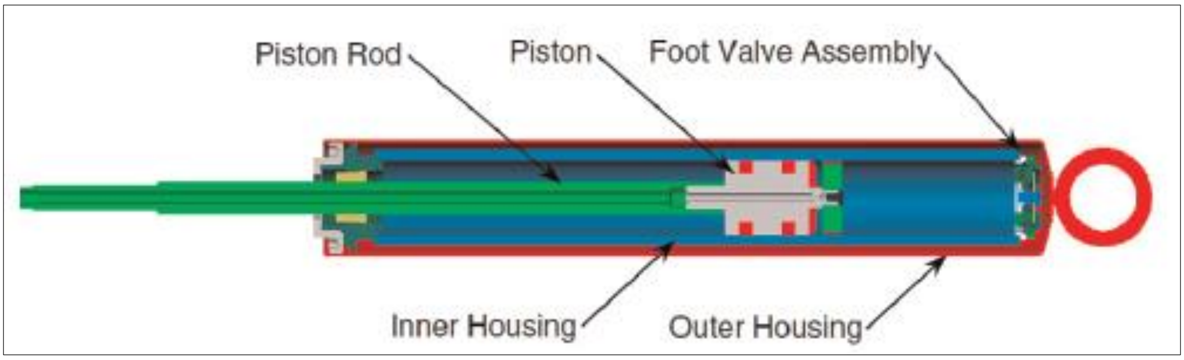

Figure 2-17: Section view of twin tube MR damper [7]

Moreover the outer housing provides additional functions like protection of the damper internal parts and transferring heat from the damper fluid to the surroundings. Note that in Fig 2-18 a valve assembly called ‘foot valve assembly’ attached to the bottom of the inner housing is used to regulate the flow between two tubes during extension and compression movement. When the damper piston enters the cylinder it compresses the MR fluid that flows from inner housing to outer housing through the foot valve assembly. The amount of fluid that enters from the inner housing to outer housing is equal to the amount of volume displaced by piston displacement. When piston retracts, the MR fluid enters back into the inner cylinder through the return path of foot valve assembly [24]. Twin tube MR dampers have advantage that it can work with lower gad pressure i.e. less than 10bars but their mechanical design is more complex and have problems in dissipating the generated heat [26].

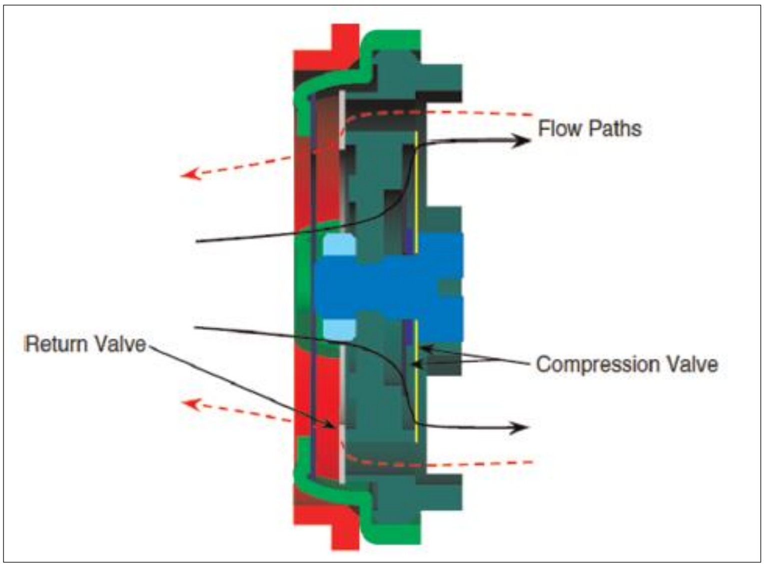

Figure 2-18: Details of foot valve assembly [7]

2.5.3 Double-ended Structure

Double-ended structure is a special configuration from Monotube structure as shown in Fig 2-19. Piston rod has been extruded from both ends of the MR damper and has the same diameter. This configuration eliminates the use of piston-rod volume compensator or accumulator in to the damper. Thus gas chamber in Monotube damper can be removed and no spring effect could be generated by itself, although small accumulator still required for compensating thermal expansion of MR fluid [27]. Double ended MR Dampers have been used for shock and impact loadings, gun recoil applications, and seismic protection in structures [27].

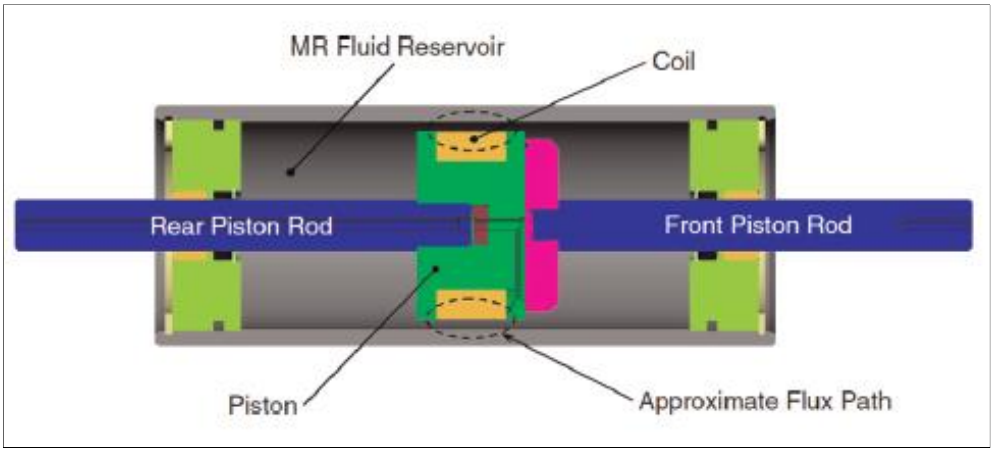

Figure 2-19: Double-ended MR fluid damper [7]. This design do not require accumulator.

2.5.4 MR damper Control Valves

MR damper control valve is basically magnetic circuit used for generating magnetic flux through which electrical control of damping force can be achieved. Figure 2-20 shows MR control valve attached to moving piston of an MR damper.

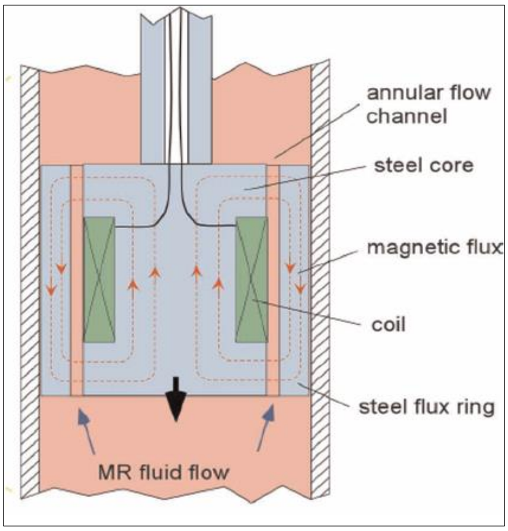

Figure 2-20: MR damper control valve with magnetic circuit [24]

Magnetic circuit control valve is based on magnetic steel core on which coil is wound, magnetic housing, and a flow channel between inside of magnetic housing and outside of magnetic core.MR fluid passes from extension chamber to compression chamber through flow channel. When current is passed through the coil the magnetic field linked to it generates magnetic flux that flows through the low reluctance path i.e. magnetic core and housing. The dynamic yield stress of MR fluid is changed with the magnetic field intensity generated by magnetic circuit. Consequently damping force is generated against the excited motion under controlled magnetic field intensity. In the absence of magnetic field thee damping force is present due to viscosity of MR fluid [28]. Usually low carbon steel is used for magnetic circuit design which has a high magnetic permeability and saturation and can effectively guide magnetic flux into the fluid path [29]. In addition bushes and washers are employed to prevent leakage of magnetic fields [30]. Grunwald et al. described two types of magnetic circuits based on coil configuration; first the MR fluid passes through the annular gap and the coil is placed in the middle of the gap, while in the second configuration the MR fluid passes through the middle of the orifice and coil is wrapped along the whole length of orifice. In first case the direction of magnetic flux is perpendicular to fluid flow while in second case the magnetic flux is parallel to fluid flow. It is noticed that high pressure capacity, fast control response and less magnetic field leakage could be achieved using internal coil than using external coil configuration [31].

2.5.5 MR dampers with integrated internal coils

Figure 2-21 shows the schematic of integrated internal coil. The coil is wound on the moving piston and piston rod has hollow structure to accommodate coil wires and separate them from interaction with MR fluid.

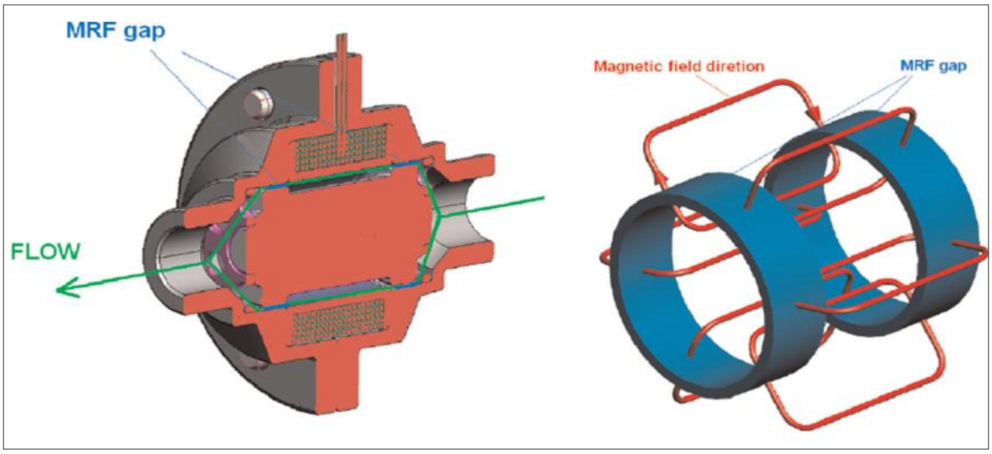

Figure 2-21: MR fluid flow and magnetic field directions in the MR damper valve [31]

This type of MR damper may work in three different modes i.e. single flow mode, mixed flow mode, direct shear mode and multimode using combination of shear mode, valve mode and squeeze mode due to the relative motion of coil and outer cylinder. Mixed mode damper has advantage of less sealing requirement but at the same time has disadvantage of being heavy due to outer body made of low carbon steel instead of aluminium.

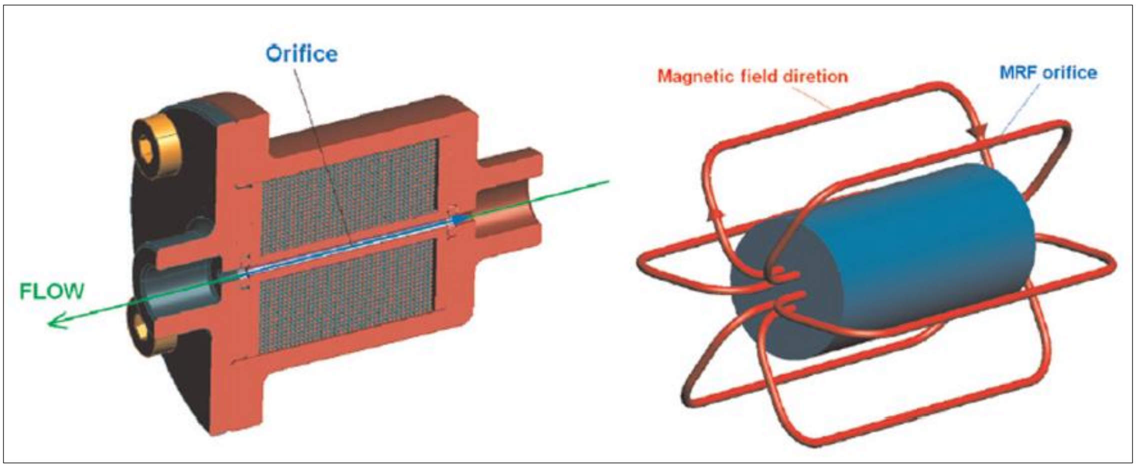

Figure 2-22: MR fluid flow and magnetic field directions in the MR damper orifice [31]

Isolators are used to isolate the transmission of vibration from excitation body to receiving body of structure. Springs are normally used as isolators. Magnetorheological isolators are also designed to change the resonance frequency of isolator if the excitation system has unpredictable dynamics. Figure 2-23 shows schematic of multimode MR isolator.

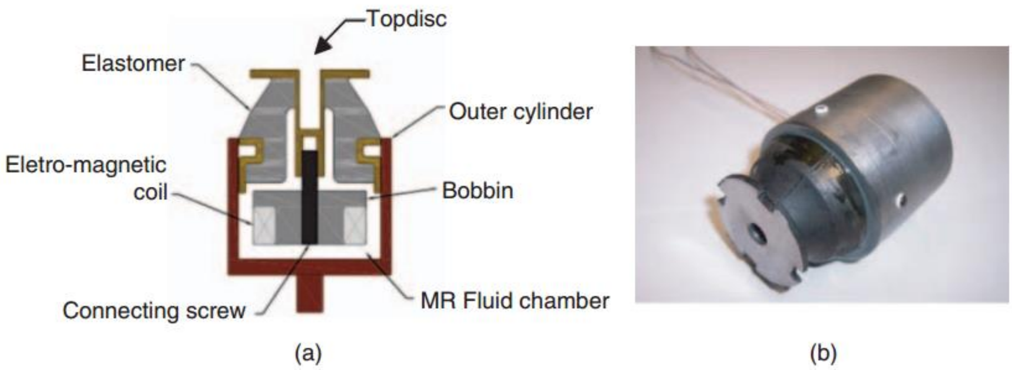

Figure 2-23: Schematic of multimode MR elastomer [32]

The electromagnetic coil is wrapped around a magnetic bobbin attached to the top elastomer through connecting screw. The outer cylinder serves as the magnetic flux return path for creating valve and shear damping during the motion of top elastomer. Squeeze mode damping is achieved in the isolator when the top elastomer moves downward and pushes the fluid against the outer cylinder walls. MR isolator design not only increase damping force but also reduces unwanted lock up state between magnetic pole gap due to high frequency and small amplitude excitations which often occurs in single valve mode isolators [32]. Integrated MR dampers with internal coil are usually characterized by good wire protection and compact structure but require complex design requirements, heavy pistons, difficult heat dissipation due to internal coil configuration, difficult assembly, maintenance and replacement of magnetic circuit [27]. Internal coil MR dampers are susceptible to heat build-up due to inside coil that causes the viscosity of MR fluid to decrease which in turn reduces the damping force [33].

2.5.6 MR dampers with integrated external coils

Figure 2-24 shows schematic of MR damper with integrated external coil. It is noted that the MR damper with simultaneously moving external coil and piston could provide more length than the MR damper with fixed external coil [24].

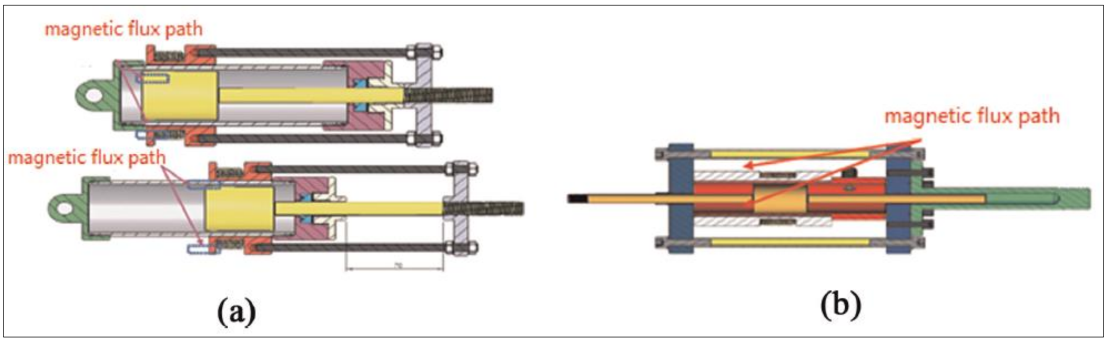

Figure 2-24: Schematic design of MR damper with external coil (a) damper with simultaneously moving external coil and piston and (b) damper with fixed external coil [24]

The external coil has the advantage that all thermal energy generated due to electrical and electromagnetic power dissipation could be released to the atmosphere and do not contribute to the dampers hydraulic system since the coil is intact with MR fluid [34]. However the damping force is less than the damper with same specification i.e. number of turns and fluid volume but with internal coils [35].

2.5.7 MR Dampers with bypass valves

In MR bypass valve damper the magnetic circuit is incorporated away from the MR fluid cylinder on a bypass duct. Bypass duct is used to create pressure difference and resistance to MR fluid to produce damping force as shown in Fig 2-25. MR bypass duct damper can only be used in valve mode since flow channel and outer housing are always fixed [24]. Bypass dampers are suitable for high impulsive force systems having large strokes and large excitation amplitude such as landing gear system, gun recoil system and transportation of dangerous objects [24] [36]. Figure 2-26 shows bypass MR damper with external coils which contains porous media and is externally wrapped by a fixed electromagnetic coil used for energy absorbing applications capable of generating high damping force with compact volume of MR damper [37].

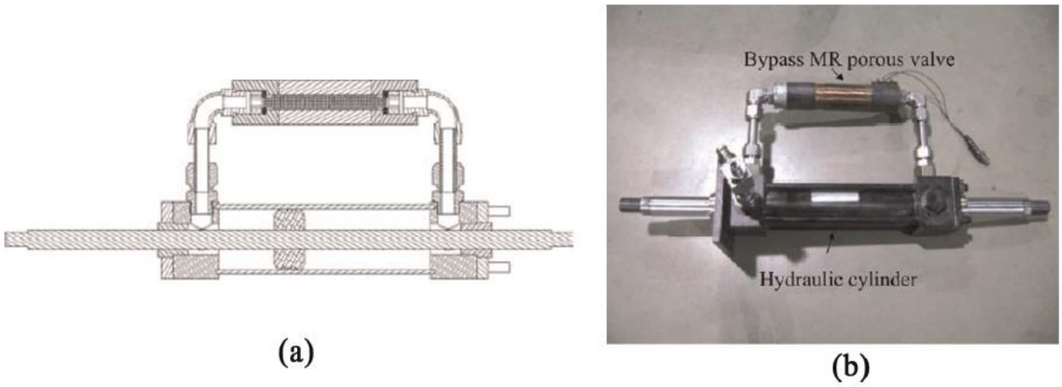

Figure 2-25: Schematic configuration and picture of porous bypass MR damper with external coil [37]

The advantage of bypass MR dampers lies in simple structural design assembly and maintenance [29]. Another benefit of bypass design is it can be fitted to any conventional hydraulic damper with slight modifications. Especially disc type bypass MR dampers has been designed for high force in large scale seismic applications [24]. The disadvantage of bypass MR damper could be its less compact design due to presence of bypass duct. Also protection of coil wires is required for external coil dampers [24].

2.5.8 Syringe-type MR dampers

Figure 2-26 shows the syringe type MR damper. It consists of two syringes connected by a plastic hollow cylinder through which the fluid flows from one syringe to another. There will be no vacuum as both the pistons shafts will move simultaneously and are connected together with a parallel rod.

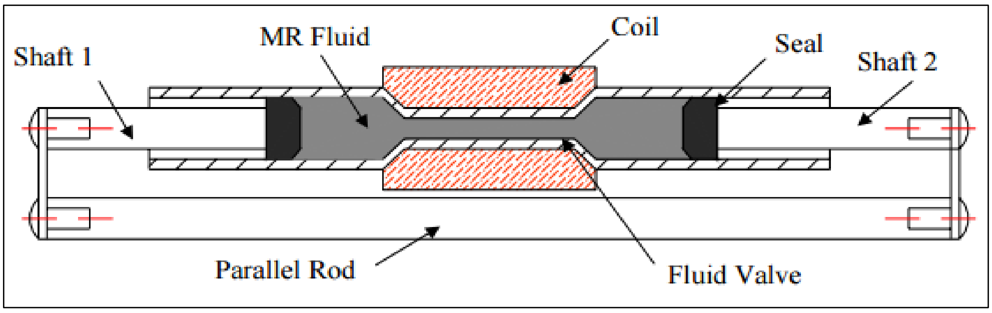

Figure 2-26: Schematic of syringe-type MR damper with external coil [24]

Main advantage of the design is that the coil is not inside the housing which helps the wiring of coil much simpler. This design has a drawback that its asymmetrical design will cause bending moments on the shaft [35]. Also there is no proper short low reluctance magnetic flux return path.

2.5.9 Sponge-type MRF dampers

A sponge type MR damper is designed such that the MR fluid is kept inside absorbent material. Sponge damper works on shear mode and has the major advantage of no sealing requirement and very less amount of MR fluid is required with minimum structural complexity. MR sponge dampers are suitable for low force and low cost applications. Figure 2-27 shows the schematic structure of MR sponge damper where outer cylinder is a hollow steel pipe and piston is comprised of electromagnetic coil and an absorbent matrix material soaked with MR fluid. Fibre, felt, polyurethane and metal foams can be used as absorbent matrix materials. Electromagnetic coil generates yielding shear force which resists the motion of piston with cylinder. Sponge type MR dampers can be operated in direct shear mode without need of hydraulic seals, bushings. No precise manufacturing and tolerance is required for the parts. The major advantage is less requirement of MR fluid which is an expensive component of MR dampers. This least requirement of MR fluid compared to all other MR damper make this design ideal for low cost, commercial, high productivity application areas. Currently low cost MR sponge damper has been used in high performance washing machines [1].

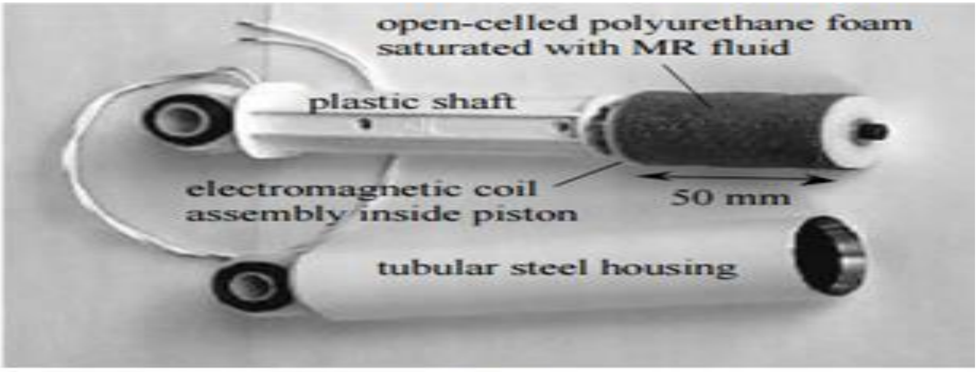

(b)

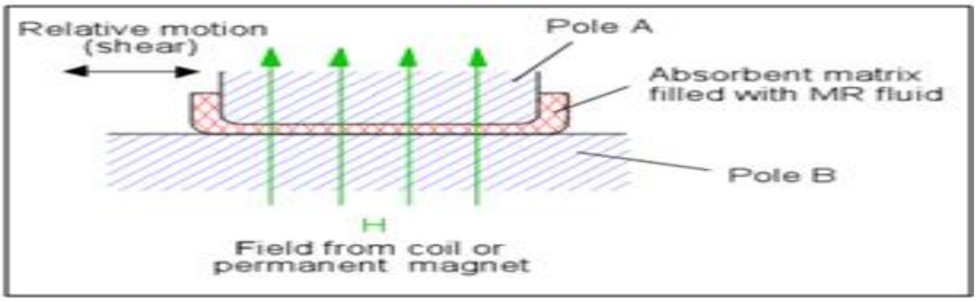

Figure 2-27: MR sponge damper (a) picture of inside parts (b) working principle with magnetic circuit [1]

Ahmadkhanlou et al. used MR sponge damper in tele robotic surgery as a force feedback sensor [13]. Spelta et al. used MR sponge damper of Lord ™ Corporation in commercial washing machine and performed various tests for vibration control. Spelta also applied adaptive control techniques to efficiently control the machine vibrations [38]. Carlson from Lord™ corporation has published first patent on field responsive Mr damper for washing machine [39].

2.6 Selection of MR damper for washing machine application

In previous section many design options has been studied for the design of suitable damper to control the vibration of washing machine. For the same purpose a front loaded washing machine has been opened and the dampers inside it were investigated. Figure 2-28 shows the inside of washing machine with rear panel opened and conventional passive damper is visible. Passive damper inside washing machine was studied. It comes out to be a friction damper with lubricated sponge material. Two similar passive dampers were installed inside the machine each capable of providing almost 110N damping force.

Figure 2-28: Rear view of front loaded washing machine. Passive damper is visible with one end attached to the base and other end connected to suspended tub.

From current machine setup and damper design many things were obvious i.e. cost and power consumption has been a major concern for white good manufacturers. European manufacturers of horizontal-axis, front-loading washing machines are pushing for increased performance and efficiency. Smaller in load capacity and typically installed in apartment kitchens, these machines are being designed for maximum energy efficiency and quiet operation (in small spaces and high-occupancy buildings, neighbors are never far away) [40].

2.7 Advantages of MR sponge damper

MR sponge damper has been selected as the most optimal solution for washing machine application due to following advantages over MR fluid dampers;

1. MR sponge damper requires neither seals nor bearings because cylinder is not filled with MR fluid therefore no fear of leakage.
2. It uses the same inexpensive components found in existing passive dampers with minimal modifications i.e. adding magnetic circuit into it and replacing lubricated fluid in sponge material with MR fluid.
3. Simpler design with ease of manufacturing installation and maintenance.
4. It consist of sponge as friction material with micron sized holes to hold MR fluid due to capillary action so MR sponge damper doesn’t require filling the cylinder with MR fluid. It is noted that 5 to 10mL of fluid is required to obtain more than 200N force.

5. Power requirement of damper is also low, only 0.3 Amps current is required to generate more than 200N force.
6. Faster response time compared to fluid damper due to less weight and using direct shear mode instead of valve mode which involves fluid flow that makes the response time slower.
7. Good heat dissipation because heat generated due to friction between sponge material and outer cylinder can be directly dissipated into surrounding air due to simpler design without seals and enclosure of fluid.
8. Cost effective because of cheap friction material required which can also be easily replaced due to ease of disassembly and less amount of MR fluid which is very expensive. MR fluid dampers are definitely expensive due to high amount of MR fluid required.
9. Less number of components i.e. only piston, sponge material, few ml of Mr fluid and outer cylinder required in making MR damper compared to MR fluid damper which require complex design with micron level finishing and polishing of piston shaft for proper sealing. High cost of seals and bearings to seal and guide the moving piston. Precise manufacturing of fluid valve parts to generate required differential pressure drop.
10. No additional components required as in fluid damper like gas accumulator for piston volume compensation.
11. Maintenance of magnetic circuit is easy compared to fluid damper because no need to open and remove any seals like in fluid dampers. If any maintenance is required in fluid dampers seals have to be removed in internal coil configuration results in loss of seals.
12. No additional friction force required due to added seal as in MR fluid dampers. Therefore passive damping can be made as low as less than 5N.

Chapter 3

3 Magnetic Circuit Finite Element Modelling and Analysis

3.1 Overview

Magnetic circuit design is the most important part of MR damper. Magnetorheological fluids yield stress changes with applied magnetic flux density B. In order to generate magnetic flux efficiently with minimum input power is the point of concern in following study. In this chapter method for generating magnetic flux and associated magnetic circuit is discussed.

3.2 Magnetic Circuit Theory

The concept of magnetic field starts with Ampere's Law. Ampere's law states that; the curl of static magnetic field intensity H equals current density J

$$\nabla \times H = J \tag{3.1}$$

Where H is the magnetic field intensity in amperes per meter and J is the current density in amperes per square meter. Magnetic flux density B is related to magnetic field intensity H in air by

$$B = \mu_o H \tag{3.2}$$

B is expressed in tesla (T) and μ_o is the permeability of free space. The value of μ_o is $4\pi \times 10^{-7}$ henrys per meter H/m. Because H is the circle or curl around current carrying conductor, another way to express H is using integral of surface area S as follows

$$\int (\nabla \times H).dS = \int J.dS \tag{3.3}$$

Units on both sides of equation are amperes. The surface S is a vector with direction normal to surface and magnitude equal to surface area. This surface integral equation is replaced by closed path integral using stokes law as follows;

$$\oint H.dl = \int J.dS = NI, \tag{3.4}$$

Where, l is the vector path length in meters and circle on left integral shows closed path. The integral of current density J can be replaced by total current I multiplied with number of current carrying conductors N. In order to generate large H or B using least current can be done by increasing the number of current carrying conductors per unit area. Number of current carrying wires wrapped in closed path is called winding and this concept is used in magnetic devices. As B is the magnetic flux density, its units are weber per square meter, the total magnetic flux of area dS which is in square meters can be calculated by integrating B over dS as follows;

$$\emptyset = \int \mathrm{B.dS} \tag{3.5}$$

Where $\emptyset$ the magnetic flux and its units are is Weber. It is important to note that for any closed surface S the total flux generated is equal to zero. Therefore we can represent the above equation by closed surface integral equation as follows;

$$\emptyset\mathrm{c} = \oint \mathrm{B.dS} = 0 \tag{3.6}$$

3.3 Magnetic Materials

Magnetic materials are those materials which easily allow magnetic flux to flow through it. The property which allows magnetic flux to flow through material is called permeability. The permeability of free space or air μ_o is 12.57 x 10^{-7} henrys per meter H/m also many other materials like copper and aluminum has permeability equal to free space. Materials with permeability other than air are represented by relative permeability defined as

$$\mu_r = \frac{\mu}{\mu_o} \tag{3.7}$$

Magnetic materials with relative permeability greater than 500 are called magnetically soft materials like ‘soft iron’ which include pure iron Fe. Nickel and cobalt are also considered magnetically soft or poses ferromagnetic properties. Iron alloys containing nickel and cobalt are also ferromagnetic with relative permeability greater than 2000. Low carbon steels are most common ferromagnetic alloys with good strength and high permeability. Steel is most used material for core in magnetic devices. Magnetic flux density can be found by multiplying H by relative permeability of material. Permeability of air and many ferromagnetic materials is a scalar quantity.

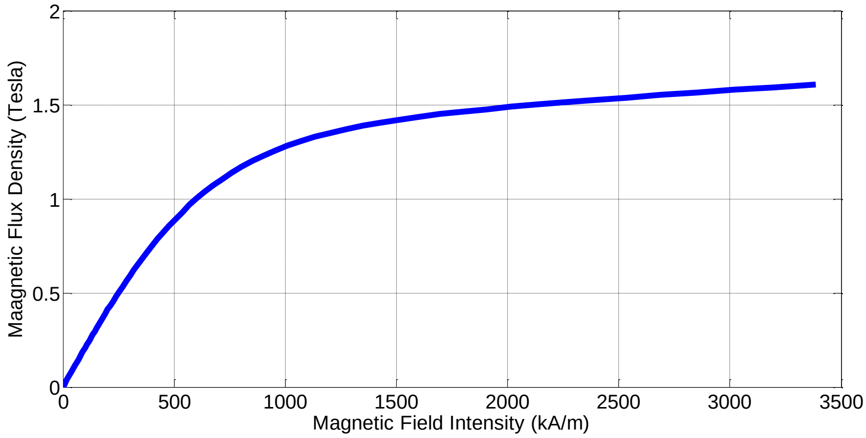

Figure 3-1: Typical BH curves of magnetic steels.

Another important property of ferromagnetic materials related to B, H and permeability is a nonlinear behavior known as BH curve. Such materials exhibit high permeability at low values of magnetic field intensity H, but as H increases B begins to saturate and permeability begins to decrease until it no longer remain constant [41]. A typical BH curve of steel is shown in Fig 3-1. Above 1.0 T the curve bends sharply that point is called a knee. After the knee the incremental permeability or the slope gradually decreases to the permeability of free space.

3.4 Magnetic Reluctance Method

Calculating magnetic path reluctance is the first step in designing of magnetic circuits. It starts with amperes law equation;

$$\oint H.dl = \int J.dS = NI \tag{3.8}$$

Where N is number of turns and I is current are selected as per requirement and H and B are calculated as;

$$\sum_{k} H_k l_k = NI \tag{3.9}$$

where' k' is a subscript that represents the line segments which make up the closed path.

Because H = B/ μ the equation (3.9) can be written as

$$\sum_{k}(B_k/\mu_k)l_k = NI \tag{3.10}$$

Magnetic flux B prefers to flow through high permeability region such as steel. If the steel has an air gap the flux try to travel through the shortest path of air gap. The total flux is the surface integral of flux density as mentioned in equation (3.5)

$$\emptyset = \int B.dS \tag{3.11}$$

Assuming that each line segment 'k' has cross section area S_k perpendicular to the direction of magnetic flux density, the total flux of each segment will be

$$\emptyset_k = B_k.S_k \tag{3.12}$$

Substituting Eq (3.12) into Eq (3.10) we get

$$\emptyset_k \sum_{k}[l_k/\mu_k.S_k] = NI \tag{3.13}$$

The term within brackets is called Reluctance represented by letter $\mathcal{R}$, Eq (3.13) becomes

$$\emptyset \sum_{k}[\mathcal{R}_k] = NI \tag{3.14}$$

Units of reluctance are ampere per weber. If reluctance of all paths is known total flux can be calculated as

$$\emptyset = NI / \sum_{k}\mathcal{R}_k \tag{3.15}$$

Thus reluctance method can be used to calculate flux densities of individual paths inside the closed flux paths. Simplifying Eq (3.15) gives following equation which is analogous to ohms law IR = V

$$\emptyset\mathcal{R} = NI \tag{3.16}$$

Thus the reluctance method is also called magnetic circuit method. In magnetic circuits reluctance is analogous to resistance and flux is analogous to current. The voltage is analogous to ampere-turns which is also called magneto motive force [41].

Table 1 describes the parameters to be used in this chapter and especially in magnetic circuit design with their symbols and units below

Table 3-1: Parameters used in magnetic circuit with symbol and units

Parameter	Symbol	Unit
Magnetic field intensity	H	A/m
Current density	J	A/m^2
Magnetic flux density	B	Tesla or Weber/m^2
Electrical Inductance	H	Henry
Magnetic Permeability	μ	Henry/m
Magnetic Vector Potential	A	Weber/m
Magnetic flux	Φ	weber

3.5 Magnetic circuit Finite Element Modelling & Analysis

There are two methods to design and analyze magnetic circuits, analytical method and finite element method. Analytical methods are time consuming as every parameter of design need to be calculated before putting it into the equations. Chances of error in writing the exact equations can be made and sometimes some crucial parameters or equation can be skipped that results in inaccurate results. Matlab is used for analytical methods. Finite element methods use FEM soft wares especially designed for such purposes for example ANSYS™ and FEM software. These soft wares have built in modules that incorporate all the necessary equations to model the magnetic circuits. Also computation is very fast and many analysis results can be obtained simultaneously. In magnetic circuit's design of MR damper, FEM software AC/DC module has been utilized to calculate magnetic flux.

3.5.1 2-D axis-symmetric design

In this study 2-D axis symmetric model of electromagnet has been built in FEM software. The magnetic circuit is symmetric along the axis of piston. Table 2 represents the parameters used for 2-D magnetic circuit design.

Table 3-2: Design parameters defined in FEM software for 2-D electromagnetic analysis

Name	Description	Unit
N	Number of turns of coil	-
wd	Wire diameter	mm
I	Current	A
$\boldsymbol{l_{coil}}$	Coil length	mm
$\boldsymbol{coil_w}$	Coil width	mm
$\boldsymbol{core_r}$	Core radius	mm
$\boldsymbol{foam_t}$	Foam thickness	mm
$\boldsymbol{cyl_t}$	Cylinder thickness	mm
$\boldsymbol{flange_r}$	Flange length	mm

Figure 3-2 shows the 2-D model of electromagnet with design parameters. Because there are no perfect boundaries without air, air gaps of 0.2 mm has been incorporated between cylinder and foam and between flange and foam in order to model the air present in the design.

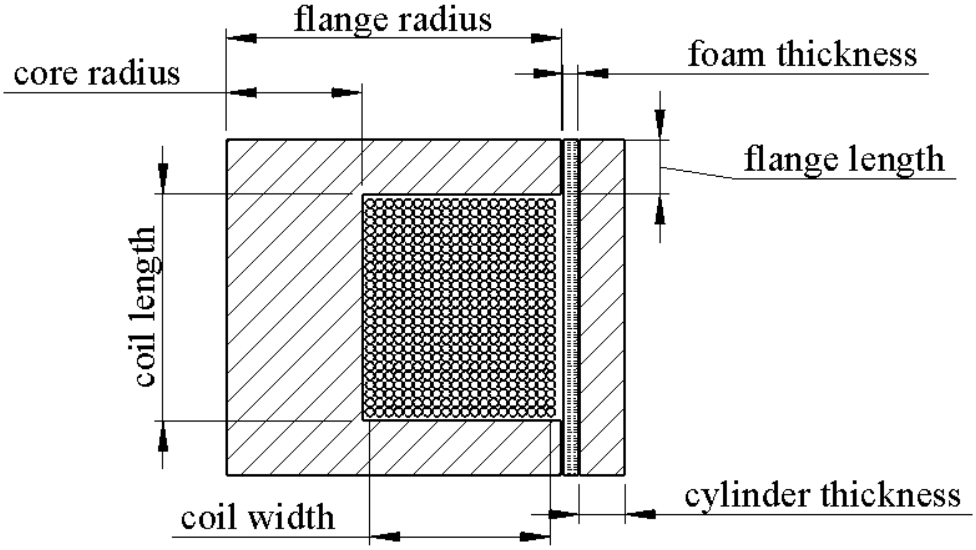

Figure 3-2: 2-D axis-symmetric model of magnetic circuit with design parameters.

After completing the geometry, each geometric block has been assigned a material for example the material of core and cylinder has been selected as steel. In materials library non-linear magnetic steel has been selected. The reason for selecting nonlinear steel is that these materials are provided with BH curve data which as mentioned before is the property of magnetic material that its magnetic flux saturates after certain applied magnetic field. Normal steels without BH curve produce incorrect results because FEM software uses different types of the constitutive relation to generate magnetic flux e.g. to model permanent magnets FEM software uses remnant flux density or magnetization (M). Similarly for steels without HB curve data FEM software calculates results based on relative permeability (μ_r) which basically represents a linear relationship between H and B. Therefore relative permeability selected as a constitutive relation will give incorrect results because if we keep on increasing H, magnetic flux density will continue to increase proportionally which is impractical because in all real world materials flux density saturates after certain point. Environment is also defined around geometry and the material assigned to environment is air. Next step is to select type of study, there are many options available depending upon the application. In magnetic flux analysis stationary analysis is chosen because the magnetic circuit design in MR damper uses dc current and the direction of current is unchanged hence the magnetic field created around coil will not change direction. The 2-D quarter model is designed and optimized on the basis of required flux which needs to be 200mT in air. For calculation of coil width an equation has been developed as follows;

$$coil_w = N.\frac{w_d^2}{l_{coil}} \tag{3.17}$$

Where N is number of turns, w_d is wire diameter and l_{coil} is the length of coil as mentioned in Fig 3-2. Equation 3.17 will give the width of coil which will define the piston diameter and overall diameter of damper. Radius of flange is calculated as follows;

$$flange_r = core_r + coil_w + 0.001 \tag{3.18}$$

Where $core_r$ and $coil_w$ is core radius and coil width respectively and 0.001 is the tolerance in meters added in coil width to provide clearance to protect coil from rubbing with foam and cylinder. Overall diameter of damper can be computed as follows;

$$damper_r = flange_r + foam_t + cyl_t + 0.0004 \tag{3.19}$$

Where $damper_r$ is the overall damper diameter and 0.0004 is the total sum of width of air gap between flange-foam and foam-cylinder respectively. These global parameters later optimized on the basis of geometry in order to obtain required 200mT flux with minimum current and space. The details of parameter optimization will be discussed later. From literature review it is recommended of using low carbon steel with carbon content less than 0.15 % is required for magnetic circuit design because low carbon steels have high permeability and saturation range. Recommended grades are AISI-12L14, AISI-1008, AISI-1010 and AISI-1018 [42]. Initially the magnetic circuit was modelled with following steel grades. Mechanical and magnetic Properties along with BH curves of steel grade are available in FEM software database. However due to unavailability of following grade, medium carbon steel was selected with carbon percentage between 0.30 to 0.50 %. Magnetic properties of these materials were tested by simple experiment in the Koc University Manufacturing and Automation Research Center. A cylinder of AISI 1030 was taken from market and a fix amount of turns were made onto the surface of cylinder then coil was energized by 0.5 A current and magnetic flux was measured on the corners by FH-55 Gauss/Teslameter. Parameters of prototype were added in to a model developed in FEM software and resultant flux was compared with physical prototype results. Magnetic flux matches with physical measurement within 5 % error.

Figure 3-3: Gauss/Teslameter used for magnetic flux density measurement.

Hence the material AISI-1030 has been verified and added into actual FEM software model for final design. AISI-1030 is chosen for core and outer cylinder as found from the market. Material was also tested in KUYTAM material testing laboratory and chemical composition has been verified. In FEM software magnetic fields (mf) parameters with ampere's law, all domains were selected except core and outer cylinder and their constitutive relation has been established according to relative permeability. If material selected has a BH curve data than the constitutive relation should be changed from relative permeability to HB curve to obtain accurate results otherwise FEM software will not cater for the saturation data and resultant magnetic field results will be incorrect. Low permeability domains include thread area and foam while high permeability domains are core and cylinder. Ampere law will not be used for coil domain because coil domain will be selected in multi turn coil settings. In next step mesh has been defined for the geometry. User defined mesh has been taken with maximum element size as 12.7mm and minimum element size as 0.057mm. Initially first prototype hardware of MR damper piston with magnet circuit was built and tested in off state and on state. By off state and on state means when current is switched off and on. Constant current i.e. 0.5A has been supplied to magnetic circuit through power supply. For computing the electromagnetic force acting on the MR fluid present in foam between flange and outer cylinder requires identification of force model. Because MR fluid consist of ferrous particles suspended in hydrocarbon oil, the particles experience a force perpendicular of the opposite poles i.e. core flange and outer cylinder. Magnetic force between flange and cylinder can be calculated by Maxwell tensile force [43]. This method of force calculation is very reliable in analytic simulations where models are based on reluctance method. This method works very well for homogeneously distributed magnetic flux density within the boundary of magnetic poles. Magnetic flux passing through a perpendicular area can be calculated using formula below

$$F = \frac{\emptyset^2}{2\mu_0 A} = \frac{B^2 A}{2\mu_0} \tag{3.20}$$

Where B the magnetic flux density of first prototype was measured using Teslameter while A the surface area of flange is computed as by using following equation

$$A = 2.\pi.R_f.l \tag{3.21}$$

Where R_f is the radius to flange and l is the length of flange. Maxwell tensile force is calculated using experimental data of magnetic flux density then the same force is verified using force dynamometer. The calculation of physical force is discussed in later chapter. The value of magnetic flux density is taken experimentally by energizing the first prototype magnetic circuit with 0.5A current and measuring the flux density at the surface of the flange using Teslameter. In next step total damping force has been measured experimentally in two steps, first damping force is measured in off-state which is the pure friction force then in second step damping force is measured in on-state which is greater than off-state force because it includes pure friction force plus magnetic force due to magnetic circuit. The difference between off-state and on-state is the Maxwell tensile force due to magnetic circuit. On-state and off-state forces are measured using dynamometer.

The Maxwell tensile force calculated by measured value of B has been compared with the tensile force obtained with difference of off-state and on-state force. Maxwell tensile force calcualted analytically using following

$$F_{MR} = F_{OFF} + F_M \tag{3.22}$$

$$F = \frac{B^2 A}{2\mu_0}$$

$$A = 2.\pi.R_f.l$$

Where F_{MR} = On-State damping force

F_{OFF} = Off-State damping force

F_M = Magnetic Force at Single Flange.

B= magnetic flux density

μo= magnetic permeability of air= 4π. 10^{-7}

A= Surface area of flange

r_f= Flange radius

l_f= length of Flange

Currently the value of B is 194.7 mT with foam soaked with MR fluid and working cylinder. The radius of the flange is 0.0124 m and length of the flange is 0.005 m respectively. The calculated F_M is 5.8336 N. This calculated value is closed to our measured F_M as shown in below table. The comparison validated the use of Maxwell tensile force model for MR damper magnetic circuit. The comparison of both forces is mentioned in table below;

Table 3-3: Comparison of Maxwell tensile force (calculated vs measured) at various frequencies.

Frequency(Hz)	Measured $\boldsymbol{F_{OFF}}$ (N)	Measured $\boldsymbol{F_{ON}}$ (N)	Measured $\boldsymbol{F_M = F_{ON} - F_{OFF}}$ (N)
23	5.5078	11.31	5.802
24	5.3760	11.103	5.727
25	5.26	11.33	6.07
30	5.2	11.11	5.91

3.6 Optimization of design parameters

From discussion of reluctance method above it is clear that besides the material property reluctance which is analog to electrical resistance highly depends upon geometric dimension. The main target of magnetic analysis was to obtain the required above 0.6T (200mT in air) average flux on the surface of flange (200mT in air) which is the area of interest to generate required magnetorheological effect and to produce 200N damping force. In order to produce the effect geometric parameters were optimized and final design parameters were obtained based on the results. Here the effect of each design parameter were discussed in detail. Zekeriya et al. did finite element analysis and discussed the effect of geometric parameters on magnetic flux density [44].

3.6.1 Effect of Flange length

An important design parameter for MR Damper magnetic circuit is flange length because it determines the surface area S_k which is mentioned in equation (3.15). Theoretically if surface area increases it reduces the flux density B similarly as flange length increases surface area S_k increases which reduces the flux density. Using finite element analysis magnetic flux density first increases from 2mm to 7mm flange length then starts to decrease and it can be seen in the Fig 3-5. An optimal flange length need to be selected which should not be large enough because it will decrease B so from Fig 3-5 6mm was selected as optimum length because above 6mm flux density begins to decrease and its keep on deceasing. As the flux density was required around 0.56T, flange length of 6mm has been selected.

Table 3-4: Comparison of Effect of flange length on magnetic flux and force.

Flange length (mm)	Average Magnetic Flux Values at Foam Opposite to Flange inside working cylinder (mT)	Magnetic Force (N)
5	540.94	173.8665
6	565.8	228.4055
7	576.79	276.9500
8	578.9	318.7161
9	572.35	351.1502
10	553.29	338.7761
15	439.56	344.7297

Results were also obtained by simulating the results in air by removing the cylinder. It is verified that if the flange length were reduced below 6 mm there is no considerable increase in magnetic flux density in air.

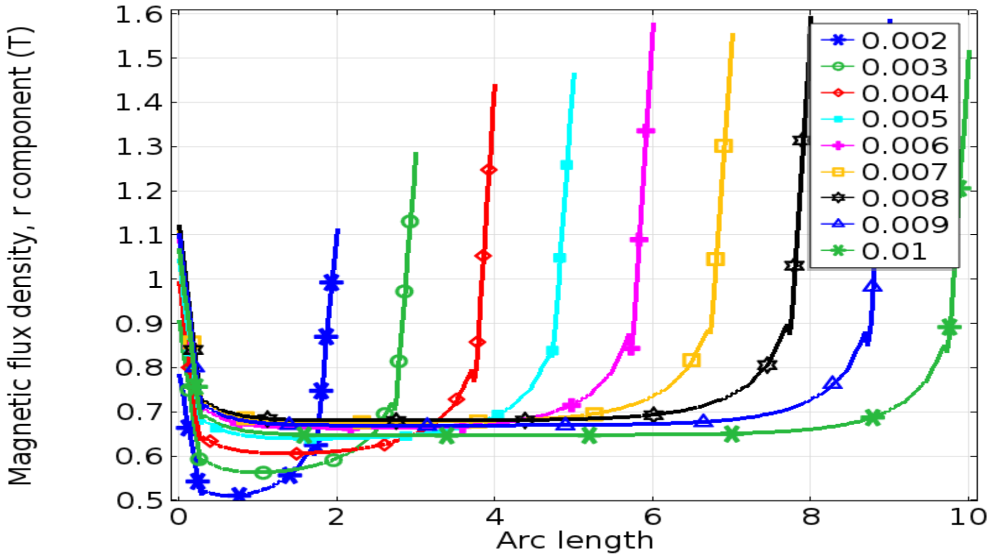

Figure 3-4: Magnetic flux density at different flange lengths

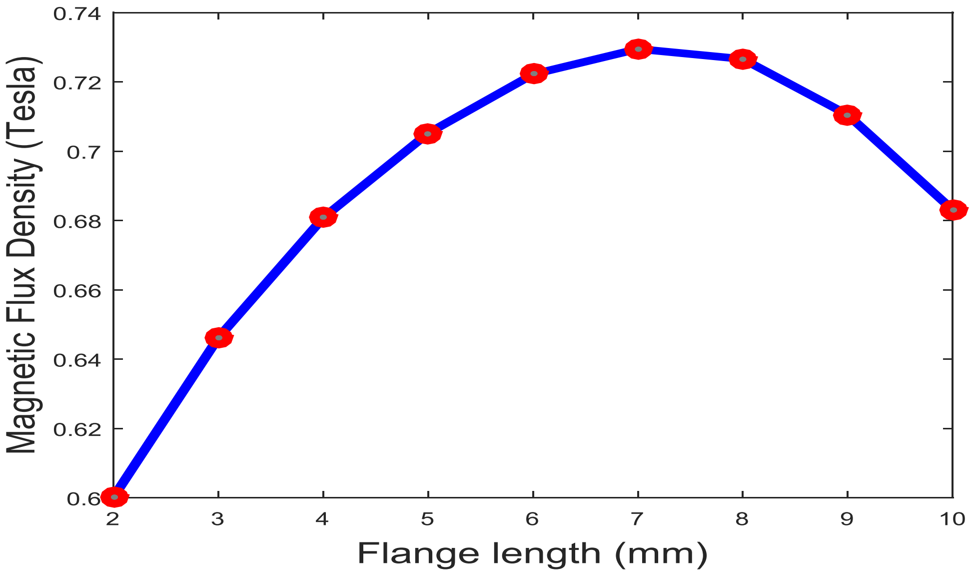

Figure 3-5: Behavior of magnetic flux density as a function of flange length

Another reason not to increase flange length more is it increases the mass of the piston. If mass of the piston increases it will decrease the natural frequency of MR damper.

3.6.2 Effect of Number of turns

In order to calculate number of turns, current has been fixed to be 0.5A and parametric sweep of number of turns selected from 1000 turns to 5500 turns. Magnetic flux density value should be 0.5 to 0.7 tesla was selected as target objective. In initial parametric sweep number of turns against 0.5 to 0.6 T comes around 3000 but the problem was wire diameter which was 0.33mm cannot withstand 0.5A for longer duration. Wire diameter greater than 0.33 cannot be used because of weight and size requirements. The American wire gauge standard 0.33mm diameter copper wire can withstand 0.3Amps continuous current [45]. Therefore parameter sweep carried out again with current set to 0.3A, number of turns computed between 2500 and 3500.

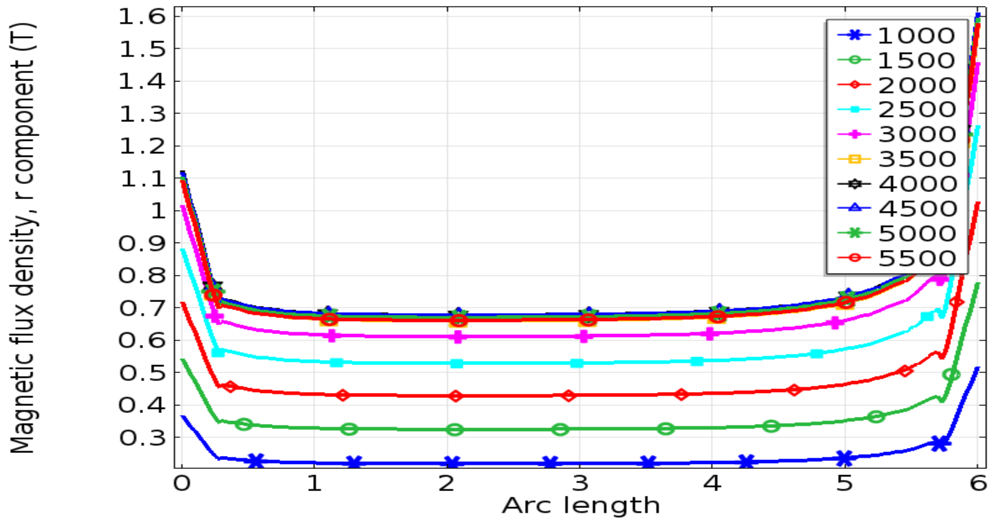

Figure 3-6: Magnetic flux density comparison against number of turns.

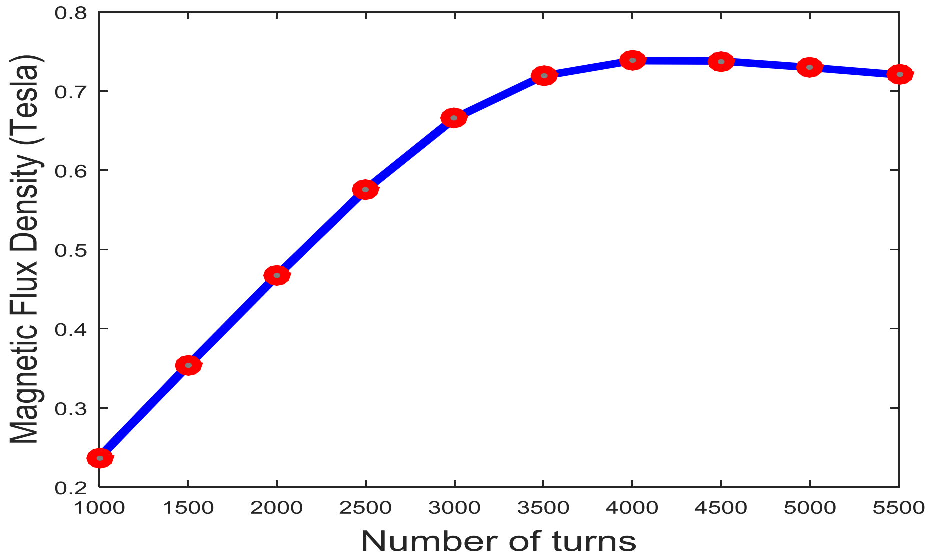

Figure 3-7: Behavior of magnetic field intensity as a function of number of turns

3.6.3 Effect of Coil length

Effect of coil length was investigated to optimize the length of damper piston. It is obvious from Fig 3-9 that flux density increases almost linearly with coil length. Due to the limitation of damper length and stroke, coil length needed to be minimized as much as possible to increase stroke length. Parametric sweep was performed for coil length from 10mm to 50mm with 5mm step. Optimized coil length was found between 25 to 30mm. another way to increase flux density using minimum overall flux length is using multiple coils in series with each other. This technique increases the number of active poles also increases the flux density.

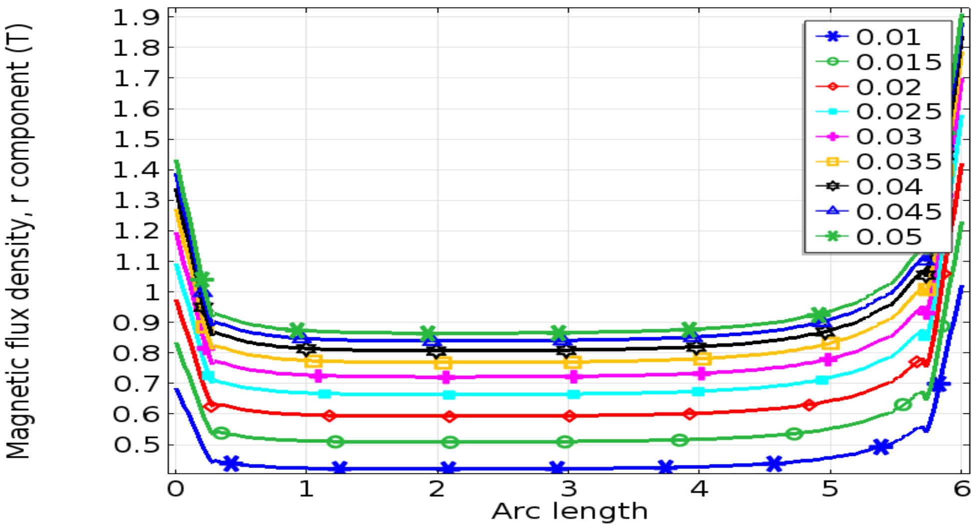

Figure 3-8: Magnetic flux density compared to coil length

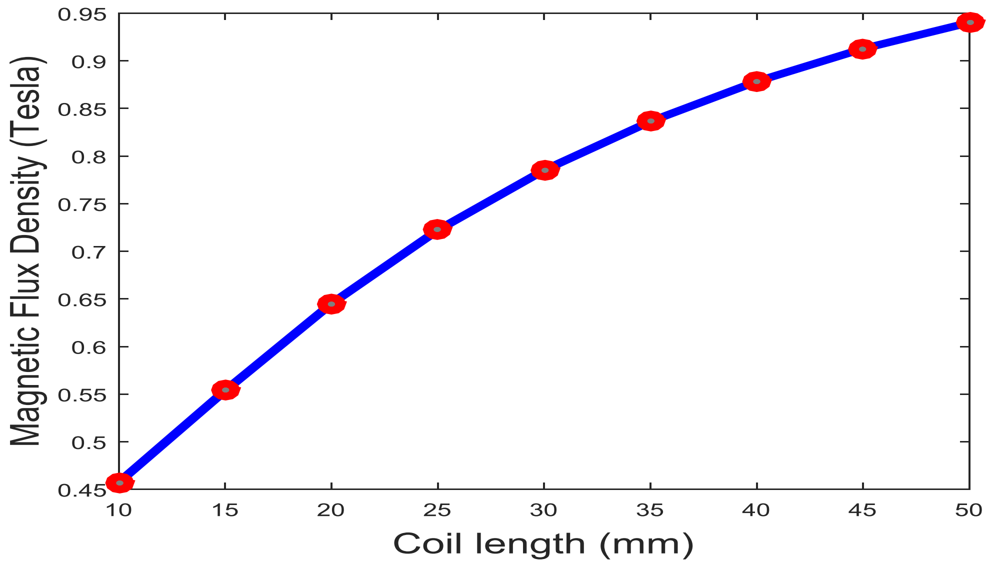

Figure 3-9: Behavior of magnetic flux density as a function of coil length

3.6.4 Effect of Core radius

Core radius is another important parameter. Parametric sweep has been performed on core radius from 2mm to 10mm and the optimized value has been computed between 5 to 10mm. Due to limitation of weight and size of MR damper 10mm has been taken as optimal value of core radius.

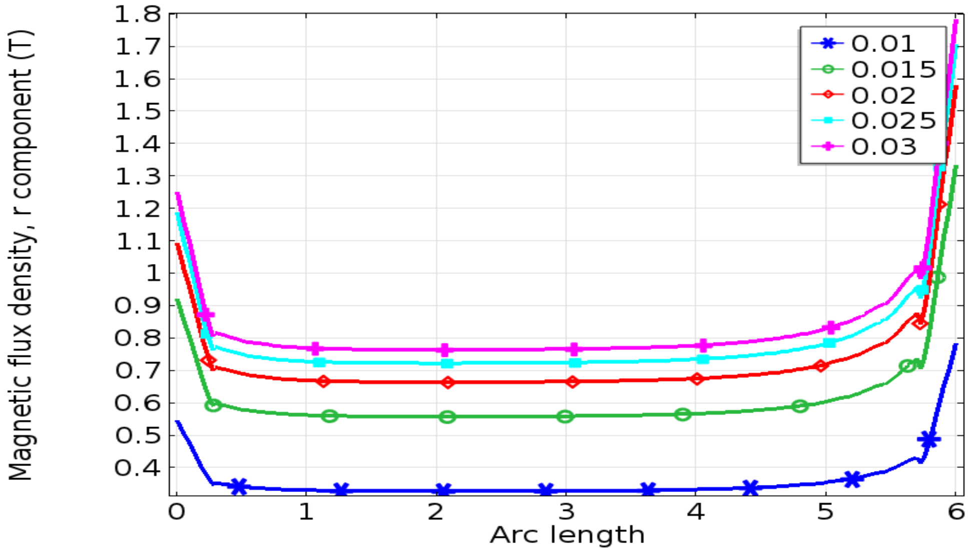

Figure 3-10: Magnetic flux density as a function of core radius.

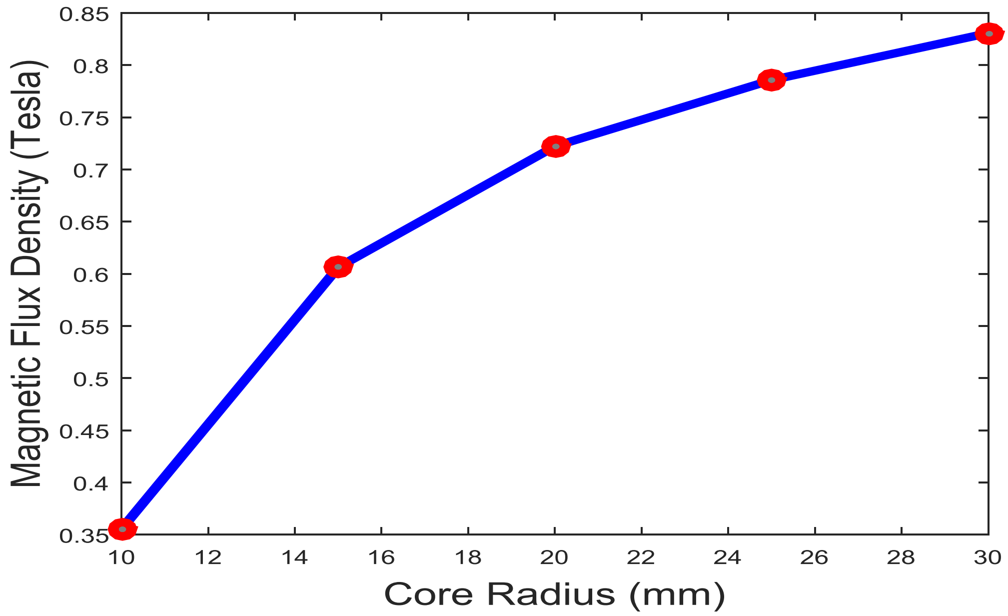

Figure 3-11: Behavior of magnetic flux density as a function of core radius

3.6.5 Effect of Cylinder Thickness

Effect of cylinder thickness was investigated with parametric sweep function and that increase in thickness increases magnetic flux density up to 4mm as shown in Fig 3-12 and 3-13. Above 4mm magnetic flux saturates hence there is no need to further increase the cylinder thickness.

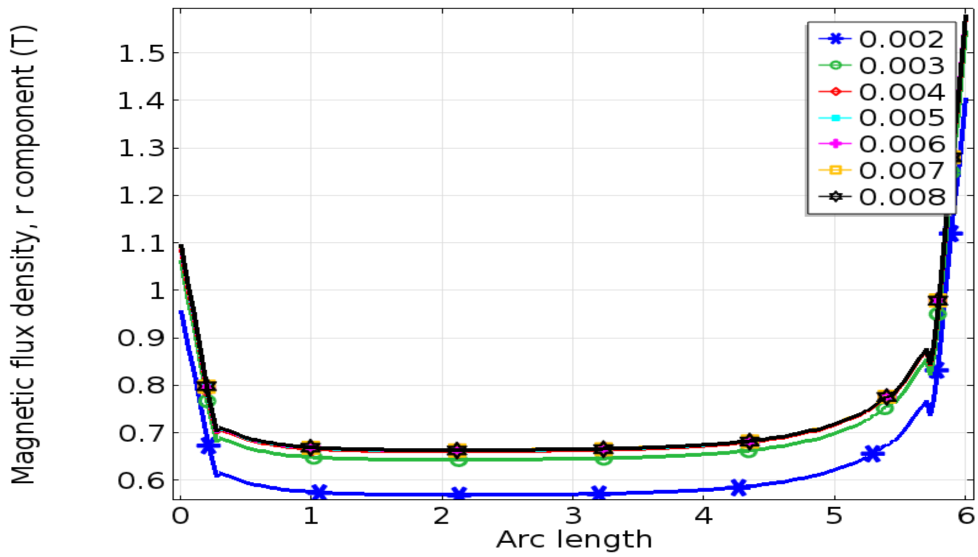

Figure 3-12: Magnetic flux density as a function of cylinder thickness.

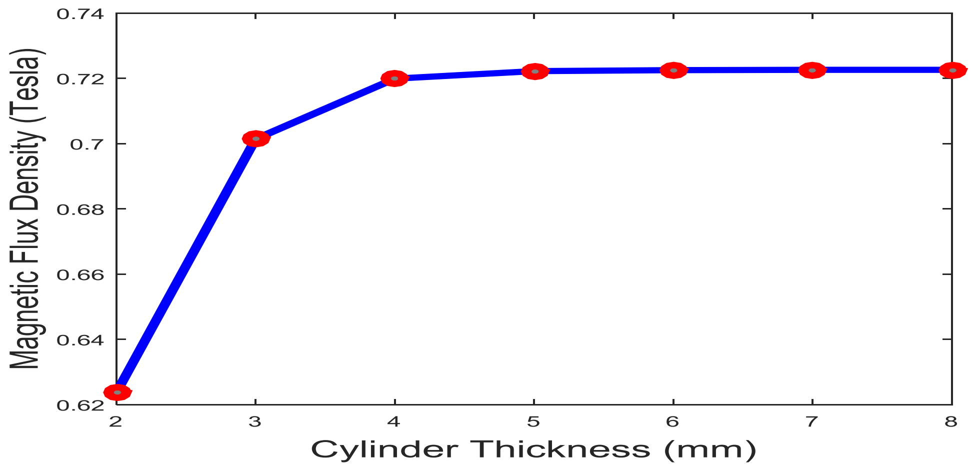

Figure 3-13: Behavior of magnetic flux density compared with cylinder thickness

3.6.6 Effect of Foam thickness

Magnetic flux density was calculated against foam thickness. Foam thickness in the circuit acts as a gap between flange and outer cylinder where flange acts as poles of electromagnet and outer cylinder acts as an object for flux return path. Parametric sweep on gap or foam thickness is applied from 0.5mm to 2mm. From Figure 3-14 it is obvious that the magnetic flux density reduces almost linearly with increasing gap thickness. Foam thickness is very important parameter from another aspect i.e. for the selection of suitable thickness absorbent material. From parametric analysis it confirmed that MR fluid absorbent material should chose to be of low thickness to improve magnetic flux density. Another important observation was permeability of absorbent material. If the permeability of material is good i.e. above 1 it will make a low reluctance flux path parallel to the outer cylinder. In that case the flux passing perpendicular to MR fluid will decrease and some flux will pass within the permeable absorbent material. This phenomenon was observed when nickel foam is used as absorbent material (which has permeability greater than 1) instead of polymeric material. Some of the flux passed within the foam and flux passing perpendicular to MR fluid weaken.

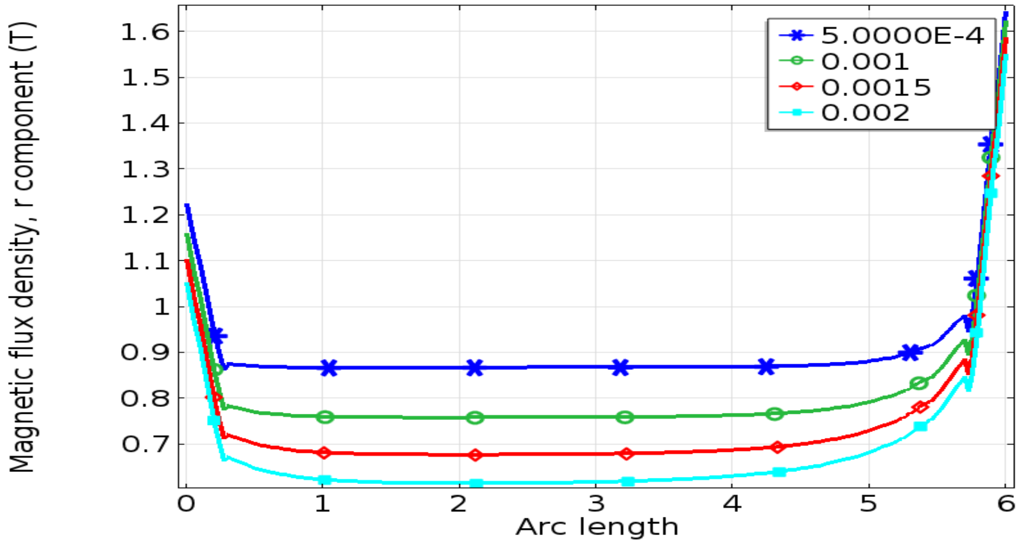

Figure 3-14: Magnetic flux density with different thickness of foam

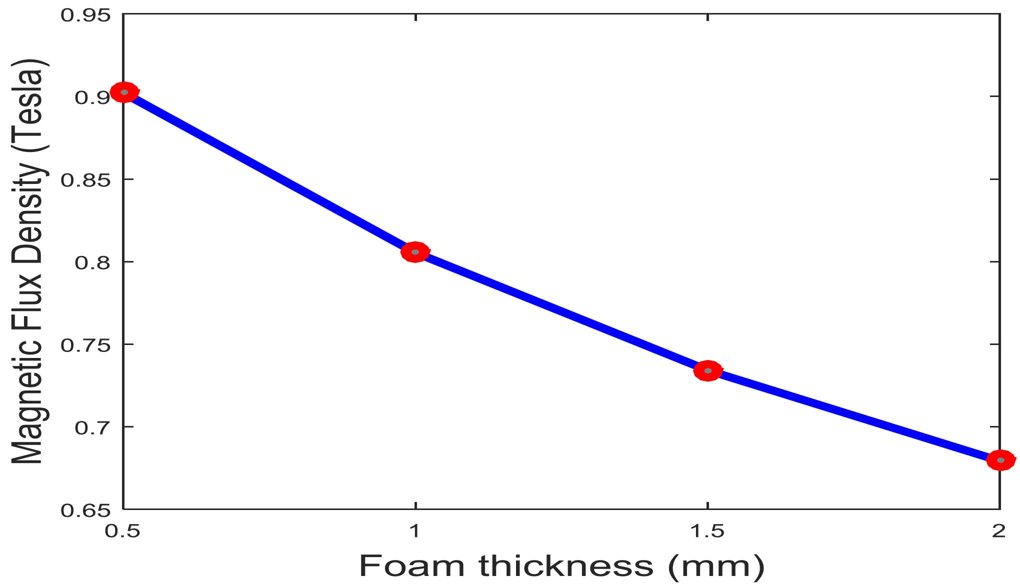

Figure 3-15: Behavior of magnetic flux density vs foam thickness

3.7 Optimized Design parameters

After complete optimization following design parameters were calculated. Number of turns is selected higher because changing the turns later in the study will not be possible. However current can be easily controllable later in the study. Coil length was selected on the basis of overall length of damper in extended and compressed positions and required length of stroke. The length of coil needed to be reduced as much as possible with maximum flux density to obtain maximum stroke length. Coil width is also selected by geometric optimization and cannot be reduced in current design because of its direct relationship with flux density. Similarly core radius has to be increased because of its direct relationship with flux density. Foam thickness was selected on the basis of available fabric and foam which are available in 1.6mm and 2.2 mm thickness in the market.

Table 3-5: Optimized design parameters of MR damper magnetic circuit.

Design Parameters of New MR Damper	Values
Number of Turns (N)	5400
Wire Diameter	0.33 mm
I (Amperes)	0.5 A
Coil Length	25 mm
Coil Width	26.7 mm
Core Radius	20 mm
Flange radius	47.7 mm
Thickness of Cylinder	5 mm
Flange length	6 mm
Surface Area of Flange	0.0015 m^2
Foam thickness	1.6 mm
Damper Diameter	109.4 mm

3.8 Electromagnetic force and flux density calculation

Based on parameters given in Table 5, magnetic flux density is calculated on the surface of single flange and on the surface of foam respectively. The Maxwell surface stress tensor is also evaluated which is used to calculate radial electromagnetic force acting on the surface of cylinder. The average value of flux density is taken and it comes out 0.68 Tesla.

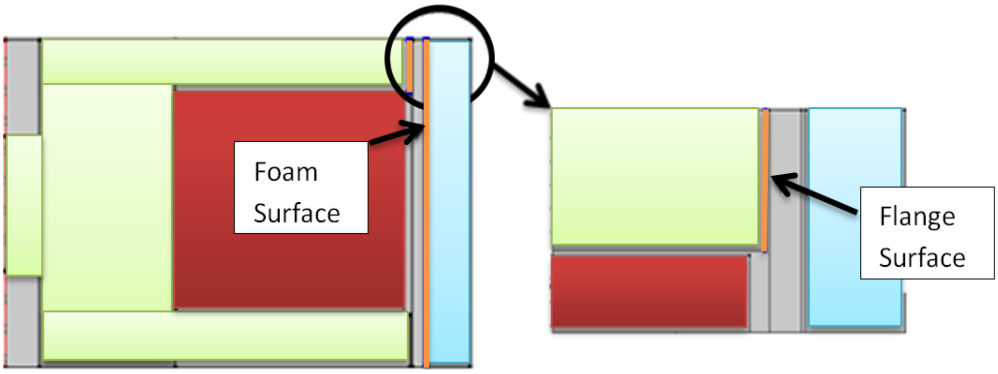

Figure 3-16: Surface for flux measurement, foam (Left) and flange (Right)

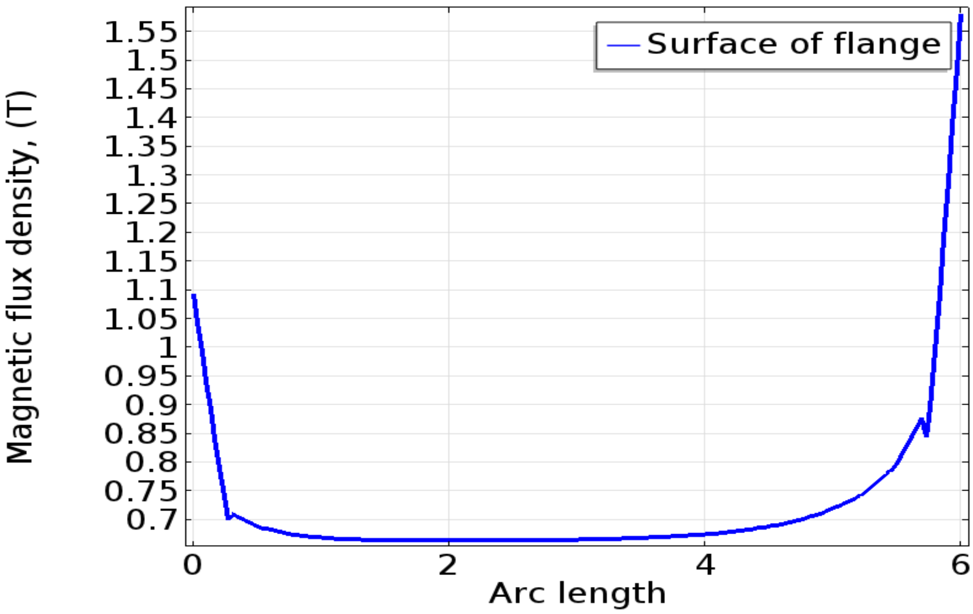

Figure 3-17: Magnetic flux density on the surface of flange.

Magnetic flux density measured at the surface of foam which is in contact with cylinder is measured as shown in Fig 3-18. It is obvious from figure that flux density decreases along the length of coil up to center of coil. From the center the direction of flux density becomes negative and starts to increase as it approaches the second pole. It is confirmed that net flux in the closed path is zero as proved by equation 3.6.

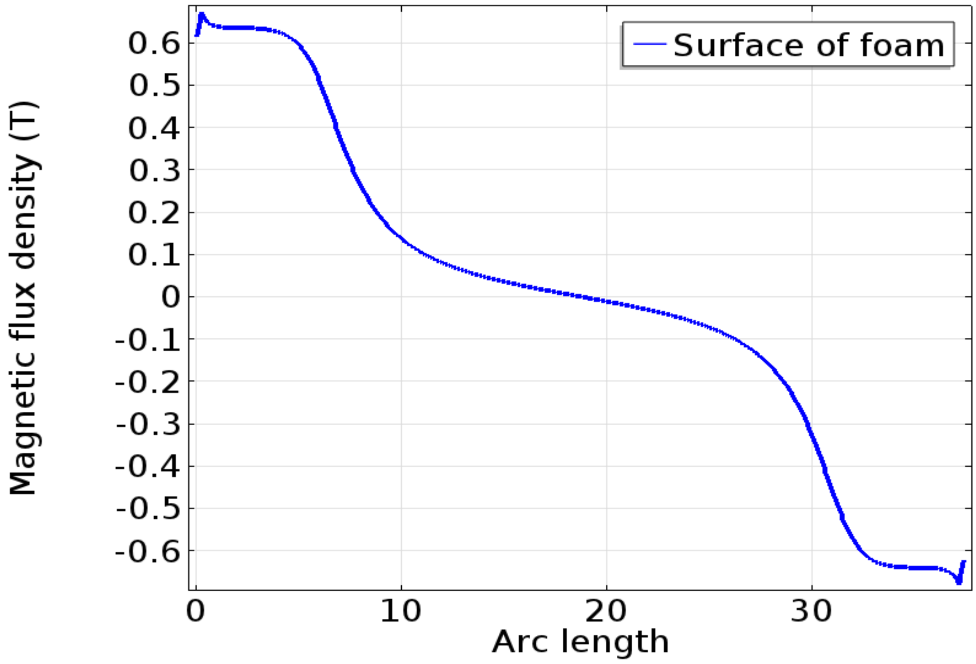

Figure 3-18: Magnetic flux density on the surface of foam.

Maxwell tensile surface stress tensor is also evaluated on the surface of foam as shown below.

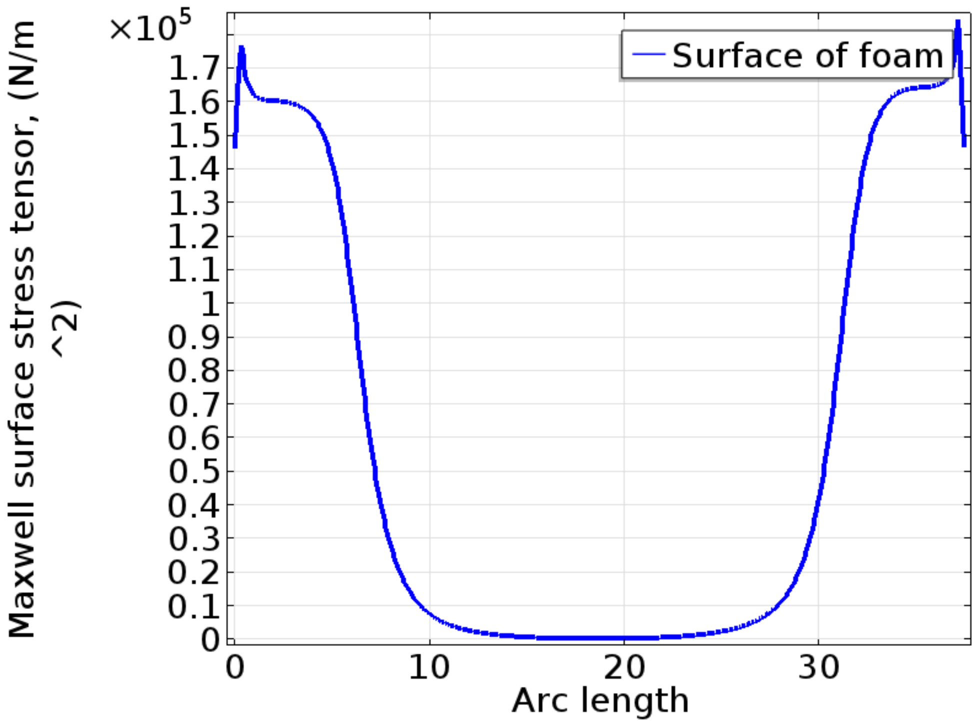

Figure 3-19: Maxwell surface stress tensor along the surface of foam.

The average values of magnetic flux density on flange and foam surface and Maxwell surface stress tensor on foam surface within active region are listed in table below. Active region is described below;

Table 3-6: Average values of magnetic flux density and Maxwell surface stress tensor in active region of MR damper magnetic circuit.

Description	Value
Average flux density on surface of flange in active region	0.780 Tesla
Average flux density on surface of foam within active region	0.682 Tesla
Average Maxwell surface stress tensor surface of foam within active region (τ_m)	165785.42 N/m^2

Magnetic flux density at the foam surface is used in equation 3.20 to calculate electromagnetic force acting in radial direction on the cylinder. Maxwell surface stress tensor value will also be used in equation below to calculate electromagnetic force acting in radial direction on the cylinder.

$$F_{maxwell} = \tau_m * A_f \tag{3.23}$$

Where $\boldsymbol{\tau_m}$ is the average value of Maxwell stress tensor evaluated in active region and A_f is the surface area of flange. Equation 3.21 is used to compute surface area. Electromagnetic forces are computed by two methods (Eq 3.20 and Eq 3.23) in Matlab and the comparison is given in table below;

Table 3-7: Comparison of electromagnetic force using magnetic flux density and Maxwell surface stress tensor.

Description	Value (N)
Electromagnetic force using magnetic flux density	242.3
Electromagnetic force using Maxwell tensile stress tensor	242.7

Chapter 4

4 Magnetic circuit design with MR fluid

4.1 Overview

A magnetorheological fluid is a smart fluid which when subjected to a magnetic field greatly increases its shear strength to a level that it becomes viscoelastic solid. Therefore the induced yield stress of the fluid can be controlled precisely by varying the magnetic field intensity (H). The ability to change the yield stress can be used to generate damping force of vibration damper. A typical vibration hydraulic damper uses oil to dissipate excessive energy generated in the machines.

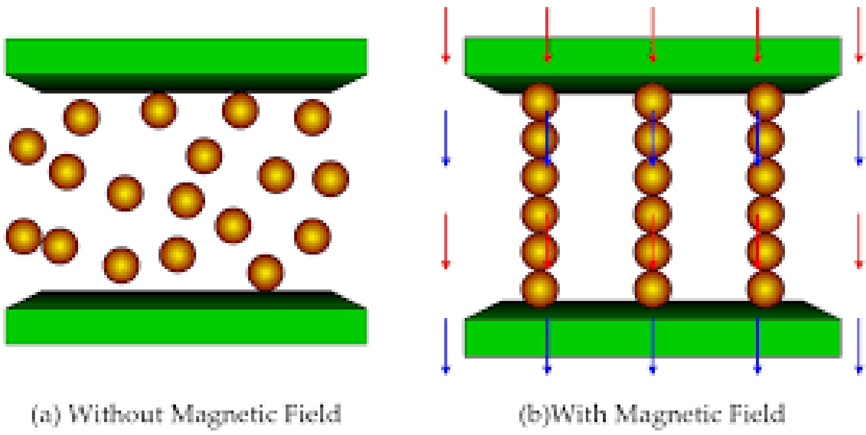

Figure 4-1: Magnetorheological fluid effect with and without magnetic field. Iron Particles suspended in fluid form a chain like structure when subject to magnetic field [2].

The yield stress represents the peak value of the stress strain curve, since the semisolid gel like structure will break and becomes liquid again when the stress would have reached yield point. MR suspensions have first received less attention than electrorheological suspensions mainly because the weight and the space required with coils to produce the magnetic field were thought to be a severe restriction for practical applications [46]. Furthermore, the response time of the fluid is limited with rising time t ¼ L=R (with L being the inductance and R the resistance of the coils) of the magnetic field which in practice is about 10_{-1}–10_{-2} s. Nevertheless, just comparing the magneto static energy density m_0H_2 for H ¼ 3000 Oe and the electrostatic energy density e_0E_2 for a field E ¼ 3 kV/ mm (close to the breakdown field); it appears that the former is larger by an order of magnitude. This is the main reason why yield stresses obtained with MR fluids are usually much larger than those obtained with ER fluids.

Yield stresses close to 100 kPa are obtained with magnetic suspensions made of carbonyl iron [4] whereas it is difficult to attain 10 kPa with an ER fluid.

4.2 Challenges in MR technology

The challenges in the area of MR fluid are still persist. For example systematic studies in terms of material science are still not being done. Durability of MR fluid in applications is still a major challenge and there is very less study being done on the factors affecting the durability. Effect of temperature is also a big concern on the performance of MR fluid. There are some non-technical issues as well such as very few manufacturers are producing MR fluid with fine iron powder. Available powders are quite expensive and are also in large grain size [47].

4.3 Magnetic Circuit design with MR fluid

The objective of this study is to design a low reluctance path to guide and focus magnetic flux density in the region of MR fluid. It is important to maximize the magnetic energy in the fluid gap while minimizing the energy loss in steel core and regions of non-working MR fluid and other areas. It is also maintained to keep the cross section of steel sufficient to keep magnetic field intensity H very low while minimizing total amount of steel in magnetic circuit. Typical design process has been explained step by step as follows;

Step 1: Select Operating Point (H_f, B_f) in the MR fluid to give yield stress (τ).From data sheet of selected MR fluid (MRF-140CG), magnetic field strength H_f is chosen from yield strength vs. magnetic field strength graph as shown in Figure 4-2. From graph it is noticeable that relationship between shear stress (τ) and magnetic field strength (H_f) is almost linear up to 40kPa which is around 80kAmp/m roughly. Therefore 80kAmp/m is chosen as operating point because of almost linear relationship also it is easy to control shear stress by changing magnetic field strength.

Step 2: After selecting Hf from Fig 4-2, Bf is selected from another graph in MRF-140CG datasheet known as typical magnetic field properties as shown in Figure 4-3. Once (H_f, B_f) selected, total magnetic flux is calculated as;

$$\emptyset_f = B_f . A'_f \tag{4.1}$$

With A'_f is the effective pole area due to fringing. A'_f is calculated as;

$$A_f' = 2\pi\left(r + \frac{g}{2}\right).(L_f + g) \quad (4.2)$$

With r is the minimum radius of coil, L is the length of steel path and in case of toroidal coil it is equal to the circumference of circle and 'g' is the magnetic field gap.

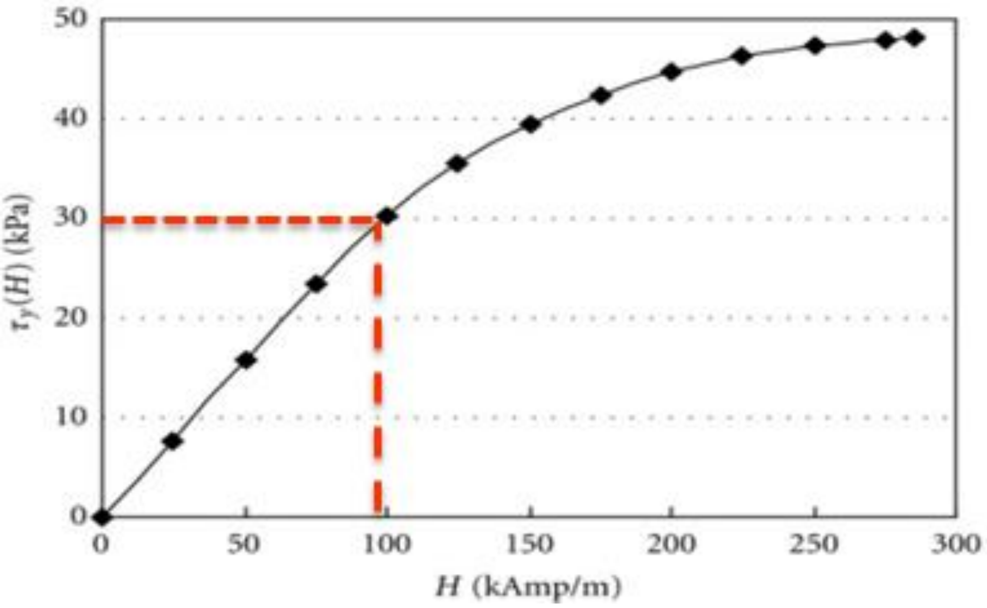

Figure 4-2: Selection of operating point from BH curve provided in MR fluid datasheet (MRF-140CG) [48]

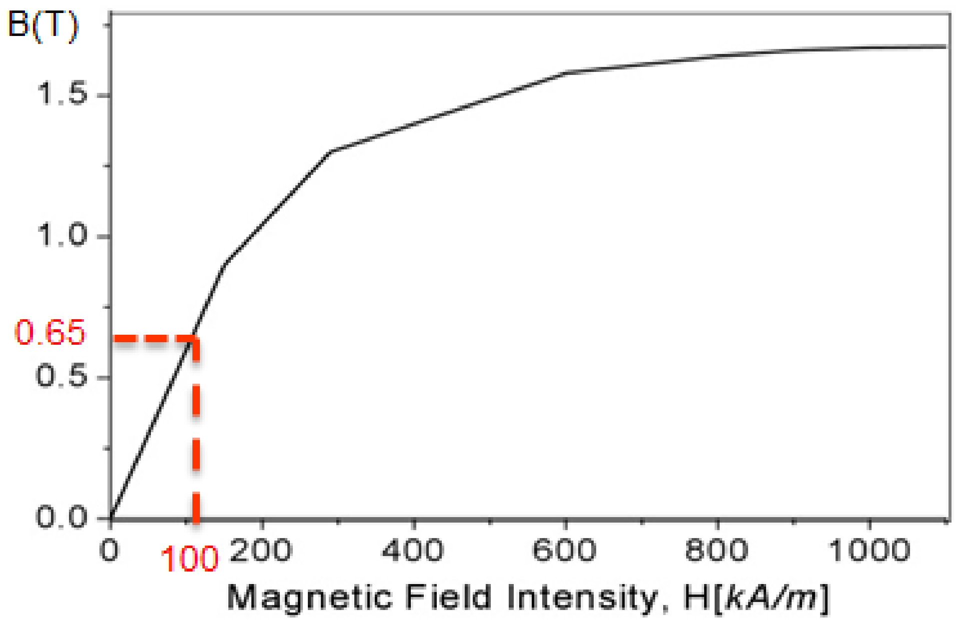

Figure 4-3: Relationship of magnetic flux density (B) vs magnetic field intensity (H) of MRF-140CG fluid [48].

The values of gap, length of coil and radius of coil are mentioned in table below;

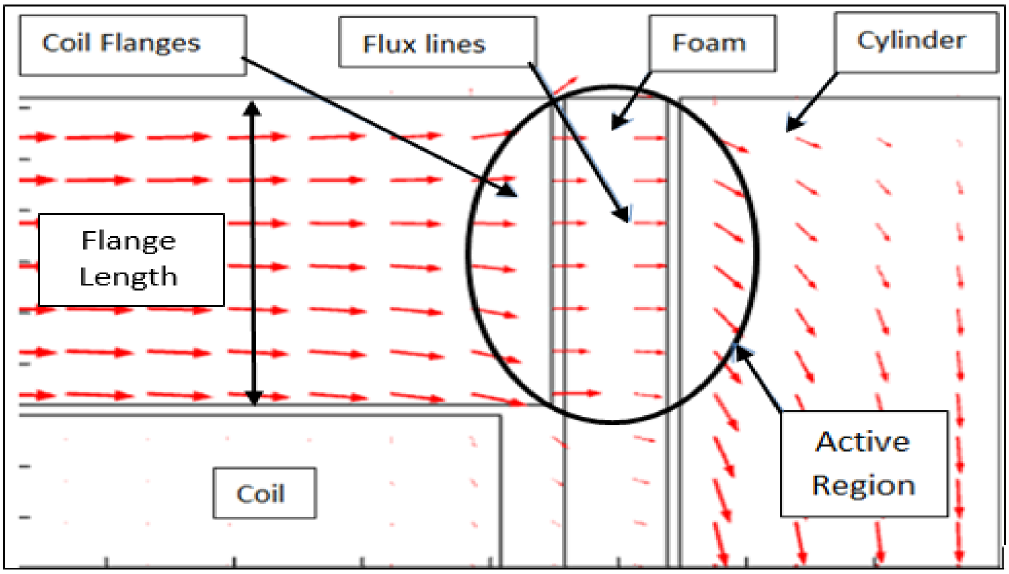

Figure 4-4: Active Region of Electro-magnet.

Step 3: Use Principal of continuity of magnetic flux to determine flux density B_s (steel) throughout flux conduit;

$$\emptyset_{fluid} = \emptyset_{steel} \tag{4.3}$$

Step 4: Determine Operating Point in steel as follows;

$$\frac{B_s = \emptyset_{steel}}{A_s} = B_f . A_f' / A_s \tag{4.4}$$

Where ‘As’ is cross section of selected steel core is calculated using Eq (3.21). Once ‘Bs’ is calculated as, determine Hs from **BH curve of selected steel**. We chose AISI 1030 magnetic steel with non-linear BH curve as shown below;

Step 5: Use Kirchhoff’s law of magnetic circuits to determine the necessary ampere-turns(NI)as follows [42] [48] [47];

$$NI = H_f . g + H_s . L_f \tag{4.5}$$

Above equation is used to optimize and generate required magnetic flux for MRF magnetic circuit.

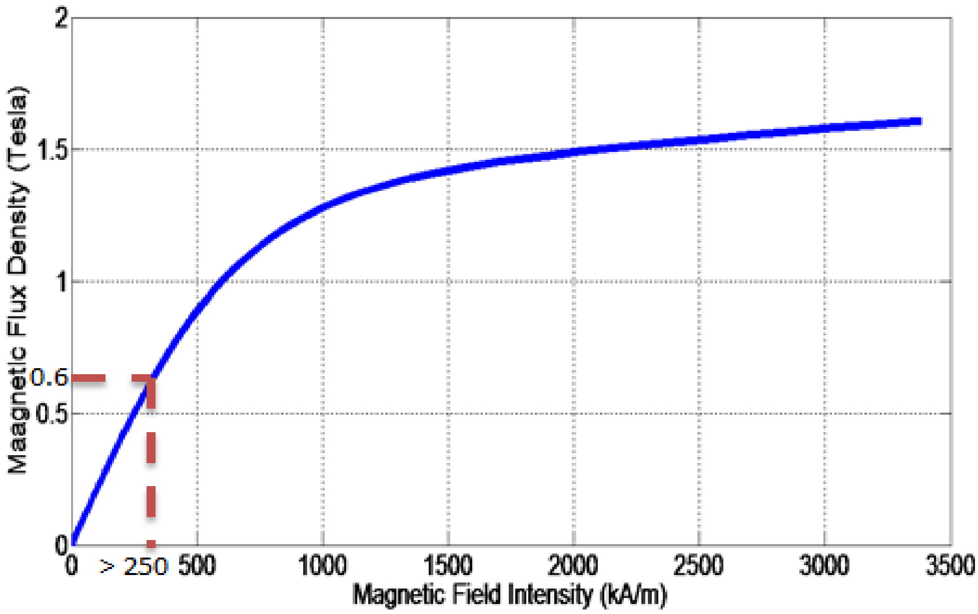

Figure 4-5: BH curve of 1030 steel.

Table 4-1: Parameters of effective pole area

Description	Value	Units
Yield stress of Mr fluid ($\boldsymbol{\tau_y}$)	40	kPa
Magnetic Field intensity of MR fluid (H)	80	kA/m
Magnetic Flux density of MR fluid	0.5	Tesla
Gap (g)	1.6	mm
Radius of flange(r_f)	47.7	mm
Length of steel path (L)	6	mm
Effective pole area ($\boldsymbol{A'_f}$)	2314.80	mm^2
Area of steel path ($\boldsymbol{A_s}$)	1797.3	mm^2
Magnetic flux density of Steel ($\boldsymbol{B_s}$)	0.64	Tesla

Chapter 5

5 Mechanical design, modal testing of MR damper with experimental test setup.

5.1 Overview

In this chapter computer aided design of proposed MR damper is discussed. Also the damper characteristics such as natural frequency, damping ratio and stiffness have been found using modal testing method is discussed. Finally the experimental test setup for testing the characteristics of MR damper is discussed.

5.2 CAD Design

The mechanical design of MR damper mainly consists of the bobbin (electromagnet), damper cylinder, cylinder cover and bottom clamp. The electromagnet (bobbin) is built on the final design parameters obtained by magnetic circuit design. The material of bobbin is medium carbon steel AISI 1030.The bobbin is covered with absorbent material such as fabric to absorb and retain MR fluid. The bobbin will move inside a damper cylinder which is a static member and clamped to a stationary structure using cover and clamp. The material of bobbin is medium carbon steel AISI 1050. The stroke of damper is set at ± 15 mm. The clamp, cover of the cylinder and shaft of the piston is manufactured using aluminum. The selection of aluminum is to avoid any leakage of magnetic flux and reducing overall weight.

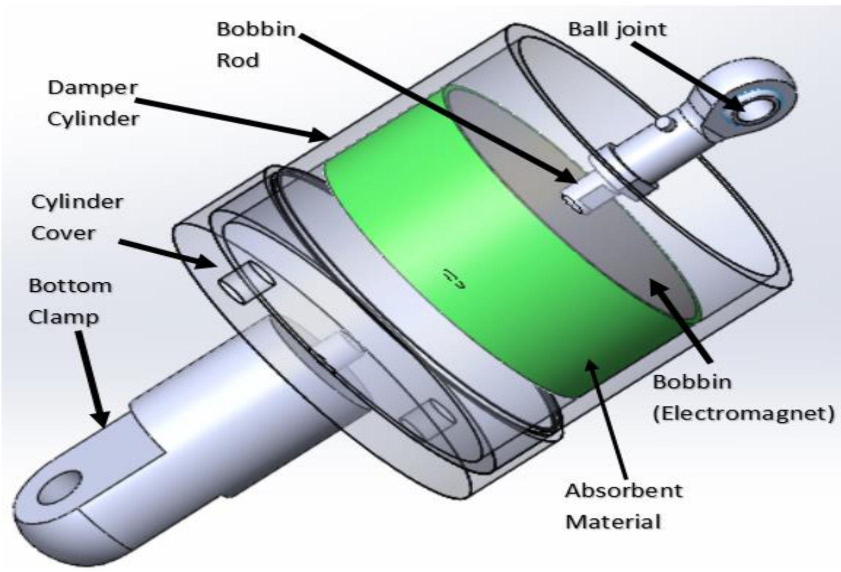

Figure 5-1: CAD model of MR damper

Two holes are made in the cylinder cover to allow passage of air in and out of the damper. These holes take away the heat built up due to friction of the piston and cylinder in other words; these holes are used to maintain the temperature of the damper. The relative movement of bobbins and the cylinder is controlled or resisted by adding a friction element between them, which in our case is foam made of polyurethane material. Polyurethane is a good liquid absorbent material, hence used for holding the MR fluid in active regions. As discussed in previous chapter active regions are those where magnetic flux lines pass perpendicular to flange surface area. Electromagnet connected to one end of piston consists of magnetic core called bobbin on which magnetic wire is wound called a coil. Two ends of the coil are taken out from a cutout slot of bobbin and connected to connector terminals to supply DC current.

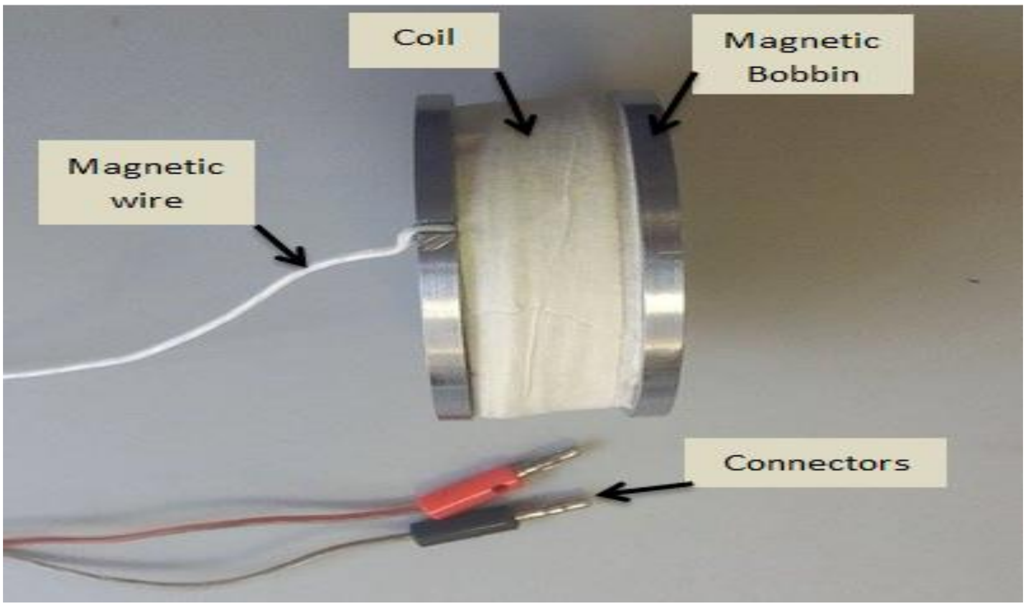

Figure 5-2: Electromagnet consisting of Magnetic bobbin, coil and magnetic wire with connectors at the end of DC current supply.

The electromagnet is wrapped with polyurethane or metal foam and soaked with MR fluid. Metal or polyurethane foam holds the fluid in contact with active region when the piston vibrates hence maintaining the flux lines always perpendicular to MR fluid. Magnetic flux generated in electromagnet passes through MR fluid in foam and enters the outer cylinder which acts as back iron to complete the flux return path. Due to this reason outer cylinder is also made of magnetic steel.

5.3 Modal Testing of MR damper

MR Damper structural dynamics such as natural frequency, stiffness and damping ration can be obtained experimentally using frequency response function (FRF). Frequency response function can be measured using modal testing techniques [50]. The structure is excited by external force; in our case force is applied by impact hammer on the head of ball joint of the piston. Impact hammer has a force sensor at the tip. The response of the piston (bobbin) is measured with vibration sensors; in our case vibration of bobbin is measured through a laser sensor as shown in Fig 5-3;

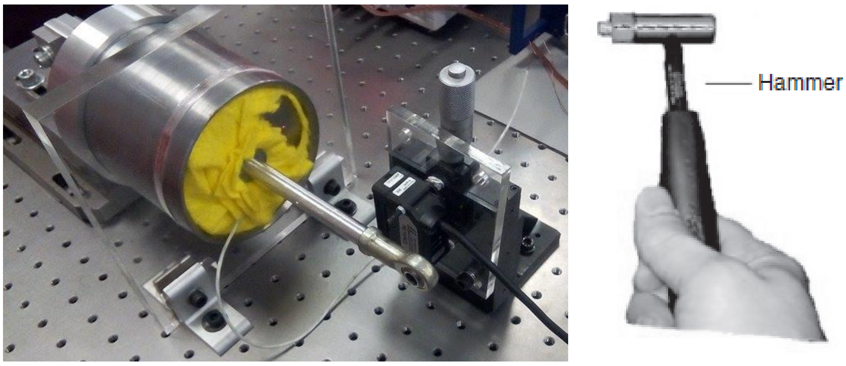

Figure 5-3: Impact hammer testing.

Make sure that the direction of applied force should be in the same direction of measured displacement. Measurements of force and displacement are recorded via data acquisition device and data is analysis is performed in CUTPRO™ software provided by MAL Inc. The flow chart of measurement and signal processing algorithm used to evaluate the FRF of damper are shown below;

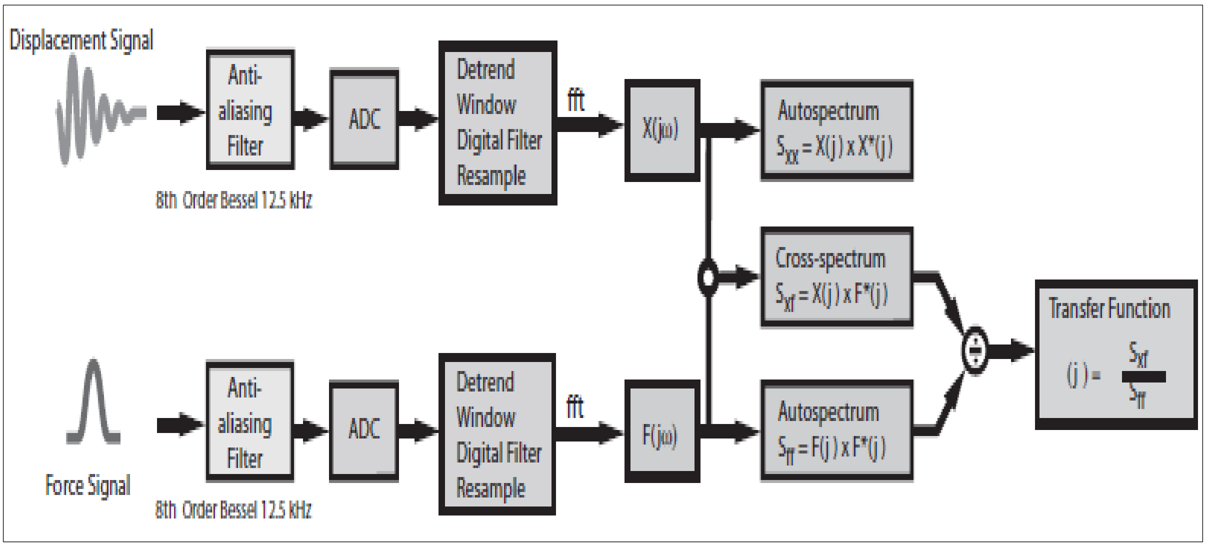

Figure 5-4: Flow chart of measurement and signal processing algorithm for FRF measurement with impact testing [50].

After signal processing in CUTPRO, the following data has been obtained. The two peaks in Fig 5-5 are the first and second mode of MR damper respectively. The first peak or first mode comes at 30.77 Hz and the second peak or mode comes at 40.5 Hz. First peak shows the first resonance hence this frequency could be the first natural frequency of RM damper.

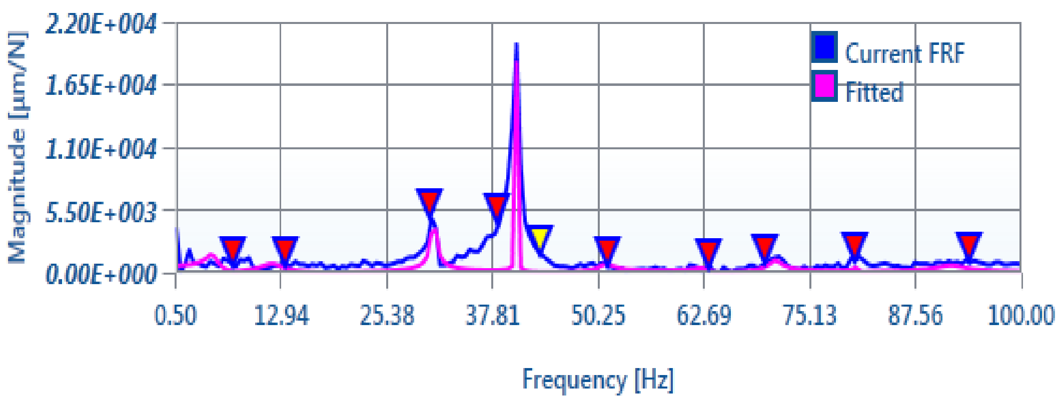

Figure 5-5: Actual and fitted magnitude plot of MR damper frequency response. This plot is actually the ratio of displacement response over force input.

The real and imaginary plots of frequency response function are given below; as clear in figure 5-6, the real magnitude first cross over frequency is 30.77Hz and second cross over is 40.5 Hz.

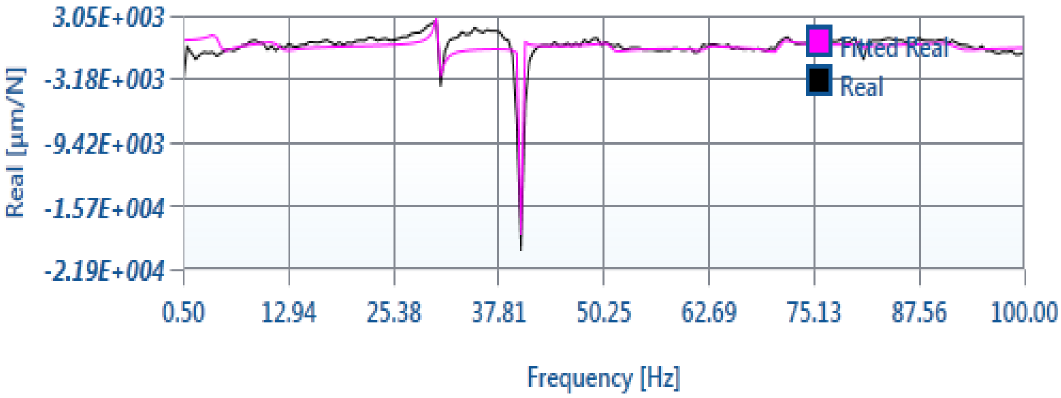

Figure 5-6: Real part of frequency response of MR damper

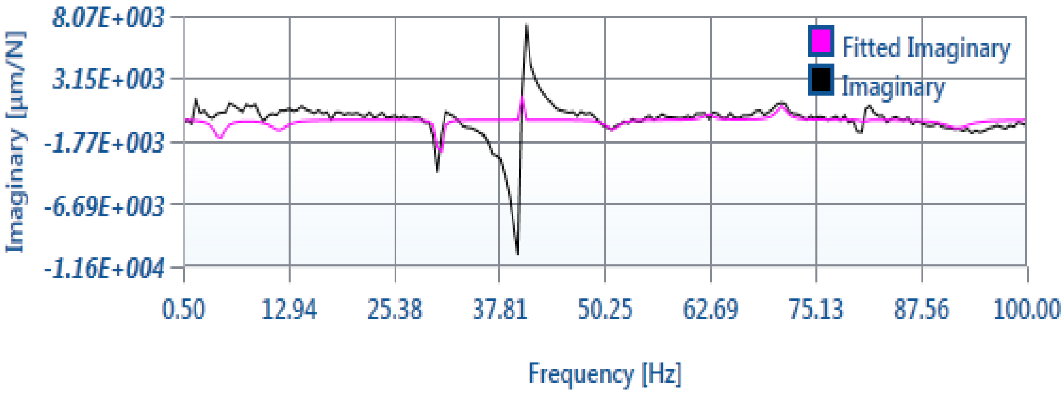

Figure 5-7: Imaginary part of frequency response of MR damper

From CUTPRO, modes, natural frequency, stiffness, mass and damping ratio can also be calculated as shown in the table 5-1 below;

Modal Stiffnesses in table 5-1 are the structural stiffness values of MR damper in on-state. In on-state the damper applies more than 200 N force which makes the structure too stiff so that impact hammer can only measure the structural displacement rather than the displacement of the piston.. Moreover the damping ration at 40.5Hz reduces to 0.01 due to resonance. At this resonance frequency the damping ration of structure is at a minimum.

Table 5-1: Optimized modes, natural frequencies, damping ratios and modal stiffness's of MR damper

Mode No.	Frequency (Hz)	Damping Ratio (%)	Modal Stiffness (N/m)
1	4.84	13.71	2.3976E03
2	11.84	9.22	6.7171E03
3	30.77	0.66	1.3077E04
4	40.50	0.01	7.6561E04
5	51.11	1.60	3.8769E04
6	62.42	1.16	1.0232E05

5.4 Experimental test setup

The experimental test setup is established for MR damper as given in Fig.5-8, which includes linear actuator with its controller, laser displacement sensor, dynamometer (force Sensor) with its charge amplifier, DAQ card and a combined power supply for linear actuator and laser displacement sensor. A linear actuator is coupled with MR damper for different ranges of input velocities. The coil inside the MR damper is energized by another power supply, which results into a magnetic force depends upon the value of input current. The laser displacement sensor measures the displacement of MR damper during its actuation from linear motor. The total damping force of MR damper is measured with dynamometer. The analog data from all these sensors are given to the DAQ card where it is used for further analysis as explained in the following sections

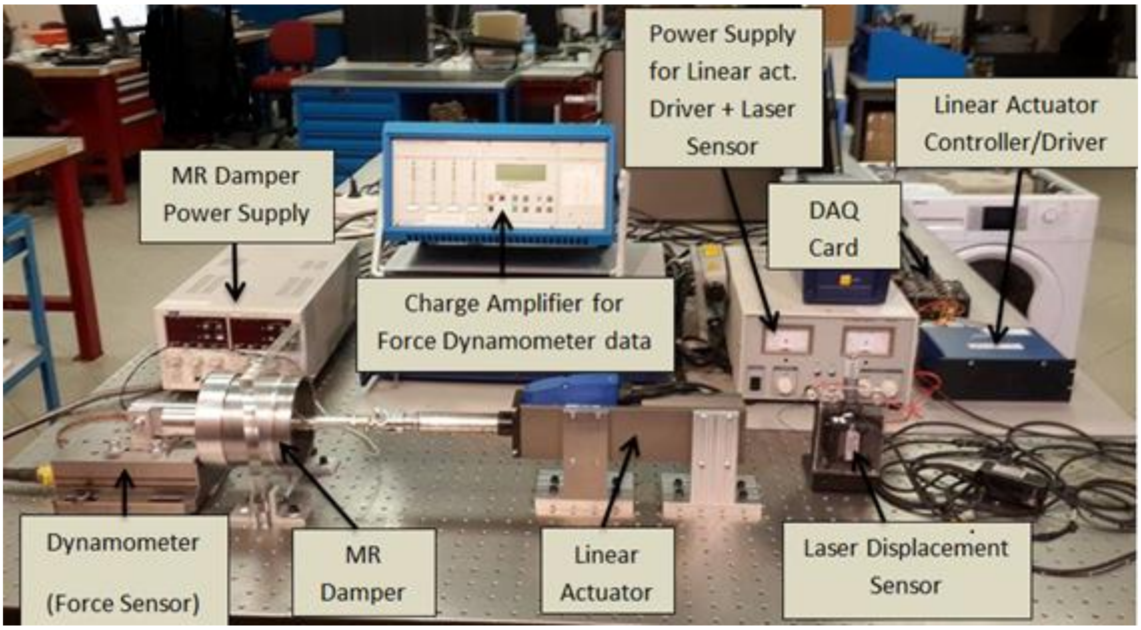

Figure 5-8: Experimental testing setup for MR damper.

5.4.1 Dynamometer (Force Sensor)

Dynamometer or force sensor is used in the test setup to measure the damping force generated by MR damper. It is a table top 3 axis piezoelectric sensor for measuring the three orthogonal components of force. It consists of four three-component force sensors fitted under high preload between a base plate and a top plate. Each sensor contains 3 pairs of quartz plates, one sensitive to pressure in the z direction and the other two responding to shear in the x and y directions respectively. The force components are measured practically without displacement [51].

Table 5-2: Specifications of Dynamometer [51]

Description	Units	Value
Force Range	kN	-5 to 5
Sensitivity	pC/N	≅ -7.5

Force range of dynamometer can be calibrated to other ranges in order to achieve better resolution, for example, in our case force range was within 500N so the calibrated range was selected to be 0 to 500N. This setting has been done on charge amplifier. MR damper is fitted in the Y-axis direction of the dynamometer.

5.4.2 Laser Displacement Sensor

Laser displacement sensor is used for measuring the displacement of the MR damper piston. Laser sensor is highly useful for generating the force displacement graphs which are the major design feature. Force displacement graph helps to determine the work done or energy dissipated by MR damper. From energy dissipation data damping coefficient of the MR damper can be calculated using an energy dissipation method which will be discussed in later chapters. Laser displacement sensor is highly accurate device with the added advantage of no hard connection with the device whose displacement measurement is required. Hence, no loading effect on the displacement of load.

Table 5-3: Specification of Laser Displacement Sensor [52]

Description	Units	Value
Reference distance from object	mm	100
Measurement range from Head	mm	75mm to 130 mm (55mm)
Sensitivity	mm/V	4
Output Range	V	± 5

Laser displacement sensor has range of ±27.5mm hence can effectively measure the maximum displacement of washing machine tub i.e. ±25mm.

5.4.3 Charge Amplifier

Charge Amplifier is used to sense and amplify charge signal coming from piezoelectric force dynamometer. Dynamometer senses force in N and gives output in the form of charge in pC (picoCoulombs). This charge is sensed, amplified and converted into voltage by charge amplifier so that the data can be fed and stored in to PC by DAQ card. The charge amplifier used is Kistler™ 9015B with following specifications

Table 5-4: Specifications of Charge Amplifier [53]

Description	Units	Value
Measuring range	pC	±10 to 999000
Sensitivity	pC/Mechanical Unit	0.01 to 9990
Scale	Mechanical Unit/Volt	0.001 to 9990000
Output Voltage	V	±10

5.4.4 Linear Actuator

In order to simulate the drum vibrations of washing machine, linear actuator or servo tube motor has been used to provide required force and displacements of the washing machine tub/drum. Linear actuator has the capability of providing high speed oscillations up to 23.3 Hz which corresponds to the maximum 1400 rpms of the washing machine. It can also provide more than 200N force at 23.3 Hz. Linear actuator also provides position, velocity and current feedback for position, speed and force control respectively. The operation of linear actuator is very smooth and noise free.

Figure 5-9: Linear tube actuator with controller.

Table 5-5: Linear Actuator Specifications [54]

Description	Units	Value
Peak Force	N	312
Peak Current	Amps	20
Sensitivity	N/Amps	15.6
Maximum speed	m/s	5.6
Maximum stroke	mm	309
Thrust rod mass	Kg/m	3.5

Linear Motor controller /driver has been used for position, velocity and force control. In MR damper testing different velocities were selected from the user interface of the linear motor controller. Software for user interface has been downloaded from internet into a PC. User interface software provides features like auto tuning of linear motor according to load attached. Different currents can be set up to fulfill the load requirements. User Interface also provides frequency change option by which at certain fixed velocity different frequencies can be set with different motion command types, for example square wave, sine wave and step forward and backward commands.

Chapter 6

6 Mathematical modelling of MR damper

6.1 Overview

In this chapter various mathematical models of MR damper are discussed, such as off state friction models for passive state performance. Several on-state models of MR damper are also discussed which include electric current as major control parameter. Harmonic analysis, i.e. forces versus displacement measurement and force versus velocity measurements is discussed. In the end Hysteresis behavior will be discussed along with the mathematical modelling and parameter identification using optimization techniques.

6.2 Friction Models of MR damper (Passive Mode)

Friction is the resisting force between two sliding bodies. In our case one body is piston composed of connecting rod and bobbin wrapped with MR fluid absorbent material and other body is outer cylinder made of magnetic steel. There are many friction models based either on the physics of the surface interactions or on the experimental observations [55]. The most widely used friction models are Maxwell-slip, Dahl and LuGre models.

6.2.1 Static Friction Models

Coulomb and linear viscous damping are the basic static friction models. Static friction Fs can be described as the friction before non-zero velocity as shown in Fig 6-1;

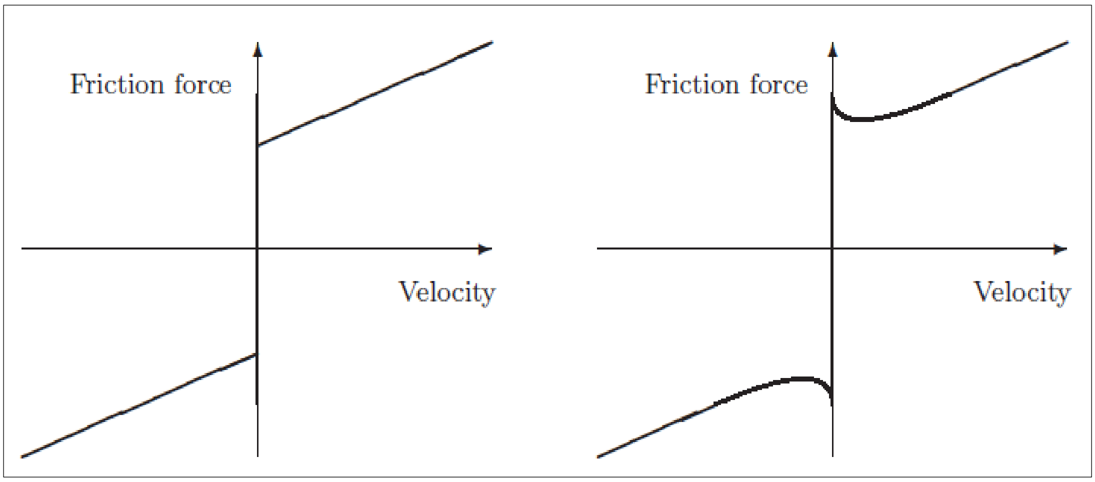

Figure 6-1: Basic static friction model depiction versus velocity (a) Coulomb, viscous and static friction (b) Stribeck friction model [56].

At certain velocity regime, friction force decreases with increasing velocity. The effect is called stribeck effect as shown in above Fig 6-1 (b). These models do not predict the behavior at zero velocity.

6.2.1.1 The coulomb, the viscous and the stribeck model

The very basic friction model is coulomb model where the friction force is given by

$$F_c = \mu F_n sign(v) \tag{6.1}$$

Where Fc is the magnitude of the coulomb friction force, Fn is the normal force, μ is the friction coefficient and v is the relative velocity of a moving object. The magnitude of the coulomb friction force is independent of the magnitude of velocity and the contact area [55].

The relationship between viscous friction force and velocity is linear as expressed below

$$F_v(v) = \sigma_v v \tag{6.2}$$

Where $\sigma_v$the viscous friction coefficient.The stribeck effect is can be expressed as Fs and is the drop in friction force in certain region of velocity.

$$F_f(v) = \mu F_n sign(v) + \sigma_v v + F_s \tag{6.3}$$

6.2.2 Switching Models

The static friction models described above explain friction forces well at steady state velocities. For velocities near zero or equal to zero or crossing zero, the static models give numerical errors. In order to overcome numerical problems switching model such as seven parameter models is discussed which further enhance these models into more accurate and complete numerical models.

6.2.2.1 The seven parameter model

The seven parameter model includes presiding displacement, coulomb and viscous friction and the stribeck curve with frictional lag. The seven parameter model is split into two halves, one for stick phenomena and other presents slip or sliding phenomena. For stick phase friction is simply modelled as spring;

$$F_f(x) = \sigma_0 x \tag{6.4}$$

With $\sigma_0$as micro stiffness and x is the displacement of the object subjected to the friction force. In the sliding phase friction is modelled as

$$F_f(\dot{x},t) = \left(F_c + F_v|\dot{x}| + F_s(\gamma, t_2) \frac{1}{1 + \left(\frac{\dot{x}(t-\tau_L)}{\dot{x}_s} \right)^2} \right) sign(\dot{x}) \tag{6.5}$$

With

$$F_s(\gamma, t_2) = F_{s.a} + (F_{s.\infty} - F_{s.a}) \frac{t_2}{t_2+\gamma} \tag{6.6}$$

With:

F_f= the friction force

F_c= the coulomb friction force

F_v= the viscous friction force

F_s= the magnitude of stribeck friction

$F_{s.a}$= the magnitude of stribeck friction at the end of previous sliding period

$F_{s.\infty}$= the magnitude of stribeck friction after long time at rest (with a slow application of force)

$\dot{x}_s$= the characteristic velocity of the stribeck friction

τ_L= the time constant of frictional memory

γ = the temporary parameter of rising static friction

t_2= dwell time, it is the time at zero velocity.

Eq (6.5) and Eq (6.6) present a model that tries to capture the dynamics of friction by introducing the time delay. This time delay oversimplifies the solution and only affects the friction in sliding phase. This model has the drawback that it does not observe the transition between presiding and sliding phase.

6.2.3 LuGre Model

Dahl presented a model which explains the transition between presiding and sliding behavior and hysteresis in a dynamic model but unable to predict other phenomena like stribeck effect [56]. Dahl forms the basis of LuGre model which can be shown

$$\frac{dz}{dt} = \frac{1}{\sigma_0}\frac{dF_f}{dx}\frac{dx}{dt} = \frac{1}{\sigma_0}\frac{dF_f}{dx}v = v - \sigma_0\frac{|v|}{F_c}z \qquad (6.7)$$

LuGre model replace Fc with velocity dependent function g (v) and add two more terms. It has an additional damping σ_1 associated with microdisplacment and a memory less velocity dependent f (v) and results in

$$\dot{z} = v - \sigma_0\frac{|v|}{g(v)}z = v - h(v)\text{z} \qquad (6.8)$$

$$F_f = \sigma_0 z + \sigma_1 \dot{z} + f(v) \qquad (6.9)$$

With F_f = the friction force, v the velocity betweenthe two surfacesin contactand zthe internal friction rate. LuGre model describes the presiding and sliding regime quite well.

6.3 Energy dissipation method and equivalent damping coefficient.

The total force of MR damper is the combination of force in off and on states as given by equation.6.10. Firstly the MR damper is tested in off state (I =0 A) having off state (passive) friction labeled as "F_{off}" between piston and surface of cylinder. The passive friction is characterized by Stribeck, Coulomb and viscous frictions as discussed previously.

$$F_{total} = F_{off} + F_{on} \qquad (6.10)$$

In On-state (when I > 0 A), the damping force is due to force generated by MR fluid "F_{mrf}" and magnetic force "F_{mag}" at a single flange. The force due to MR fluid "F_{mrf}" is given by equation 6.11

$$F_{mrf} = T_y . A_p \qquad (6.11)$$

Where “T_y” the yield stress of MR fluid is due to applied magnetic field intensity “H” and A_p is the active pole area of a single flange given by equation.6.12

$$A_p = 2\pi . R_{flange} . l_{flange} \qquad (6.12)$$

Where R_{flange} and l_{flange} is the radius and length of flange respectively. The relationship between induced yield stress of MR fluid and magnetic field “H” is obtained in Fig 4-2. The magnetic force "F_{mag}” at a single flange is calculated by Maxwell tensile force [43] and is given by equation.6.13. Where B is the magnetic flux density at a single flange μ_o is permeability of air and A_p is the active pole area. The flux lines originate from the flange as shown in chapter 3. The total On-State damping force is given by equation.6.5

$$F_{mag} = \frac{B^2 A_p}{2\mu_o} \qquad (6.13)$$

$$F_{on} = F_{mrf} + F_{mag} \qquad (6.14)$$

The performance of MR damper is compared with a conventional viscous damper by determining equivalent damping coefficient C_{eq} [7, 8, and 10]. The equivalent damping coefficient is found by using equation.6.6, where W the energy is dissipated by MR damper in one cycle, w_e is the excitation frequency and X is the excitation amplitude.

$$C_{eq} = \frac{W}{\pi w_e X^2} \qquad (6.15)$$

The relations of energy dissipation and equivalent damping coefficient of MR damper are investigated for different sets of amplitudes, input currents and at a fixed excitation frequency of 3 Hz as given in table.6-1.

Table 6-1: Experimental conditions for testing of MR damper

Excitation Amplitude (mm)	Frequency (Hz)	I (Amperes)				
4	3	0	0.05	0.1	0.15	0.2
5	3	0	0.05	0.1	0.15	0.2
6	3	0	0.05	0.1	0.15	0.2
7	3	0	0.05	0.1	0.15	0.2

It is observed that for a fixed frequency and different values of excitation amplitudes, the dissipation of energy and equivalent damping coefficient are increased by varying input current as shown in figures 6-2 & 6-3.

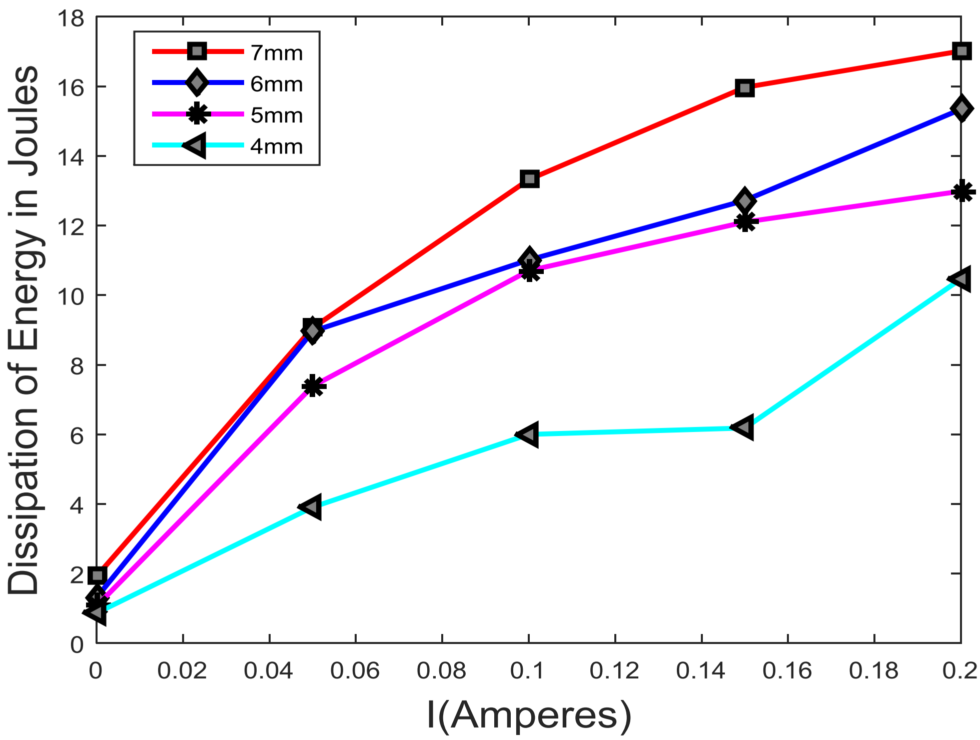

Figure 6-2: Energy dissipation for various amplitudes at 3Hz.

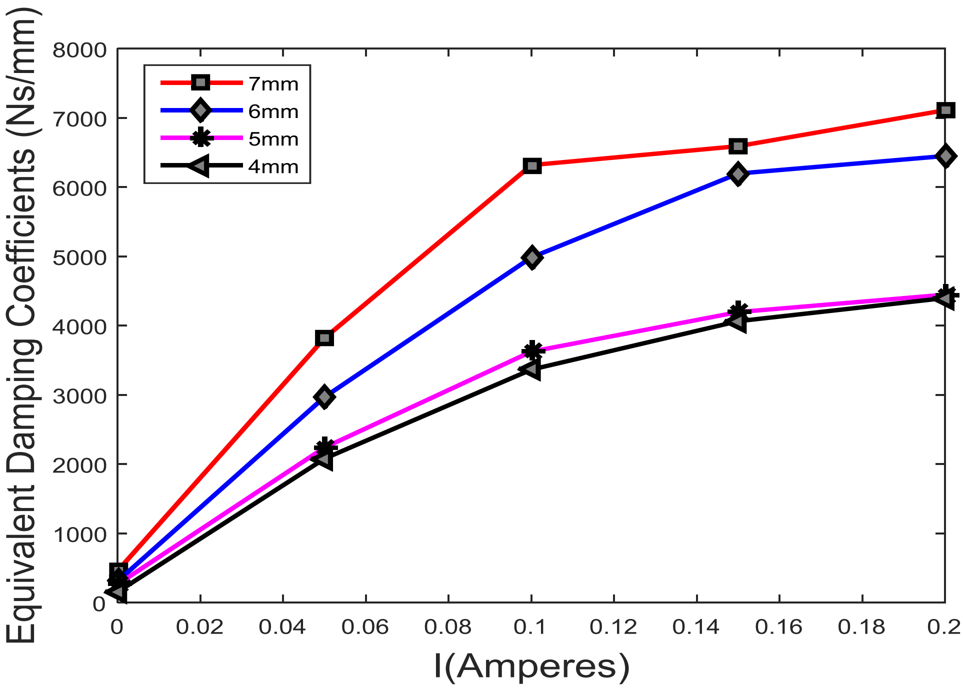

Figure 6-3: Equivalent damping coefficient for various amplitudes at 3Hz

However if excitation amplitude is varied for a fixed frequency and varying current, the energy dissipation shows increasing trend whereas the equivalent damping coefficient dramatically decreases as shown in Fig.6-4 and 6-5.

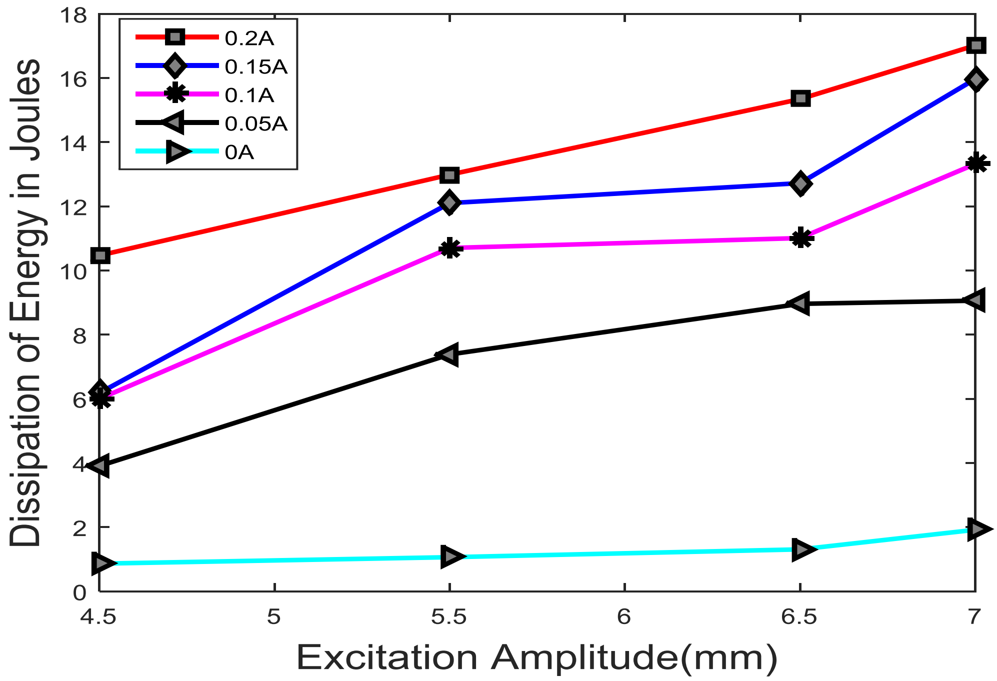

Figure 6-4: Energy dissipation with changing amplitude at different values of current.

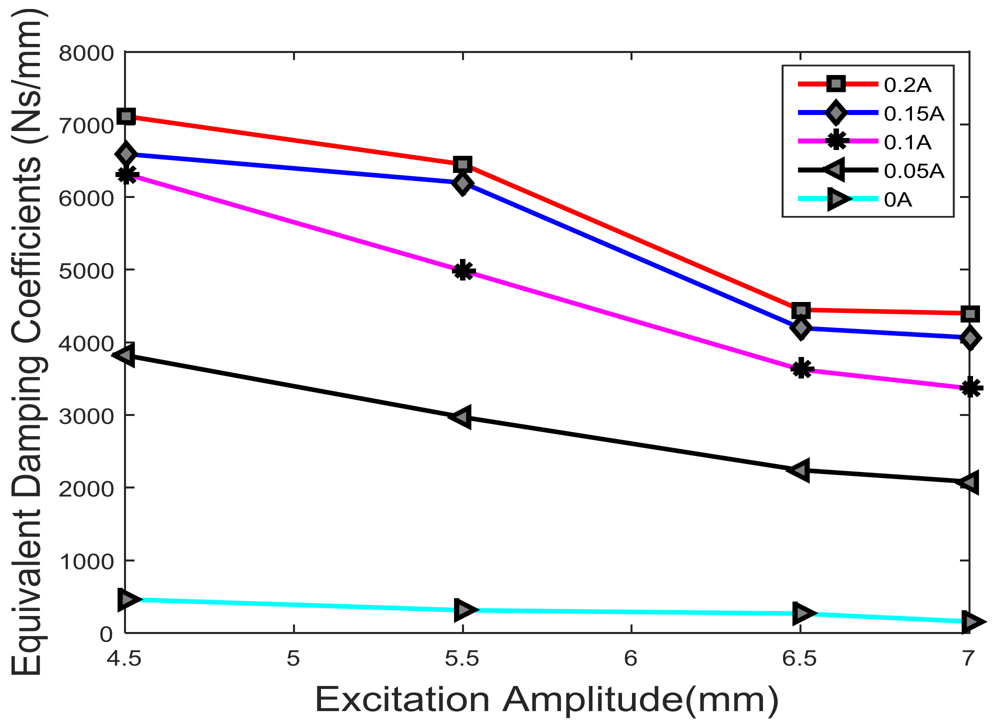

Figure 6-5: Equivalent damping coefficient with changing amplitudes at 3Hz for different values of current.

6.4 Hysteretic Model and parametric identification

The MR damper is mathematically modeled using hysteretic model [57]. The model consists of dashpot which modeled viscous damping, spring represents stiffness and hysteresis component as shown in Fig 6-6 and given by equation 6.16 & 6.17. Where c represents viscous damping k represents stiffness, α shows the scale factor and the tangent hyperbolic function which is used for modeling the hysteresis behavior of MR damper is represented by z. The offset force of MR damper is shown as f_o.The hysteretic model is chosen due to the efficient computation of tangent hyperbolic function. This function proved helpful in terms of parametric identification of MR damper. The identified parameters play vital role in the overall geometry of hysteresis as shown in Fig 6-7. The sharp slope at both ends of hysteresis curve is made by c$\dot{x}$. The ellipse along horizontal axis is due to kx. β represents the basic hysteresis loop, which defines the slope of the hysteresis curve. The width of hysteresis curve is determined byδx. The height of hysteresis curve is achieved with factor α. The larger hysteresis curve can be obtained byα.

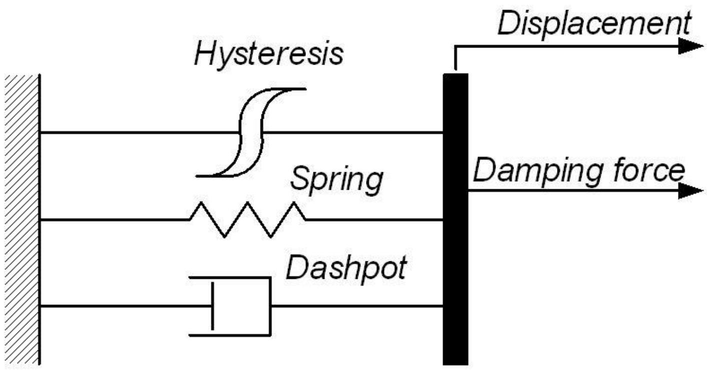

Figure 6-6: Hysteretic model of MR damper [57]

$$f = c\dot{x} + kx + \alpha z + f_o \tag{6.16}$$

$$z = \tanh\left(\beta\dot{x} + \delta sign(x)\right) \tag{6.17}$$

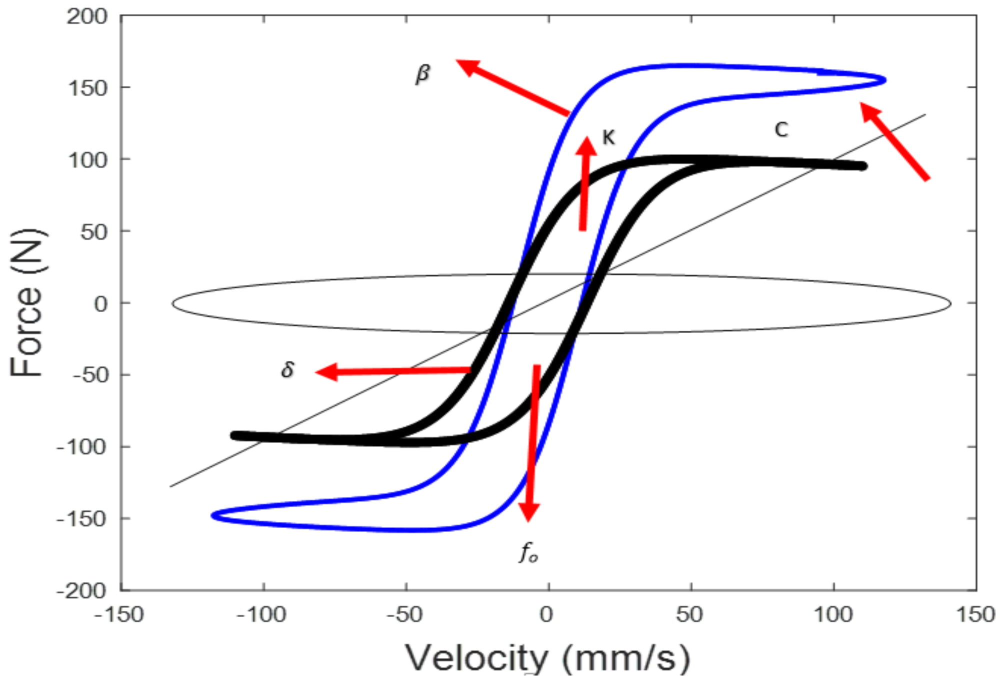

Figure 6-7: Parameters of Hysteretic Model and their effects on hysteretic behavior.

The root mean square error between experimental and hysteretic model is chosen as objective function for parametric identification of MR damper as given by Eq (6.18) where F_{exp} is the MR damper force is, F_{hm} is the hysteretic model force and n shows the number of data points to be taken. Furthermore the minimum of objective function is obtained using lsqcurvefit in Matlab.

$$J = \sqrt{\frac{1}{n}\sum_{i=1}^{n}(F_{exp}^{i} - F_{hm}^{i})^2} \tag{6.18}$$

The mathematical modeling and parametric identification of MR damper is done by using different sets of experiments which are given in table 6-2. The trend of each parameter is studied and approximated with corresponding polynomials given by Figures 6-8 to 6-12. In addition to this, it is important to mention that the offset force $f_o \approx 0$ is approximately considered negligible due to absence of accumulator in our MR damper.

Table 6-2: Experimental details for mathematical modelling of MR damper

Excitation Amplitude (mm)	Frequency (Hz)	I (Amperes)				
4	2	0	0.05	0.1	0.15	0.2
5	2	0	0.05	0.1	0.15	0.2
6	2	0	0.05	0.1	0.15	0.2
4	3	0	0.05	0.1	0.15	0.2
5	3	0	0.05	0.1	0.15	0.2
6	3	0	0.05	0.1	0.15	0.2

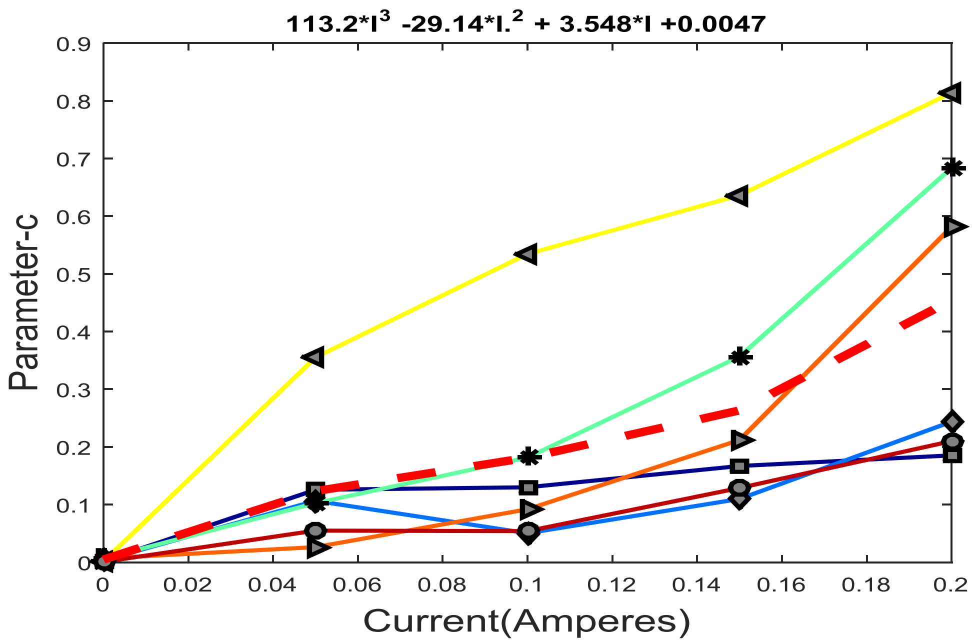

Figure 6-8: Trend of damping coefficient of Hysteretic Model. Damping coefficient shows increasing trend with increase in current.

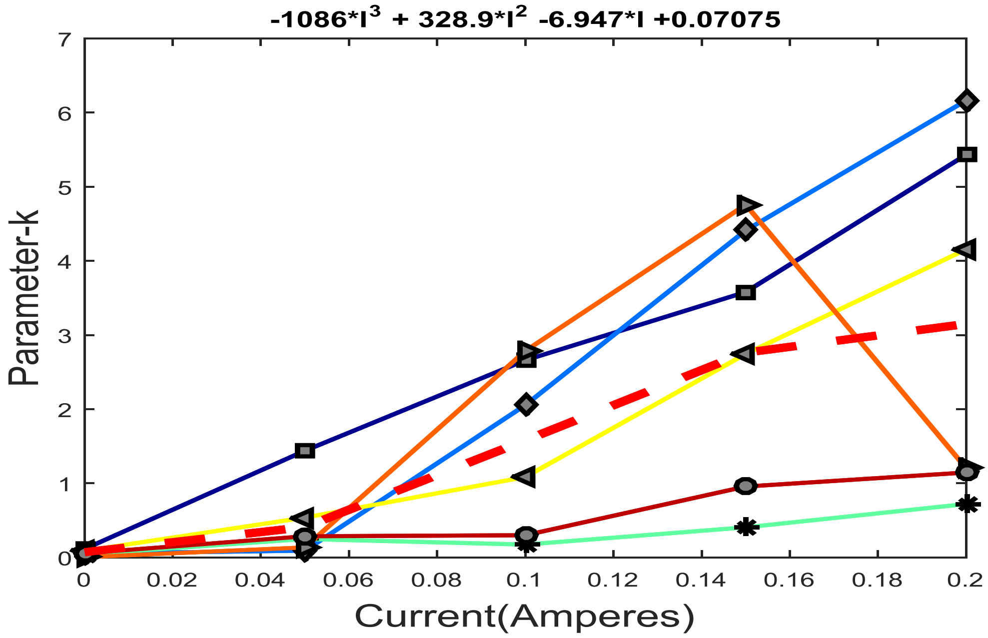

Figure 6-9: Trend of stiffness of MR damper Hysteretic Model. Stiffness shows increasing trend with increase in current.

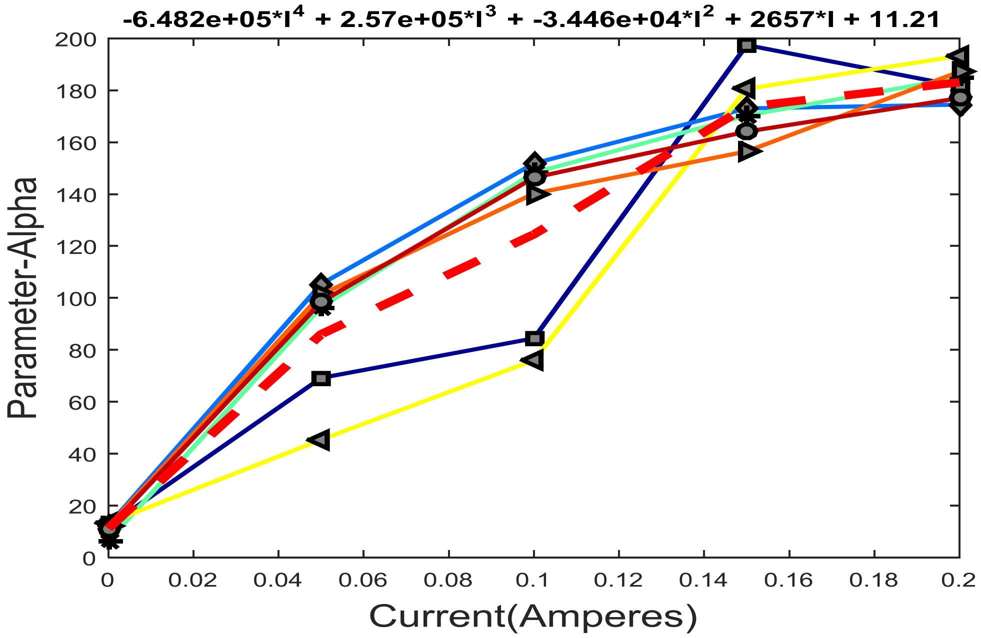

Figure 6-10: Trend of Alpha (α) parameter of Hysteretic Model. Alpha shows increasing trend with increase in current.

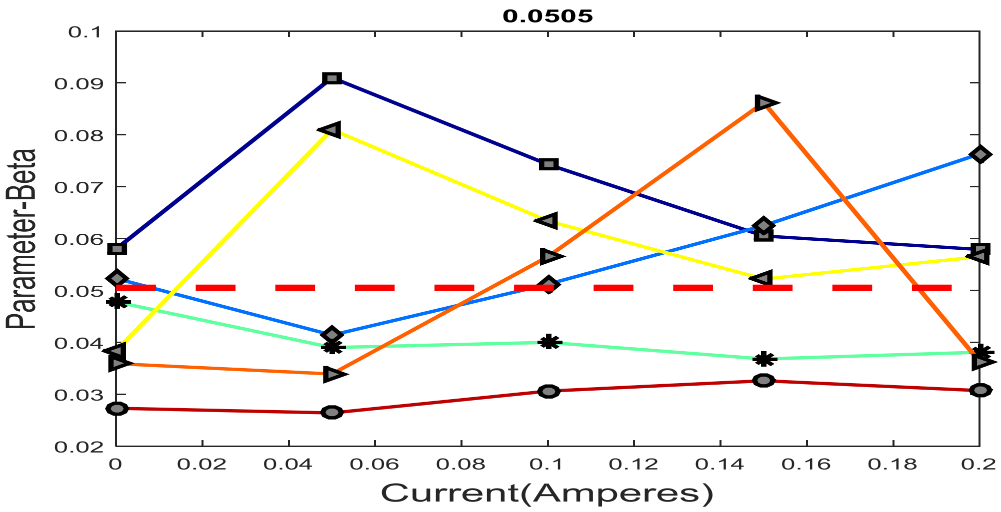

Figure 6-11: Trend of Beta (β) parameter of Hysteretic Model. Beta remains constant with increase in current.

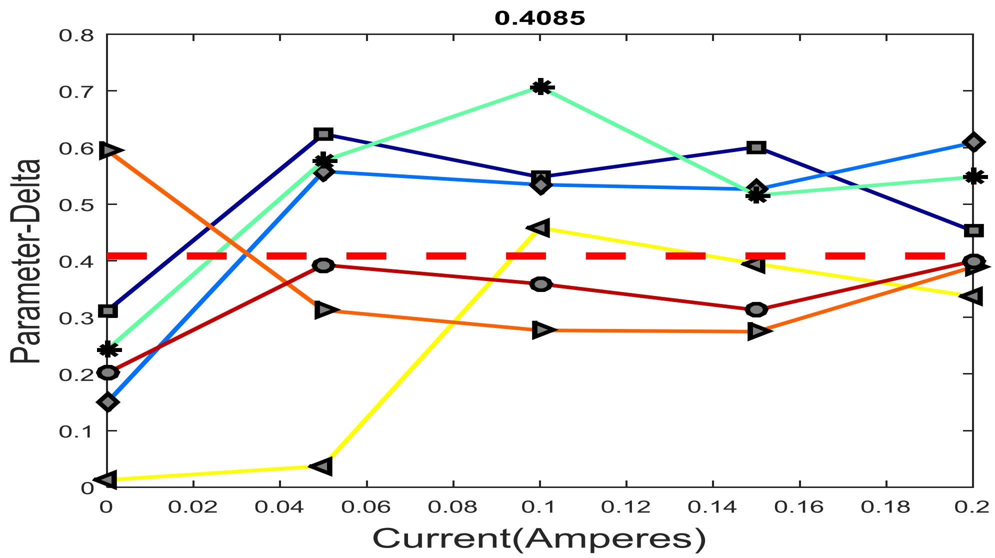

Figure 6-12: Trend of Delta (δ) parameter of Hysteretic Model. Delta also remains constant with increase in current.

The force-velocity & force-displacement hysteresis curves for the experimental and mathematical model are investigated by varying current at different excitation amplitudes and frequencies are shown in Figures 6-13 and 6-14. It is clearly observed that RMSE increases as the current varies from 0A to 0.2 A as shown in Figure.6-15.

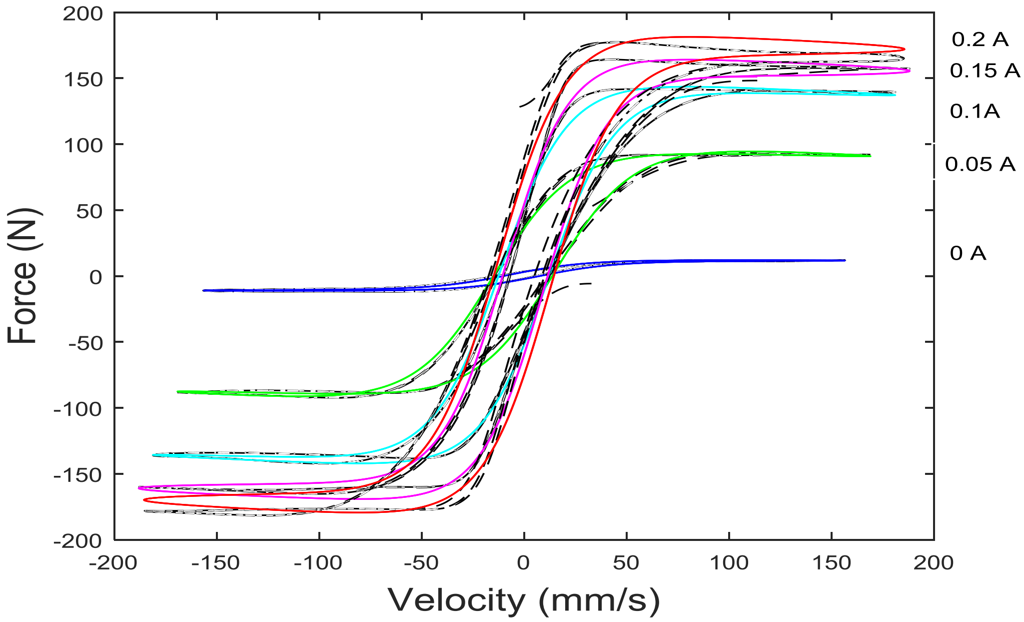

Figure 6-13: Force-Velocity hysteresis curves at 6mm amplitude and 3Hz frequency. Dotted lines are the experimental data and solid lines represent the fitted data using least square curve fit method.

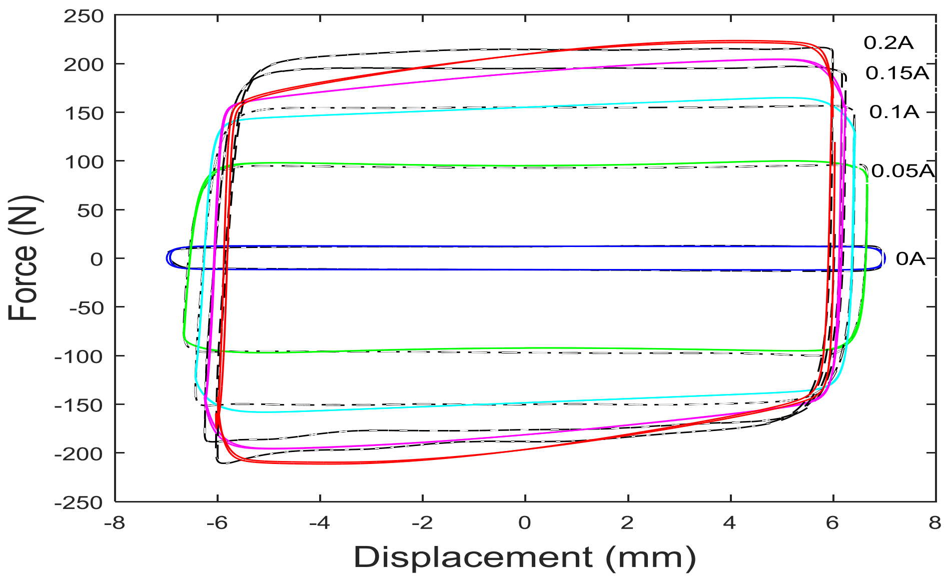

Figure 6-14: Force-Displacement hysteresis curves at 5mm amplitude and 2Hz frequency. Dotted lines are the experimental data and solid lines represent the fitted data obtained using least square curve fit method.

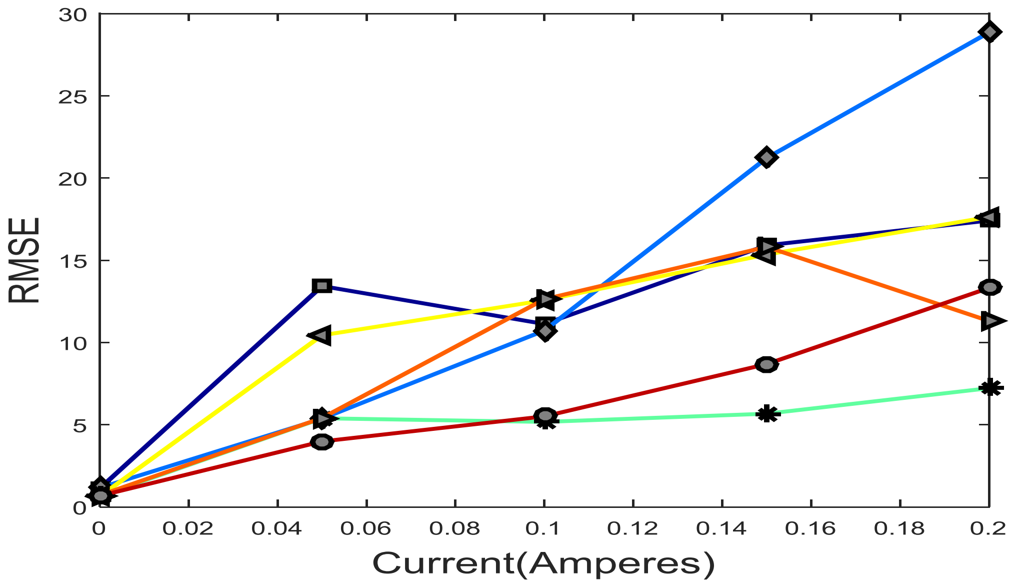

Figure 6-15: RMSE (Root Mean Square Error) between experimental data and mathematical model

Chapter 7

7 Performance comparison of MR and Passive dampers on washing machine

7.1 Overview

This chapter describes the performance comparison of MR damper with available passive dampers onto the washing machine. First the displacement data of washing machine drum has been recorded with passive dampers. The drum speed (RPM) is also measured simultaneously with displacement. In next step passive dampers are replaced by MR dampers and displacement data is again recorded for similar drum speeds. During operation MR damper current is controlled by on-off controller. The controller switches current based on drum speed. In the end comparison of both passive and MR damper performance is compared. Experimental Setup

7.2 Experimental Setup

An experimental set-up is established to compare the performance of MR and passive dampers in washing machine drum vibration. Experimental setup of both dampers is shown in Figure 7-1 and 7-2. In Figure 7-1, an NI-DAQ card is used with LabVIEW to acquire the data of displacement, RPM and electric current. A laser displacement sensor is fixed on a beam which is attached to vibration isolation table to isolate any disturbance such as ground vibrations to displacement signal. A power supply is used for continuous supply of electric current to MR dampers. The axes of washing machine are defined such that z-axis is pointing towards outside of the paper, y-axis is pointing and x-axis is pointing towards the front end of machine. Moreover RPM are measured using hall-effect sensor fixed on plexi-glass, which senses the magnetic field of permanent magnet attached at the back side of drum as shown in Figure 7-2.

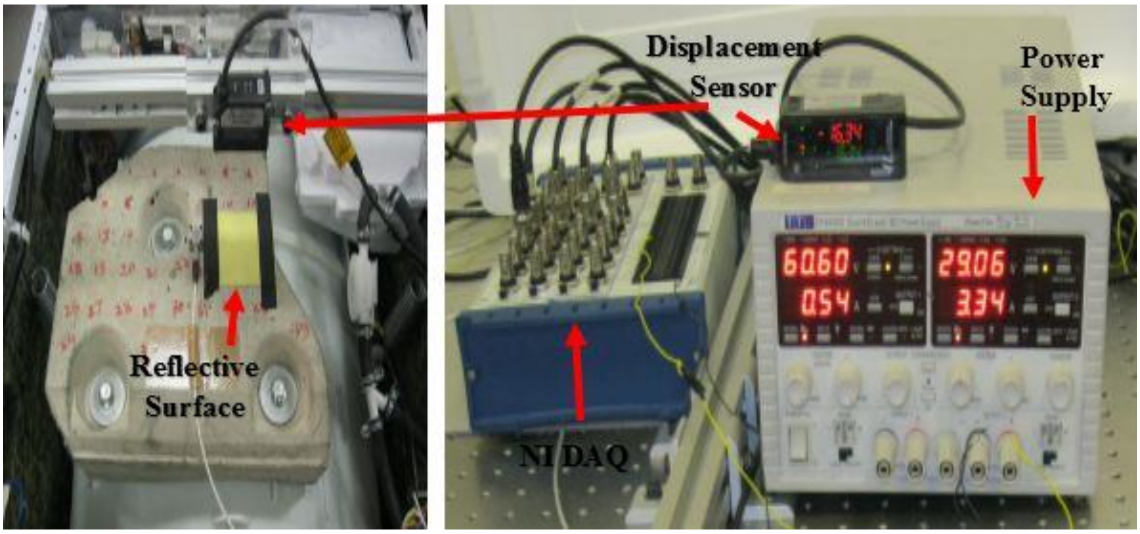

Figure 7-1: Experimental setup for measuring the displacement of washing machine drum in both passive and MR damper testing.

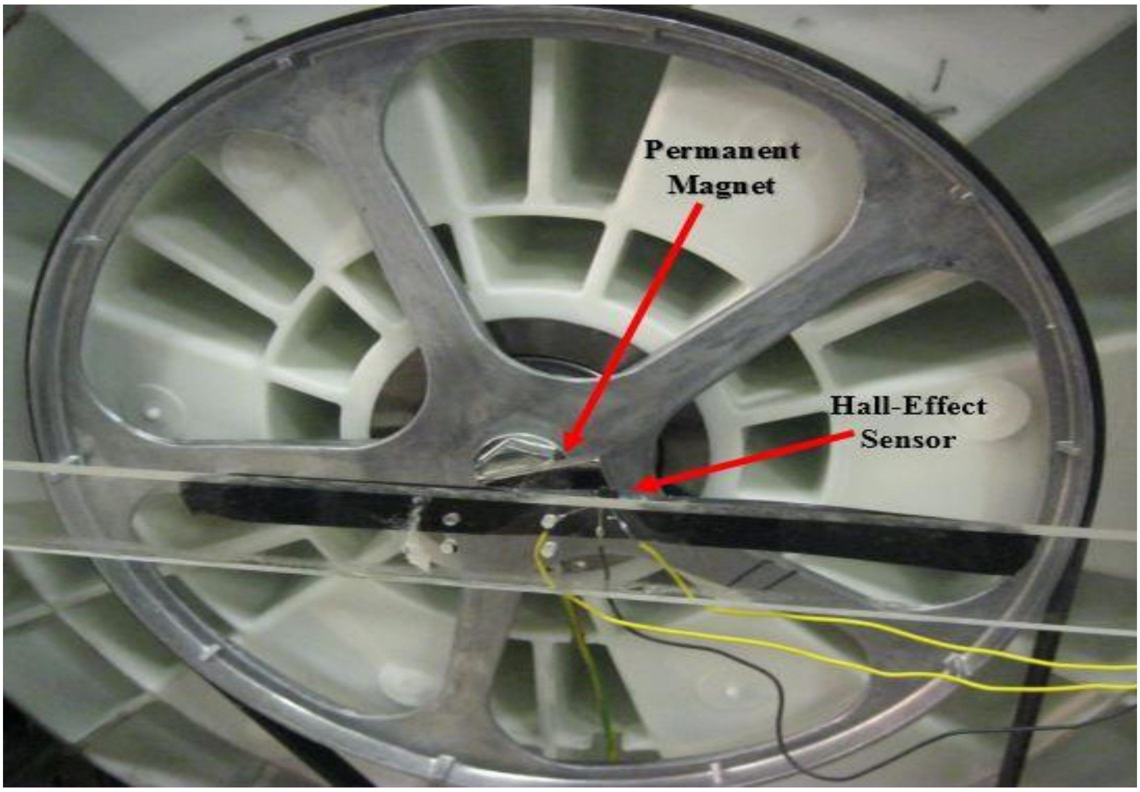

Figure 7-2: Permanent magnet and Hall effect sensor setup for measurement of drum RPM.

7.3 Controller Design

A look up on-off control technique has been developed reducing the drum vibration in resonance and steady state conditions. The decision of the controller is totally based on number of RPMs measured with Hall-effect sensor. A complete control block diagram of LabVIEW is given in Figure 7-3 showing the acquired & generated data of all sensors along with On-Off controller in real-time. Damper current is controlled by generating the pulse width modulated signal based on RPM. Three pwm duty cycles are set based on three regions of drum speeds, first region from 0 to 200 rpm duty cycle of voltage output are set to 65%; second region of speed is 200 to 400 rpm in which there comes machine resonance so the duty cycles are set to 100%. Third region is steady state region from 400 up to 1400 rom which is the maximum speed of washing machine. In this region the voltage duty cycles are set 20% so that transmissibility can be minimized.

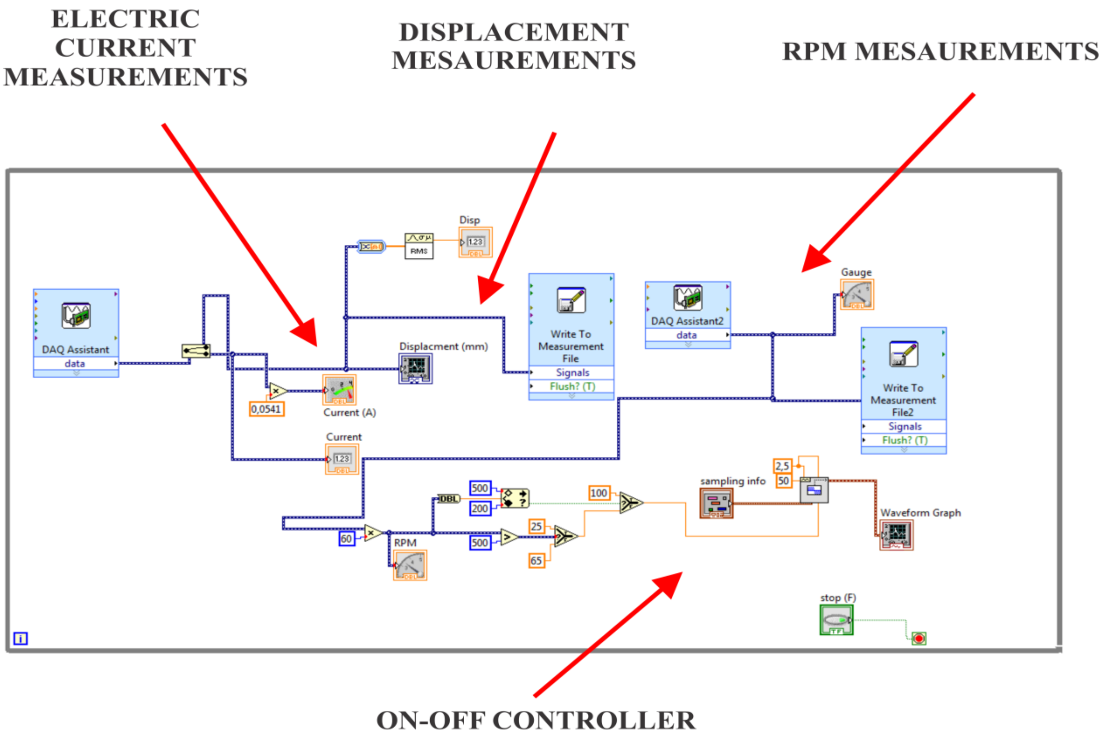

Figure 7-3: Block diagram for data acquisition and on-off control in LabVIEW.

7.4 Performance Comparison

After establishing the experimental testing set-up, the performance of passive & MR dampers are compared. For this purpose the passive & MR dampers are installed in washing machine one after another as shown in Figure 7-4.

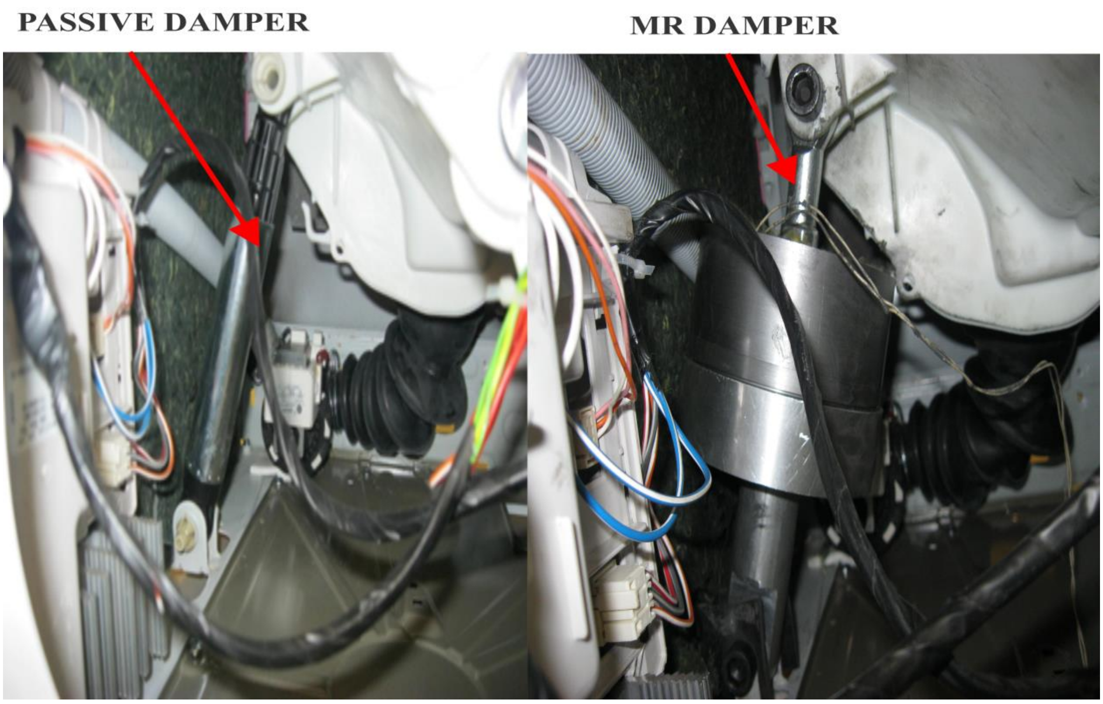

Figure 7-4: Passive and MR dampers are installed separately in washing machine.

The washing machine is tested at different ranges of cycles from 0 to 1400 RPM. The performance of both dampers is compared in terms of displacement as shown in Figure 7-5.The value of electric current is varied for different ranges of RPMs and the On-Off controller performs the required switching operation. An electric current of 0.1A is applied to each MR damper in resonance band (200 to 400 RPM). It is quite clear that when washing machine operates in resonance band the MR dampers greatly reduce the displacement as compared with passive dampers. Furthermore as washing machine starts to enter in steady state (400 to 1400 RPM) the controller switches current to 0.025A and MR dampers also give better performance than passive dampers.

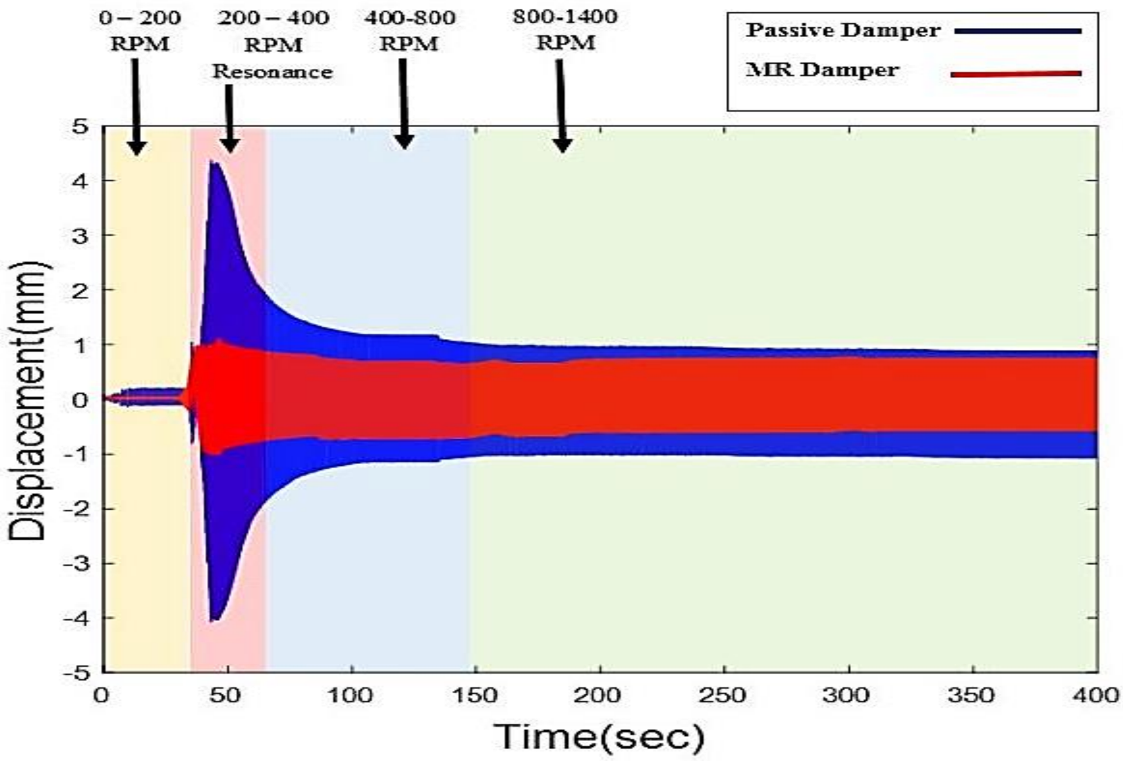

Figure 7-5: Performance comparison of passive and MR dampers.

7.5 Conclusion & Discussion

In this study a novel magnetorheological damper was developed to suppress the vibration of washing machine. Conventional passive dampers were studied and performance is analyzed in washing machine. The performance of passive dampers was found inefficient at resonance and high speeds. This problem brought the need of variable damping device that can adjust damping force according to disturbances. Magnetorheological fluid damper was selected and analyzed as variable damping device because of its good performance both in passive and active modes, millisecond response time and low electrical power requirement. Magnetic circuit of the damper was designed and analyzed both experimentally and using finite element methods. Structural design of damper was made as per requirement of force, stroke and space inside washing machine and approach is followed such as design should be closer to passive design, cost effectiveness because of its usage in high production machines spare parts availability and maintenance. Experimental results on test rig have proven the analytical analysis in terms of force and response time. The MR damper was finally tested on washing machine and results proved that MR damper is the required solution to the vibration in current high tech washing machines.

BIBLOGRAPHY

[1] M. J. Chrzan and J. D. Carlson, “MR fluid sponge devices and their use in vibration control of washing machines,” *SPIE’s 8th Annu. Int. Symp. Smart Struct. Mater.*, vol. 4331, pp. 370–378, 2001.

[2] D. Truong and K. Ahn, “MR Fluid Damper and Its Application to Force Sensorless Damping Control System,” *Smart Actuation Sens. Syst. - Recent Adv. Futur. Challenges*, pp. 383–424, 2012.

[3] “SmartMaterials.”Available: http://webdocs.cs.ualberta.ca/~database/MEMS/sma_mems/smrt.html.

[4] W. Kordonski and A. Shorey, “Magnetorheological (MR) Jet Finishing Technology,” *J. Intell. Mater. Syst. Struct.*, vol. 18, no. 12, pp. 1127–1130, 2007.

[5] H. B. Cheng, Y. Yam, and Y. T. Wang, “Experimentation on MR fluid using a 2-axis wheel tool,” *J. Mater. Process. Technol.*, vol. 209, no. 12–13, pp. 5254–5261, 2009.

[6] A. Sidpara and V. K. Jain, “Analysis of forces on the freeform surface in magnetorheological fluid based finishing process,” *Int. J. Mach. Tools Manuf.*, vol. 69, pp. 1–10, 2013.

[7] Poynor, James C. Innovative designs for magneto-rheological dampers. Diss. Virginia Polytechnic Institute and State University, 2001.

[8] Singh, Anant Kumar, Sunil Jha, and Pulak M. Pandey. "Mechanism of material removal in ball end magnetorheological finishing process." *Wear*302.1 (2013): 1180-1191.

[9] B. Jung, K. I. Jang, B. K. Min, S. J. Lee, and J. Seok, “Magnetorheological finishing process for hard materials using sintered iron-CNT compound abrasives,” *Int. J. Mach. Tools Manuf.*, vol. 49, no. 5, pp. 407–418, 2009.

[10] A. Pettersson, S. Davis, J. O. Gray, T. J. Dodd, and T. Ohlsson, “Design of a magnetorheological robot gripper for handling of delicate food products with varying shapes,” *J. Food Eng.*, vol. 98, no. 3, pp. 332–338, 2010.

[11] Z. J. Wang, P. Y. Wang, and H. Song, “Research on sheet-metal flexible-die forming using a magnetorheological fluid,” *J. Mater. Process. Technol.*, vol. 214, no. 11, pp. 2200–2211, 2014.

[12] T. H. Yang, H. J. Kwon, S. S. Lee, J. An, J. H. Koo, S. Y. Kim, and D. S. Kwon, “Development of a miniature tunable stiffness display using MR fluids for haptic application,” *Sensors Actuators, A Phys.*, vol. 163, no. 1, pp. 180–190, 2010.

[13] Ahmadkhanlou, Farzad. *Design, modeling and control of magnetorheological fluid-based force feedback dampers for telerobotic systems*. Diss. The Ohio State University, 2008.

[14] J. D. Carlson, W. Matthis, and J. R. Toscano, “Smart prosthetics based on magnetorheological fluids,” *Proc. SPIE*, vol. 4332, pp. 308–316, 2001.

[15] M. H. Prasad and K. V Gangadharan, “Research Trends in Controllable Fluids for Landing Gear Applications,” vol. 5, no. 7, pp. 1340–1343, 2014.

[16] S. Dong, K. Q. Lu, J. Q. Sun, and K. Rudolph, “Adaptive force regulation of muscle strengthening rehabilitation device with magnetorheological fluids,” *IEEE Trans.*

Neural Syst. Rehabil. Eng., vol. 14, no. 1, pp. 55–63, 2006.

[17] H. Tomori, Y. Midorikawa, and T. Nakamura, “Vibration control of an artificial muscle manipulator with a magnetorheological fluid brake,” *J. Phys. Conf. Ser.*, vol. 412, p. 012053, 2013.

[18] L. Kong, J. H. Chin, Y. Li, Y. Lu, and P. Li, “Targeted suppression of vibration in deep hole drilling using magneto-rheological fluid damper,” *J. Mater. Process. Technol.*, vol. 214, no. 11, pp. 2617–2626, 2014.

[19] D. Case, B. Taheri, and E. Richer, “Dynamical modeling and experimental study of a small-scale magnetorheological damper,” *IEEE/ASME Trans. Mechatronics*, vol. 19, no. 3, pp. 1015–1024, 2014.

[20] D. Mei, T. Kong, A. J. Shih, and Z. Chen, “Magnetorheological fluid-controlled boring bar for chatter suppression,” *J. Mater. Process. Technol.*, vol. 209, no. 4, pp. 1861–1870, 2009.

[21] S. B. Choi, S. R. Hong, K. G. Sung, and J. W. Sohn, “Optimal control of structural vibrations using a mixed-mode magnetorheological fluid mount,” *Int. J. Mech. Sci.*, vol. 50, no. 3, pp. 559–568, 2008.

[22] B. F. Spencer, G. Yang, J. D. Carlson, and M. K. Sain, “Smart Dampers for Seismic Protection of Structures : A Full-Scale Study,” *Proc. 2nd World Conf. Struct. Control*, pp. 1–10, 1998.

[23] “MagneRide.”Available:http://www.magneride.com/magneride.com/magneride home page.html.

[24] X. Zhu, X. Jing, and L. Cheng, “Magnetorheological fluid dampers: A review on structure design and analysis,” *J. Intell. Mater. Syst. Struct.*, vol. 23, no. 8, pp. 839–873, 2012.

[25] G. Xinchun, H. Yonghu, R. Yi, L. Hui, and O. Jinping, “A novel self-powered MR damper: theoretical and experimental analysis,” *Smart Mater. Struct.*, vol. 24, no. 10, p. 105033, 2015.

[26] B. Ebrahimi and B. Hamesee, “Development of Hybrid Electromagnetic Dampers for Vehicle Suspension Systems,” *Dep. Mech. Mechatronics Eng.*, vol. Doctor of , p. 172, 2009.

[27] G. Yang, S. Jr, D. Carlson, and K. Sain, “Large-scale MR uid dampers: modeling and dynamic performance considerations,” *Eng. Struct.*, vol. 24, pp. 309–323, 2002.

[28] H. Boese and J. Ehrlich, “Performance of Magnetorheological Fluids in a Novel Damper with Excellent Fail-safe Behavior,” *J. Intell. Mater. Syst. Struct.*, vol. 21, no. 15, pp. 1537–1542, 2010.

[29] M. Unsal, C. Crane, and C. Niezrecki, “Vibration control of parallel platforms based on magnetorheological damping,” *Florida Conf. Recent …*, pp. 1–6, 2006.

[30] W. H. Li, X. Y. Wang, X. Z. Zhang, and Y. Zhou, “Development and analysis of a variable stiffness damper using an MR bladder,” *Smart Mater. Struct.*, vol. 18, no. 7, p. 074007, 2009.

[31] A. Grunwald and A. G. Olabi, “Design of magneto-rheological (MR) valve,” *Sensors Actuators, A Phys.*, vol. 148, no. 1, pp. 211–223, 2008.

[32] M. Brigley, Y.-T. Choi, N. M. Wereley, and S.-B. Choi, “Magnetorheological Isolators Using Multiple Fluid Modes,” *J. Intell. Mater. Syst. Struct.*, vol. 18, no. 12, pp. 1143–1148, 2007.

[33] M. B. Dogruoz, E. L. Wang, F. Gordaninejad, and A. J. Stipanovic, “Journal of Intelligent Material Systems and Structures Augmenting Heat Transfer from Fail-safe Magneto-rheological,” *J. Mater. Syst. Struct.*, vol. 14, no. 79, 2003.

[34] G. H. Hitchcock, X. Wang, and F. Gordaninejad, “A New Bypass Magnetorheological Fluid Damper,” *J. Vib. Acoust.*, vol. 129, no. 5, p. 641, 2007.

[35] Olabi, Abdul-Ghani, and Artur Grunwald. "Design and application of magneto-rheological fluid." *Materials & design* 28.10 (2007): 2658-2664.

[36] Y.-J. Nam and M.-K. Park, “Performance Evaluation of Two Different Bypass-type MR Shock Dampers,” *J. Intell. Mater. Syst. Struct.*, vol. 18, no. 7, pp. 707–717, 2007.

[37] W. Hu, R. Robinson, and N. M. Wereley, “A design strategy for magnetorheological dampers using porous valves,” *J. Phys. Conf. Ser.*, vol. 149, p. 012056, 2009.

[38] C. Spelta, F. Previdi, S. M. Savaresi, G. Fraternale, and N. Gaudiano, “Control of magnetorheological dampers for vibration reduction in a washing machine,” *Mechatronics*, vol. 19, no. 3, pp. 410–421, 2009.

[39] Carlson, J. David. "Washing machine having a controllable field responsive damper." U.S. Patent No. 6,151,930. 28 Nov. 2000.

[40] “Controlling Vibration with Magnetorheological Fluid Damping | Sensors.” Available: http://www.sensorsmag.com/sensors/electric-magnetic/controlling-vibration-with-magnetorheological-fluid-damping-999.

[41] Brauer, John R. *Magnetic actuators and sensors*. John Wiley & Sons, 2006.

[42] Ueno, Toshiyuki, Jinhao Qiu, and Junji Tani. "Magnetic circuit design method for magnetic force control systems using inverse magnetostrictive effect: Examination of energy conversion efficiency depending on ΔE effect." *Electrical Engineering in Japan* 140.1 (2002): 8-15.

[43] O. Vogel and J. Ulm, “Theory of Proportional Solenoids and Magnetic Force Calculation Using COMSOL Multiphysics,” *Proc. 2011 COMSOL Conf. Stuttgart*, 2011.

[44] Z. Parlak, T. Engin, and İ. Çallı, “Optimal design of MR damper via finite element analyses of fluid dynamic and magnetic field,” *Mechatronics*, vol. 22, no. 6, pp. 890–903, 2012.

[45] “American Wire Gauge table and AWG Electrical Current Load Limits with skin depth frequencies and wire breaking strength.”Available: http://www.powerstream.com/Wire_Size.htm.

[46] G. Bossis, S. Lacis, a. Meunier, and O. Volkova, “Magnetorheological fluids,” *J. Magn. Magn. Mater.*, vol. 252, no. 1–3 SPEC. ISS., pp. 224–228, 2002.

[47] Phule, Pradeep P. "Magnetorheological (MR) fluids: Principles and applications." *Smart Materials Bulletin* 2001.2 (2001): 7-10.

[48] “MRF-140CGTechData.pdf.”Available: http://www.lordfulfillment.com/upload/DS7012.pdf

[50] Altintas, Yusuf. *Manufacturing automation: metal cutting mechanics, machine tool vibrations, and CNC design*. Cambridge university press, 2012.

[51] A. Examples and T. Data, “Multicomponent Dynamometer –5 ... 10,” *Measurement*, pp. 1–4, 2009. Available: https://www.kistler.com/?type=669&fid=29887

[52] U.Type,“CMOSMulti-FunctionAnalogLaserSensor.Available: http://www.hasmak.com.tr/keyence/application_sensor/keyence_CMOS_Multi-Function_Analog_Laser_Sensor_il_series.pdf

[53] M. C. Amplifier, “Measure & Analyze – MCA,” no. 052, pp. 1–4.Availabe: http://www.copleycontrols.com/Motion/pdf/Xenus_XTL.pdf

[54] M. Velocity, M. Handling, and A. Assembly, “Models sta2504-2510 servotube actuator,” vol. 44, no. 0, pp. 1–8, 2011.

[55] Drincic, Bojana. *Mechanical models of friction that exhibit hysteresis, stick-slip, and the Stribeck effect*. Diss. The University of Michigan, 2012.

[56] Van Geffen, V. "A study of friction models and friction compensation." *DCT* 118 (2009)

[57] N. M. Kwok, Q. P. Ha, T. H. Nguyen, J. Li, and B. Samali, “A novel hysteretic model for magnetorheological fluid dampers and parameter identification using particle swarm optimization,” *Sensors Actuators A Phys.*, vol. 132, no. 2, pp. 441–451, 2006.